

**Identification and initial characterization of the gene
sticks and stones as a new regulator of dendrite
morphogenesis in *Drosophila***

Dissertation

Zur Erlangung des Doktorgrades
der Naturwissenschaften (Dr.rer.nat)
der Fakultät für Biologie
der Ludwig-Maximilians-Universität München

Angefertigt am Max-Planck-Institut für Neurobiologie
Abteilung Molekulare Neurobiologie,
Abteilungsgruppe Differenzierung von Dendriten

Vorgelegt von
Andre Reissaus
München 2007

Datum der Abgabe: 20.09.2007

1.Gutachter: Prof. Alexander Borst

2.Gutachter: Prof. John Parsch

3.Gutachter: Prof. Rüdiger Klein

4.Gutachter: PD Dr. Angelika Böttger

Tag der mündlichen Prüfung: 14.12.2007

Ehrenwörtlicher Versicherung

Ich versichere hiermit, dass die vorgelegte Dissertation von mir selbstständig und ohne unerlaubte Beihilfe angefertigt wurde. Sämtliche Experimente wurden von mir selbst durchgeführt. Ich habe weder anderweitig versucht, eine Dissertation oder Teile einer Dissertation einzureichen bzw. einer Prüfungskommission vorzulegen, noch eine Doktorprüfung durchzuführen.

München, den
(Unterschrift)

1. Gutachter: Prof. Alexander Borst
2. Gutachter: Prof. John Parsch

Die vorliegende Arbeit wurde unter Leitung von Frau Dr. Gaia Tavosanis am Max-Planck-Institut für Neurobiologie in Martinsried durchgeführt.

Table of Content

Table of Content.....	i
Figures and Tables.....	iv
Abbreviations.....	vii
1. Summary	1
2. Introduction.....	3
2.1. Role of the cytoskeleton for dendrite morphogenesis	4
2.2. Activity-dependent regulation of dendrite development.....	5
2.3. External cues that control dendrite morphogenesis.....	6
2.4. Intrinsic programs that control dendrite morphogenesis	7
2.5. Dendritic development of md-da neurons	8
2.6. Functions of md-da neurons.....	12
2.7. Formation of somatic muscles in <i>Drosophila</i>	14
2.8. Scope of the project.....	20
3. Material and Methods	21
3.1. General fly stocks	21
3.2. Antibodies	22
3.3. Instruments	22
3.4. Consumables.....	23
3.5. Solutions/Chemicals	23
3.6. Fly maintenance	24
3.7. Staging and collection of <i>Drosophila</i> embryos and larvae	24
3.8. Visualisation of md-da neurons	25
3.9. Preparation of <i>Drosophila</i> embryos and larvae for confocal microscopy.....	28
3.10. MARCM	28
3.11. Antibody staining in <i>Drosophila</i> embryos and third instar larvae	29
3.12. Confocal microscopy and processing of images.....	30
3.13. Quantifications of dendritic arbours of md-da neurons	31
3.14. Deficiency mapping	31

3.15. Local P-element hop.....	31
3.16. SNP-Mapping	33
3.17. Preparation of genomic DNA from adult <i>Drosophila</i>	35
3.18. PCR	36
3.19. Mapping of P-element insertions.....	37
3.20. Agarose gel electrophoresis	37
3.21. Sequencing of PCR products	38
4. Results	39
4.1. Deficiency mapping	41
4.2. Approaches to map the recessive lethal mutation in line 797	45
4.3. Mapping of the recessive lethal mutation in the line 904	48
4.4. Local P-element hop in the line 904	50
4.5. SNP-mapping in the line 904.....	56
4.6. Sequencing of the remaining candidate genes	61
4.7. Verification of the mapping results	63
4.8. Expression of <i>sns</i> in md-da neurons of mutant line 904 rescues the dendritic phenotype	65
4.9. Expression analysis of <i>sns</i> in <i>Drosophila</i> embryos and larvae	66
4.10. Analysis of dendrite morphology of class I and class IV md-da neurons in <i>sns</i> mutants	69
4.11. An approach to analysedendritic morphology of the remaining md-da neurons	76
4.12. MARCM of <i>sns</i> in md-da neurons of the dorsal cluster.....	77
4.13. Analysis of dendritic morphology of md-da neurons in a <i>blown fuse</i> mutant.....	79
5. Discussion.....	83
5.1. Summary of the results.....	83
5.2. A genetic screen to identify new genes involved in dendrite morphogenesis of md-da neurons.....	84
5.3. Limitations of the screen.....	84
5.4. The dendritic phenotype of md-da neurons in the six mutant lines.....	85
5.5. Approaches to map recessive lethal mutations in <i>Drosophila</i>	86
5.6. Deficiency mapping of recessive lethal mutations	88
5.7. Mapping of the recessive lethal mutation in the line 797	89

5.8. Mapping of the recessive lethal mutation in the line 904	89
5.9. Local P-element hop.....	90
5.10. SNP-mapping	92
5.11. Mapping of the recessive lethal mutation to the gene <i>sns</i>	92
5.12. Does <i>sns</i> affect the dendrite differentiation of md-da neurons directly	93
5.13. Does <i>sns</i> have a cell-autonomous function in the dendrite morphogenesis of md-da neurons.....	95
5.14. What is the role of <i>sns</i> in the dendritic development of md-da neurons	96
5.15. The role of <i>Sns</i> during the formation of dendrites	98
5.16. Outlook	101
6. Bibliography	103
7. Acknowledgements	118
8. Curriculum Vitae	119

Figures and Tables

Figures

Figure 1. Overview of the dendritic morphologies and positions of md-da neurons	9
Figure 2. The cellular environment of md-da neurons at the embryonic and larval body wall	13
Figure 3. Model of intermediate steps in myoblast fusion	15
Figure 4. Schematic overview of the structural domains of the Sticks and stones (Sns) protein.....	16
Figure 5. Signal transduction to the actin cytoskeleton during myoblast fusion.....	20
Figure 6. Expression pattern of the <i>109(2)80 GAL4</i> driver in abdominal md-da neurons.....	25
Figure 7. Expression pattern of the <i>2-21 GAL4</i> driver in abdominal class I md-da neurons	26
Figure 8. Expression pattern of the <i>ppk::GFP</i> transgene in abdominal class IV md-da neurons	27
Figure 9. Crosses for a local P-element hop	32
Figure 10. SNP-mapping crosses.....	33
Figure 11. Dendritic phenotypes of the dorsal cluster md-da neurons in the lines 969, 904 and 797	40
Figure 12. Dendritic phenotypes of the dorsal cluster md-da neurons in the lines 774, 566 and 562	41
Figure 13. Dendritic phenotypes of dorsal cluster md-da neurons in 19-21h old embryos that are hemizygous for the recessive lethal mutations in the lines 904; 797; 774; 566 chromosomes	46
Figure 14. Overview of the complementation analysis in 2L:34A3-34B9 of the line 797	47
Figure 15. Overview of the complementation analysis in 2R:44D1-44F12 of line 904	49
Figure 16. Positions of the P-elements <i>P{EPgy2}EY02398</i> and <i>P{SUPor-P}KG06087</i> in 2R:44F.....	51
Figure 17. Phenotype of the class I md-da neuron <i>vpda</i> in the line P66	53
Figure 18. Quantification of the dendritic morphology of the class I md-da neuron <i>vpda</i> in line P66	54
Figure 19. Gel picture of the iPCR in the mutant line P66	55

Figure 20. SNP-analysis in the line 904 from the right side of 2R:44E3-44F7	59
Figure 21. SNP-analysis in the line 904 from the left side of 2R:44E3-44F7	61
Figure 22. Sequence analysis of the genes <i>sns</i>	62
Figure 23. Schematic overview of the structural domains of the Sns protein	63
Figure 24. Examination of the somatic musculature in line 904.....	64
Figure 25. Rescue of the dendritic phenotype in the mutant line 904.....	67
Figure 26. Anti- <i>sns</i> staining in the 15-16h old embryos and third instar larvae filet	68
Figure 27. Dendritic morphology of the class I md-da neuron vpda in <i>sns</i> mutant embryos	69
Figure 28. Quantifications of the dendritic phenotype of vpda neurons in <i>sns</i> mutant embryos	70
Figure 29. Dendritic morphology of the class I ddaE md-da neuron in <i>sns</i> mutant embryos	72
Figure 30. Quantifications of the dendritic features of ddaE md-da neurons in <i>sns</i> mutant embryos	73
Figure 31. The dendritic phenotype of the class IV md-da neuron ddaC in control and <i>sns</i> ^{S660} embryos	74
Figure 32. Quantifications of dendritic termini in the class IV md-da neuron ddaC in control and <i>sns</i> ^{S660} embryos	75
Figure 33. FLP-out technique to visualize individual md-da neurons in 20-21h AEL old embryos	76
Figure 34. Examples of ddaD MARCM clones.....	78
Figure 35. Examples of ddaC MARCM clones.....	79
Figure 36. The body wall musculature in <i>blown fuse</i> ¹ mutant embryos	80
Figure 37. Dendritic phenotypes of the class I md-da neuron vpda in <i>blown fuse</i> ¹ mutant embryos	81
Figure 38. Quantifications of the dendritic phenotype of the class I md-da neuron vpda in <i>blown fuse</i> ¹ mutant embryos	82

Tables

Table 1. Results of the deficiency mapping.....	42
Table 2. Overlapping deficiencies in mutant lines 969 and 774.....	43
Table 3. Size and gene number of the identified deficiencies.....	44
Table 4. Refined deficiency mapping of the recessive lethal hit in the line 797	47
Table 5. Refined deficiency mapping of the recessive lethal mutation in the line 904	48
Table 6. P-elements that were used as donors for the local hop in 2R:44E3-44F7	51
Table 7. Summary of the local P-element hop	52
Table 8. Potential reference chromosomes for SNP-mapping in 2R:44E3-44F7 of mutant line 904	58

Abbreviations

AEL	After egg laying
Ants.....	Antisocial
BDNF	Brain derived neurotrophic factor
BLAST	Basic local alignment search tool
CaMK.....	Calcium/calmodulin dependend kinase
CBP	CREB-binding protein
CKII.....	Casein kinase II
cM	Centimorgan
CNS	Central nervous system
CREB.....	cAMP response element binding
CREST.....	Calcium-responsive transactivator
d.....	day
ddaA	dorsal dendritic arborization A
ddaB	dorsal dendritic arborization B
ddaC	dorsal dendritic arborization C
ddaD	dorsal dendritic arborization D
ddaE	dorsal dendritic arborization E
ddaF.....	dorsal dendritic arborization F
DEG	Degenerin
Df	Deficiency
DNA	Deoxyribonucleic acid
Dscam.....	Down syndrom cell adhesion molecule
Duf	Dumbfounded/Kirre
EDTA	Ethylenediamine tetraacetic acid
EMS	Ethyl methanesulfonate
EnaC.....	Epithelial Na channel
FCM	Fusion-competent myoblast
FL.....	Full length
g.....	Gramm
gDNA	genomic DNA
GABA.....	γ -amino butyric acid
GEF	Guanine exchange factor
GFP	Green fluorescent protein
GOF	Gain of function
h.....	hour
Ig.....	Immunglobulin
kbp.....	kilobasepair

LOF.....	Loss of function
mM.....	Milli Molar
ml.....	Milliliter
MAP1A.....	Microtubule associated protein 1A
MAP1B.....	Microtubule associated protein 1B
MAPK.....	Mitogen activated kinase
MARCM.....	Mosaic analysis with a repressible cell marker
Mbc.....	Myoblast city
md.....	multiple dendritic
md-bd.....	multiple dendritic-bipolar dendrite
md-da.....	multiple dendritic-dendritic arborization
md-td.....	multiple dendritic- tracheal dendrite
MHC.....	Myosin heavy chain
min.....	Minute
µm.....	Micrometer
µl.....	Microliter
mRNA.....	Messenger ribonucleic acid
N-terminus.....	Amino-terminus
NDR.....	Nuclear Dbf2-related
NGF.....	Nerve growth factor
NMDA.....	N-methyl-D-aspartic acid
NTP.....	Nucleoside triphosphate
ORF.....	Open reading frame
ORN.....	Olfactory receptor neuron
PBS.....	Phosphate buffer solution
PCR.....	Polymerase chain reaction
PDZ.....	PSD95/Disc large/Zona occludentes
Pfu.....	<i>Pyrococcus furiosus</i>
PKA.....	Protein kinase A
PMT.....	Preferred mean temperature
PN.....	Projection neuron
PNS.....	Peripheral nervous system
Ppk1.....	Pickpocket 1
RNA.....	Ribonucleic acid
RNAi.....	RNA interference
Rols7.....	Rolling pebbles7
rpm.....	rounds per minute
Rst.....	IrreC-Roughest
RT.....	Room temperature

SOP	sensory organ precursor
SH	Src homology
SNP	Single nucleotide polymorphism
Sns	Sticks and stones
Taq	<i>Thermus aquaticus</i>
TRK	Tropomyosin-related kinase
TRP	Transient receptor potential
UAS	Upstream activator sequence
USA	United States of America
UTR	Untranslated region
VGCC	Voltage gated calcium channels
vpda	Ventral posterior dendritic arborization
Wasp	Wiscott-Aldrich syndrome protein
WT	Wildtyp

1. Summary

The accurate control of dendritic development is a requirement for the creation of functional neuronal networks. Genetic screens allow to identify genes involved in the dendritic morphogenesis and to expand the fragmentary understanding of the genetic and cellular mechanisms that govern these developmental processes. Such a screen was performed in *Drosophila*, to produce mutants with recessive lethal mutations on the second chromosome and abnormal dendritic phenotypes in md-da neurons of the embryonic PNS (Gao *et al.*, 1999). The aim of this project was to map the recessive lethal mutations in six of the mutant lines, in which dendrites of the embryonic md-da neurons showed overbranching phenotypes. A successful identification of the mutations that are responsible for these abnormal dendritic structures would provide a chance to find new genes involved in the regulation of branch formation during dendritic development. In one of these lines, namely the mutant line 904, a recessive lethal mutation was mapped via deficiency mapping and subsequent SNP-mapping to the gene *sticks and stones* (*sns*). The molecule encoded by *sns* belongs to the Ig-superfamily and is localized to the cell membrane of a subpopulation of myoblasts during early embryonic stages (Bour *et al.*, 2000). Its function is required for the formation of the body wall musculature, which consequently fails to form in *sns* mutants (Bour *et al.*, 2000). In the course of myoblast fusion, Sns has been shown to recruit the adaptor protein D-Crk and the Wasp/Arp2-3 complex to the contact site between myoblasts (Kim *et al.*, 2007; Massarwa *et al.*, 2007). Thus, actin polymerisation is forced specifically at the fusion site, which directs also the transport of exocytotic vesicles (Kim *et al.*, 2007; Massarwa *et al.*, 2007).

The expression of Sns in md-da neurons of the mutant line 904 recovered the dendritic overbranching to control levels, which suggested a cell-autonomous function for this molecule in the dendritic branch formation. In *sns* mutant embryos, the class I neuron vpda showed an increased number of high order branches, whereas other arbour characteristics were not altered. Since the loss of the body wall musculature in *sns* mutants might have an unspecific effect for the development of md-da neurons, the dendritic structure of the

vpda neuron was checked in *blown fuse* mutant embryos that also fail to form a somatic musculature. Interestingly, the dendrites of the vpda neurons were not altered in this mutant, which indicates that the musculature is not required for the development of this neuron. In contrast, the dendritic morphologies of the two other class I md-da neurons, namely ddaD and ddaE, were mildly affected but did not show any overbranching. No morphological changes were observed on the dendrites of class IV md-da neurons *sns* mutants. At later larval stages, expression of *Sns* was detected in md-da neurons. Taken together, this study suggests *Sns* as a new molecule involved in dendrite branch formation.

2. Introduction

A characteristic feature of neurons is the formation of subcellular compartments with striking morphological and cellular specializations that are named axons and dendrites (Craig and Banker, 1994). Axons represent the major presynaptic component of neurons that connect them to often far-away targets, whereas dendrites mainly receive and process incoming information from other neurons or the environment (Yamamoto *et al.*, 2002). The development of these polarized morphologies with extended axons and branched dendrites is a crucial requirement for the correct wiring and function of a neuron within a nervous system (Craig and Banker, 1994; Kaufmann and Moser, 2000; Parrish *et al.*, 2007b; Yamamoto *et al.*, 2002).

Neurons generate individual dendritic arbors with a stereotyped morphology from animal to animal, which suggests that the addition and elongation of branches in developing dendrites is a highly regulated process. In addition, dynamic retraction and elimination of branches during neuronal differentiation, also contributes to the final dendritic shape (Parrish *et al.*, 2007b; Wong and Ghosh, 2002). Moreover, dendritic morphology is an important determinant of information processing in neurons (Hausser *et al.*, 2000; London and Hausser, 2005). The interrelation between neuronal structure and function is well exemplified by the stereotyped organisation of neuronal networks that are responsible for direction-selective responses in visual systems (Borst and Haag, 2002; Taylor and Vaney, 2003) or odor representation in the olfactory systems of rodents and flies (Jefferis and Hummel, 2006; Lin *et al.*, 2007; Wong and Ghosh, 2002).

Hence, different aspects of dendrite patterning need to be appropriately controlled in the context of a complex cellular environment to achieve functional neuronal networks. But despite the recent progress, it still can not be definitely answered, how neurons manage to build their individual dendritic arbors and how the astonishing variety of different dendritic architectures in a nervous system is generated (Parrish *et al.*, 2007b). A short summary of the main mechanisms that are known to regulate dendrite morphogenesis is given below.

2.1. Role of the cytoskeleton for dendrite morphogenesis

During neuronal differentiation, axonal and dendritic growth requires a precise organisation of the cytoskeleton and the secretory trafficking machinery (Horton and Ehlers, 2004; Luo, 2002). The components of the neuronal cytoskeleton, actin, microtubules, myosin and neurofilaments, represent the intracellular scaffold that allows the establishment and maintenance but also dynamic rearrangements of axonal and dendritic morphologies (Luo, 2002). An adequate regulation of actin dynamics is required for the formation of filopodia and lamellipodia on growth cones, which represent specialised structures at the leading end of growing axons and dendrites, or during branch formation (Acebes and Ferrus, 2000; Faix and Rottner, 2006; Luo, 2002). Moreover, the development, maintenance and motility of dendritic spines depends on a precise control of actin organisation and turnover (Johnson and Ouimet, 2006; Matus, 2005). Spines are actin-enriched protrusions that are formed along dendritic branches and represent the major site of excitatory input in mammalian brains (Calabrese *et al.*, 2006; Matus, 2005).

Organisation and stability of microtubules is interrelated with the action of different microtubule associated proteins (MAPs; (Matus, 1994)) that mainly stabilize but also crosslink them to actin (Pedrotti *et al.*, 1994; Togel *et al.*, 1998). MAP1A is needed for the stabilisation and elongation of dendritic branches in a activity dependent manner (Szebenyi *et al.*, 2005). The loss of the MAP1B-related protein in *Drosophila* causes alterations of the microtubule scaffold in neurons that lead to defects in axonal and dendritic development (Bettencourt da Cruz *et al.*, 2005; Hummel *et al.*, 2000). Furthermore, MAP1B is involved in growth cone stabilisation, which is required for correct axon steering in developing neurons, as well as for positioning of GABA receptors (Hanley *et al.*, 1999; Mack *et al.*, 2000).

Hence, the adequate manipulation of different cytoskeletal members, offers the possibility for a guided morphogenesis of dendrites. Monomeric GTPases of the different Rho/Rac subfamilies, especially RhoA, Rac1 and Cdc42, are key regulators of signal pathways that govern the organisation of the actin-

cytoskeleton (Bustelo *et al.*, 2007; Luo, 2002). These Rho GTPases influence many developmental processes, including the formation of dendritic morphology (Luo, 2002; Van Aelst and Cline, 2004; Van Aelst and D'Souza-Schorey, 1997). Rac1 and to lesser extent Cdc42 promote the addition and stabilisation of dendritic branches as well as the formation and maintenance of spines (Calabrese *et al.*, 2006; Van Aelst and Cline, 2004). In contrast, the GTPase RhoA affects more the growth of dendrites and elongation of branches. There is intensive crosstalk between the different Rho GTPases that influences the activity of these molecules and their downstream effectors (Van Aelst and Cline, 2004).

2.2. Activity-dependent regulation of dendrite development

An important role of afferent innervations for dendritic development has been shown to be linked to the action of NMDA receptors and voltage gated calcium channels (VGCC) in different vertebrate model systems (Wong and Ghosh, 2002). Several studies could demonstrate that such effects of neuronal activity on dendrite morphogenesis are mediated through calcium depended signal pathways (Konur and Ghosh, 2005). Moreover, calcium signalling has also profound influence on spine motility and synaptic plasticity in mammalian neurons (Bonhoeffer and Yuste, 2002) as well as local branch dynamics (Lohmann *et al.*, 2002). The major effectors of calcium influx seem to be calcium-dependent protein kinases (CaMKs) and mitogen-activated kinases (MAPKs; (Konur and Ghosh, 2005; Wong and Ghosh, 2002)). CaMKI and different isoforms of CaMKII are localized to the cytoplasm of neurons and control distinct morphological features of dendrites. In contrast, CaMKIV is a nuclear protein and a key player of a calcium-dependent pathway that controls gene expression and dendrite growth, via the transcription factors CREB, CREST and CBP (Konur and Ghosh, 2005; Redmond *et al.*, 2002; Wong and Ghosh, 2002; Wu and Cline, 1998). In addition, there are also indications for a calcium mediated activation of Rho-GTPases through neuronal activity (Schubert and Dotti, 2007; Sin *et al.*, 2002).

2.3. External cues that control dendrite morphogenesis

During the development of neurons within a nervous system, many extrinsic cues serve as dynamic regulators of a variety of important developmental events, including dendritic growth, branching and guidance (Van Aelst and Cline, 2004). The classical example for such extrinsic cues are the mammalian neurotrophins, like brain derived neurotrophic factor (BDNF) or nerve growth factor (NGF), that bind and activate one or more members of the tropomyosin related-kinase (TRK) family of receptor tyrosine kinases or the p75 receptor (Kaplan and Miller, 2000). Binding of neurotrophins to TRK receptors causes the activation of numerous intracellular signalling pathways, including Ras and RhoGTPase controlled cascades (Kaplan and Miller, 2000; Patapoutian and Reichardt, 2001). In the nervous system, neurotrophins are involved in the regulation of cell survival, synapse formation as well as axonal and dendritic growth (Huang and Reichardt, 2003; Van Aelst and Cline, 2004). The action of BDNF on dendritic growth depends on neuronal activity, which is mediated through NMDA receptors (McAllister *et al.*, 1996). In addition, calcium signalling induces the expression of BDNF and neuronal activity enhances the TRK receptor trafficking to the cell surface (Meyer-Franke *et al.*, 1998; Van Aelst and Cline, 2004).

The Wnt/N-cadherin/ β -catenin signal pathway is required for several developmental events in the nervous system and has been shown to enhance dendrite arborisation in dependence of neuronal activity (Yu and Malenka, 2003). Furthermore, semaphorin3A, a classical axon guidance molecule (Dickson, 2002), controls some aspects of dendrite development, like attraction and branching as well as spine maturation. (Morita *et al.*, 2006; Polleux *et al.*, 2000). In addition, a recent publication shows a cell-autonomous function of semaphorin in dendrite targeting in the olfactory system of *Drosophila* ((Komiyama *et al.*, 2007)). Robo and Frazzled, which are cell-surface receptors for the well characterized axon guidance cues Slit and Netrin respectively (Dickson, 2002), are needed for guidance (Furrer *et al.*, 2003) or branching (Whitford *et al.*, 2002) of dendrites in the central nervous system (CNS).

Interaction between dendrites of neighbouring neurons can regulate the dendritic growth and field organisation of sensory neurons to achieve an optimal coverage of receptive fields, as it is exemplified by heteroneuronal tiling of dendrites in neurons of the peripheral nervous system (PNS) of *Manduca* and *Drosophila* (see below, (Grueber *et al.*, 2002; Parrish *et al.*, 2007b)). The cell-adhesion molecule N-cadherin is required for the precise formation of glomeruli in the antenna lobe of *Drosophila* through sub-class specific sorting of olfactory receptor neuron (ORN) axons and restriction of the dendritic targeting of projection neurons (PNs) via the mediation of dendro-dendritic interactions between adjacent subclasses of these interneurons (Hummel and Zipursky, 2004; Zhu and Luo, 2004). In addition, the proto-cadherin *flamingo* is needed for dendrite routing and growth control of sensory neurons in the *Drosophila* PNS (Gao *et al.*, 1999; Gao *et al.*, 2000). Dscam is another cell-adhesion molecule with important functions in neuronal wiring and dendrite morphogenesis, like the elaboration and patterning of PN dendrites in the *Drosophila* antenna lobe (Chen *et al.*, 2006; Zhu *et al.*, 2006) as well as organisation of dendritic branches of sensory neurons in the *Drosophila* PNS (Hughes *et al.*, 2007; Matthews *et al.*, 2007; Soba *et al.*, 2007).

2.4. Intrinsic transcriptional programs that control dendrite morphogenesis

The stereotyped morphologies of individual neurons, suggest that intrinsic transcriptional programs are involved in the regulation of dendrite development. This idea is supported by the identification and characterization of transcription factors that control distinct aspects of dendrite arborisation in the PNS of *Drosophila* (see below, (Komiyama *et al.*, 2003; Parrish *et al.*, 2007b; Parrish *et al.*, 2006)). Likewise, the transcription factor neurogenin2 is required for the migration and the formation of the subtype specific dendritic morphology in pyramidal neurons of the mouse cortex (Hand *et al.*, 2005).

2.5 Dendritic development of *Drosophila* md-da neurons

A subpopulation of the sensory neurons in the PNS of *Drosophila*, the multiple dendritic-dendritic arborization neurons (md-da), was used as a model system in this PhD project. Therefore, a short summary of the development and function of these neurons is given below.

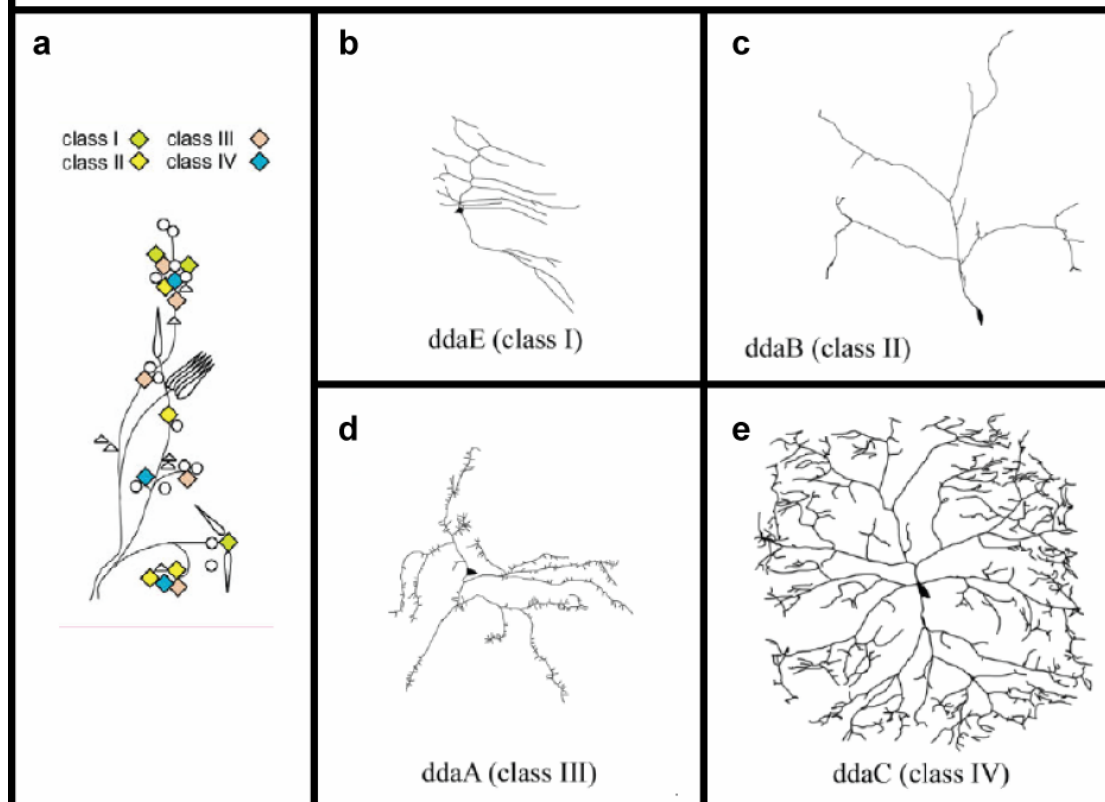
The embryonic and larval PNS of *Drosophila* is composed of sensory neurons, motoneurons and the larval photoreceptors, which constitute the Bolwig's organs (Bodmer and Jan, 1987; Jan and Jan, 1993). All sensory neurons have a bipolar morphology and are grouped based on the number and morphology of their dendrites (Bodmer and Jan, 1987; Jan and Jan, 1993; Sweeney *et al.*, 2002). The type I sensory neurons develop only one unbranched dendrite and are associated with specialized support cells to form external sensory organs or chordotonal organs (Bodmer and Jan, 1987; Jan and Jan, 1993). All type II neurons have multiple dendrites (md-neurons) and are further subdivided into bipolar dendrite neurons (md-bd neurons), tracheal dendrite (md-td neurons) and dendritic arborisation neurons (md-da neurons; see Figure 1; (Bodmer and Jan, 1987)). At 6-9h after egg laying (AEL) all sensory neurons are generated through repeated divisions of sensory organ precursor (SOP's) that originate from the epidermal layer (Brewster and Bodmer, 1995; Jan and Jan, 1993). The dendritic development of type II neurons starts not before 14h AEL, after they have already sent out their axons (Bodmer and Jan, 1987; Gao *et al.*, 1999).

On the basis of their final dendritic morphology, which they achieve in later larval stages, md-da neurons are subdivided into four different classes (Figure 1 b (Grueber *et al.*, 2002)). Among all md-da neurons, the class I neurons develop dendritic arbors with the lowest complexity. Class II md-da neurons (see Figure 1 c) form longer and more sinuous primary dendrites with few more high order branches than class I md-da neurons. Dendritic complexity of class II md-da neurons is only slightly increased in comparison to class I md-da neurons (Grueber *et al.*, 2002). The main characteristics of class III md-da neurons (see Figure 1 d) are many spike-like protrusions along their

secondary branches and at the end of their major trunks. Due to the presence of these small protrusions, dendrites of class III md-da neurons have a significantly higher complexity than dendrites of class I or class II md-da neurons (Grueber *et al.*, 2002). The dendrites of class IV md-da neurons (see Figure 1 e) develop the most sophisticated dendritic arbours among all classes and cover the larval epidermis completely (Grueber *et al.*, 2002). These class-specific differences in dendritic morphology are also reflected in distinct axonal projection of md-da neurons to the CNS (Grueber *et al.*, 2007).

Figure 1. Overview of the dendritic morphologies and positions of md-da neurons

Panel **a** shows a schematic view on the arrangement of sensory neurons in a abdominal hemisegment of *Drosophila* embryos/larvae (image is taken from (Grueber *et al.*, 2007). Diamonds=md-da neurons (color indicates the particular class), md-bd neurons =triangles, external sensory neurons=circles and chordotonal neurons=drop-like. Md-td neurons are not shown. The panels **b-d** show the dendritic morphology of each class of md-da neurons (image is taken from (Grueber *et al.*, 2003b)); **b**=class I (ddaE), **c**=class II (ddaB), **d**=class III (ddaA) and **e**=class IV (ddaC).



Class I and class IV md-da neurons achieve their particular dendritic morphologies through different modes of branching (Sugimura *et al.*, 2003). The primary dendrites of the class I md-da neurons ddaD and ddaE form lateral second order dendrites through interstitial branching, whereas class IV neurons mainly split dendritic growth cones to increase arbour complexity (Sugimura *et al.*, 2003). Furthermore, class I md-da neurons attain their final dendritic morphology much earlier (~50h AEL) than class IV neurons that dynamically increase arbour complexity throughout early larval development (Sugimura *et al.*, 2003).

The dendrites of each md-da neuron coat a specific area of the embryonic or larval body wall. Among md-da neuron of the same class, these dendritic territories are separated from each other, whereas dendritic fields of different md-da classes overlap extensively (Grueber *et al.*, 2002; Grueber *et al.*, 2003b). Two distinct mechanisms have been identified that regulate the organisation of dendritic branches, which cover the corresponding receptive field of a given md-da neuron. First, self-recognition between branches of the same neuron induces repulsive response that consequently prevent overlap between them (self-avoidance, (Hughes *et al.*, 2007; Matthews *et al.*, 2007; Soba *et al.*, 2007)). The second mechanism employs like-repel-like and fill-in responses to organize the dendritic fields of class IV md-da neurons, to achieve a complete and non-redundant coverage of the larval body wall (heteroneuronal tiling, (Grueber *et al.*, 2002; Grueber *et al.*, 2003a; Sugimura *et al.*, 2003)). Both mechanisms, self-avoidance and heteroneuronal tiling, are required to ensure efficient and unambiguous dendritic representations of receptive fields.

In recent years, many novel genes were shown to be crucial for the formation or maintenance of dendritic branch pattern and receptive fields of md-da neurons. These findings allow the characterisation of cellular mechanisms that neurons employ to develop their specific dendritic architectures (Parrish *et al.*, 2007b; Van Aelst and Cline, 2004). The transcription factors Cut, Abrupt and Spineless, regulate independently of each other the establishment of class-specific dendritic complexity in a combinatorial fashion (Grueber *et al.*, 2003a; Li *et al.*, 2004; Sugimura *et al.*, 2004), whereas several products of

polycomb genes are crucial for the maintenance of dendrites of class IV md-da neurons (Parrish *et al.*, 2007a). Hence, different intrinsic programs are required to control distinct aspects of dendrite development in md-da neurons (Grueber *et al.*, 2003a; Kim *et al.*, 2006; Li *et al.*, 2004; Moore *et al.*, 2002; Parrish *et al.*, 2007a; Parrish *et al.*, 2006; Sugimura *et al.*, 2004).

The sophisticated morphologies of dendrites are depended on a precise arrangement of the subcellular cytoskeleton. Dendritic shafts of md-da neurons are mainly filled with tubulin, whereas high order branches and especially spike-like protrusions of class III md-da neurons or filopodia are actin enriched (Andersen *et al.*, 2005; Hummel *et al.*, 2000; Li *et al.*, 2005). Known organizer of the actin-cytoskeleton, like the small GTPases Rac1 and Cdc42 or the non-receptor tyrosine kinase Abl and its downstream target Ena, affect mainly the formation of branches in all md-da neurons (Emoto *et al.*, 2004; Gao *et al.*, 1999; Lee *et al.*, 2003; Li *et al.*, 2005), whereas CaMKII has been shown to regulate formation and dynamics of actin enriched spike-like protrusions/filopodia in class III md-da neurons, through modulation of the actin turnover (Andersen *et al.*, 2005). Additionally, the development of high order branches in class III and IV md-da neurons seems to depend on the specific transport and the local control of mRNA expression in dendrites of md-da neurons (Lee *et al.*, 2003; Ye *et al.*, 2004). Interestingly, the action of Rac1 appears to be partially regulated through the control of its mRNA expression in dendrites (Lee *et al.*, 2003).

The Ste20-like kinase Hippo and the two *Drosophila* NDR kinases, Warts and Tricornered, form a signalling pathway that is involved in dendritic maintenance (Emoto *et al.*, 2006; Parrish *et al.*, 2007a), branch formation and heteroneuronal tiling of class IV md-da neurons (Emoto *et al.*, 2004). Warts interacts genetically with products of several *Polycomb* genes to ensure the maintenance of dendritic architecture of class IV md-da neurons in the later larval stages (Parrish *et al.*, 2007a), whereas Tricornered controls branch formation, through regulation of Rac1 activity, and like-repel-like navigation between dendrites of class IV neurons (Emoto *et al.*, 2004). Both NDR-kinases are coordinated by the Ste20-like kinase Hippo (Emoto *et al.*, 2006). The immunoglobulin Dscam has been shown to be responsible for self-

avoidance of isoneuronal branches (Hughes *et al.*, 2007; Matthews *et al.*, 2007; Soba *et al.*, 2007).

All md-da neurons are located in a layer between the epidermis and the somatic musculature at the body wall of *Drosophila* embryos and larvae (see Figure 2; (Bodmer and Jan, 1987)). In addition, the survival (Sepp and Auld, 2003) and dendritic development of md-da neurons (Yamamoto *et al.*, 2006) depends on their interaction with peripheral glia. Neuroglian, a member of the Ig-superfamily, has been shown to be required for the normal axonal ensheathment of the class I md-da neuron ddaE by its corresponding glia. During the embryonic development, Neuroglian restricts axonal sprouting and controls dendrite branching of the ddaE neuron (Yamamoto *et al.*, 2006). A specific influence of the epidermis or musculature on the differentiation of md-da neurons has not been shown.

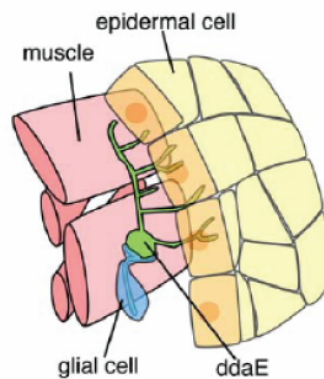
2.6. Functions of md-da neurons

All md-da neurons are sandwiched between the epidermis and the somatic musculature at the body wall of *Drosophila* embryos and larvae, which indicates a somatosensory function of these neurons (see Figure 2). Due to their class-specific dendritic morphologies, it is suggested that each md-da subpopulation has a specific sensory function, which is supported by class-specific axonal projections to the CNS (Grueber *et al.*, 2002; Grueber *et al.*, 2007). Therefore, sensory information from different classes of md-da neurons are separately processed within the CNS (Grueber *et al.*, 2007).

Several studies could show that larval md-da neurons are sensitive to temperature and mechanical stimuli (Lee *et al.*, 2005; Liu *et al.*, 2003; Tracey *et al.*, 2003). This feature of md-da neurons is connected to the action of two transient receptor potential (TRP) channels, pyrexia and painless, that are expressed in these neurons at larval stages (Lee *et al.*, 2005; Tracey *et al.*, 2003). Pyrexia, encodes a TRP channel that opens upon heightening of the environmental temperature. It was identified in a screen for mutants with a changed preferred mean temperature (PMT) and endows stress tolerance against high temperatures in adult *Drosophila* (Lee *et al.*, 2005).

The TRP channel encoded by the *painless* gene is responsible for a specific avoidance behaviour of larvae against noxious temperature and strong mechanical stimuli. Both, the temperature-sensing function of *pyrexia* and the nociceptive function of *painless* have not been specified to individual md-da neurons.

Figure 2. The cellular environment of md-da neurons at the embryonic and larval body wall (taken from (Yamamoto *et al.*, 2006)). All md-da neurons are located at the body wall, where they develop their dendrites in a layer between the epidermis and musculature. Axons as well as parts of the soma and dendrites are ensheathed by peripheral glia (Yamamoto *et al.*, 2006)).



Additionally, md-da neurons have an important proprioceptive function in the *Drosophila* larvae (Hughes and Thomas, 2007; Song *et al.*, 2007). The precise course of peristaltic waves, which is required for larval locomotion, depends on the action of class I md-da neurons in collaboration with the dorsal md-bd neurons, which project both to the same dorsal area of the CNS (Grueber *et al.*, 2007; Hughes and Thomas, 2007; Song *et al.*, 2007). Furthermore, larval locomotion is modulated through the action of the DEG/EnaC channel Ppk1 that is expressed exclusively in class IV md-da neurons (Ainsley *et al.*, 2003).

2.7. Formation of somatic muscles in *Drosophila*

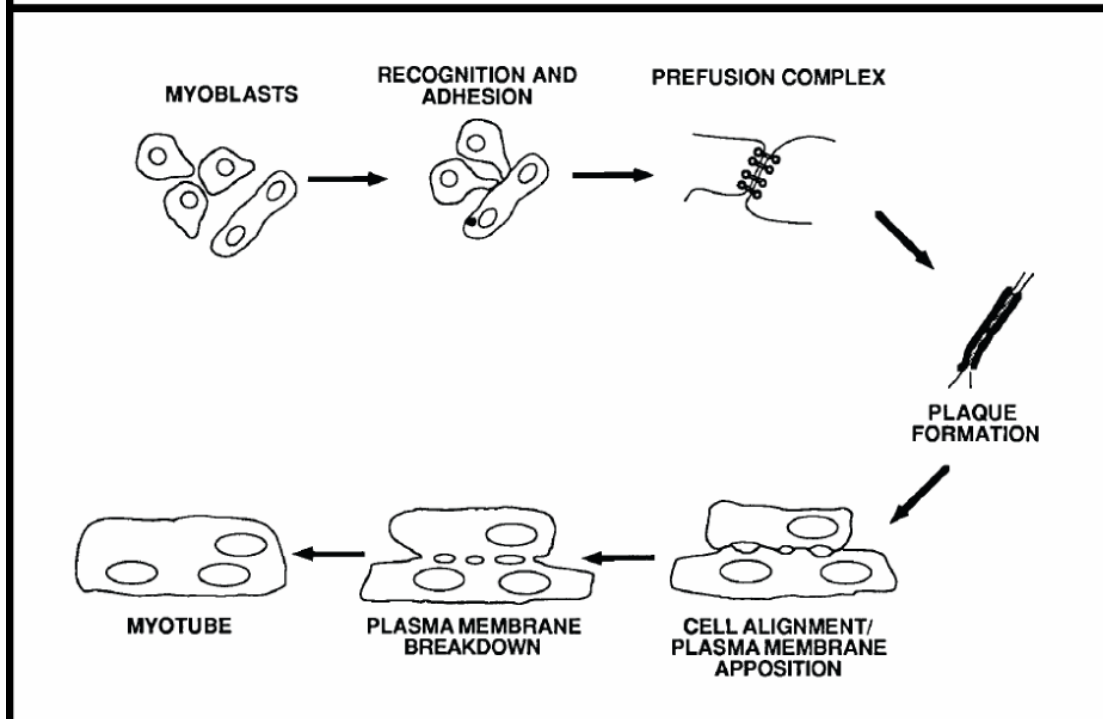
Since, md-da neurons function as proprioceptors, they need to interact with the epidermis or the body wall musculature to sense muscle contractions during the peristaltic waves in larvae. Hence, the development of md-da neurons could be influenced by the underlying musculature to control appropriate dendrite differentiation. Particular molecules that are crucial for the formation of the musculature might also be involved in the dendritogenesis of the md-da neurons. Thus, a short summary of the development of the somatic body wall musculature is given below.

The multinucleated myotubes that constitute somatic muscles in *Drosophila* are generated by the fusion of two types of myoblasts: muscle founder cells and fusion competent myoblasts (FCMs; (Bate, 1990; Carmena *et al.*, 1995; Rushton *et al.*, 1995)). At early stage 12 (7.45h AEL), muscle founder cells and FCMs are derived via Notch-mediated lateral inhibition from clusters of *lethal of scute* expressing cells in the somatic mesoderm (Carmena *et al.*, 1995; Ruiz-Gomez, 1998; Ruiz Gomez and Bate, 1997; Rushton *et al.*, 1995). Founder cells become specified through the expression of an individual set of transcription factors that determines the identity and final position of the future muscle (Bate, 1993; Baylies *et al.*, 1998).

In contrast, FCMs seem to differentiate through the action of a more general transcriptional program and therefore represent a more homogeneous population (Duan *et al.*, 2001; Dworak and Sink, 2002; Ruiz-Gomez *et al.*, 2002). Through the fusion of both types of myoblasts, FCMs adopt the identity of the founder cell with which they fuse, and enable the growth of the corresponding myotube to its final size and shape (Bate, 1990; Rushton *et al.*, 1995). Fusion of myoblasts occurs asynchronously, myoblasts in the ventral region fuse earlier than those more dorsal (Bate, 1990). Unfused myoblasts have a teardrop-like shape with a single pseudopod. These cells need to orient, recognize and adhere to appropriate fusion partners (Figure 3, (Doberstein *et al.*, 1997; Dworak and Sink, 2002)). When contact between unfused myoblasts is established, electron-dense vesicles appear near the juxtaposed plasma membranes that form the prefusion complex (Doberstein

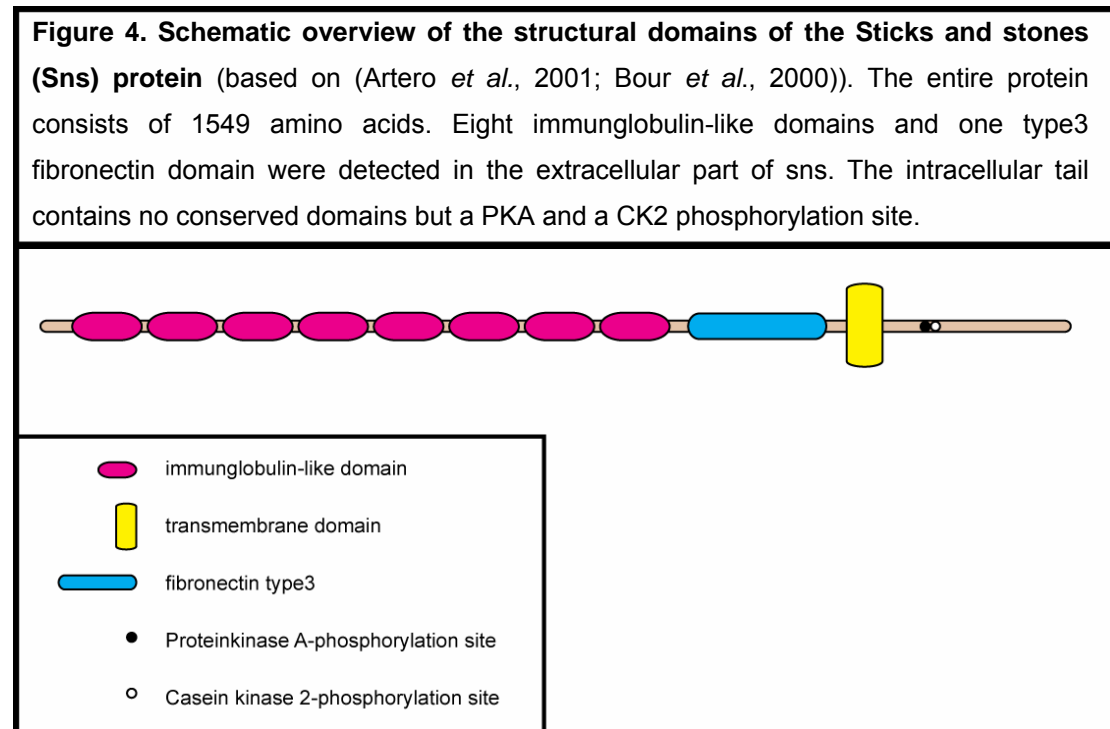
et al., 1997). Upon formation of the prefusion complex, myoblasts align with each other and start to break down the plasma membranes (Doberstein *et al.*, 1997).

Figure 3. Model of intermediate steps in myoblast fusion (adapted from (Doberstein *et al.*, 1997)). FCMs adhere to founder cells after they have recognized each other. Electron dense vesicles appear between the two opposed membranes that will form the prefusion complex. After cell alignment, plasma membrane starts to break down and both myoblasts fuse finally.



Three transmembrane molecules of the immunoglobulin (Ig) superfamily were found to play critical roles in the first steps of myoblast fusion (Bour *et al.*, 2000; Ruiz-Gomez *et al.*, 2000; Strunkelnberg *et al.*, 2001). In *sticks and stones* (*sns*) mutants, myoblast fusion is completely abolished and consequently no somatic musculature is formed (Bour *et al.*, 2000). All myoblasts differentiate, but fail to cluster prior to muscle formation, which indicates an early abort of the myoblast fusion pathway in *sns* mutants (Bour *et al.*, 2000). Sequence analysis revealed that *sns* encodes a transmembrane protein of the Ig superfamily with a predicted size of 162kDa and strong

homology to human Nephrin (Bour *et al.*, 2000). Its N-terminus contains eight putative Ig domains, a single fibronectin type III domain and a putative transmembrane domain (Figure 4; (Artero *et al.*, 2001; Bour *et al.*, 2000)).



Additionally, several SG doublets that serve as potential attachment sites for heparine sulfate can be found in the extracellular domain (Artero *et al.*, 2001; Bour *et al.*, 2000). The intracellular domain of Sns harbours two potential target sites for Protein-kinase A (PKA) and Casein-kinase II (CKII; (Artero *et al.*, 2001)). During embryogenesis *sns* is expressed in the visceral mesoderm and in FCMs of the somatic mesoderm, where it becomes localised to discrete sites in the plasma membrane (Bour *et al.*, 2000). After fusion of FCMs to muscle founders/precursors Sns protein becomes degraded rapidly (Bour *et al.*, 2000). At embryonic stage 17, Sns expression is also seen in muscle attachment sites (Bour *et al.*, 2000).

A similar myogenic phenotype as seen in *sns* mutants, occurs in embryos that are double mutants for *dumbfounded/kirre (duf)* and *IrreC-roughest (rst)* (Ruiz-Gomez *et al.*, 2000; Strunkelnberg *et al.*, 2001). The gene *duf* encodes a transmembrane Ig-protein of the DM-GRASP/BEN/SC1 subfamily, which is

expresses in all muscle founder cells (Ruiz-Gomez *et al.*, 2000). Additional expression can be detected in the visceral mesoderm and few CNS-neurons during embryogenesis (Dworak and Sink, 2002; Ruiz-Gomez *et al.*, 2000). The function of Duf seems to be the attraction of myoblasts to muscle founder cells, since its misexpression in epidermal cells causes myoblasts to migrate and aggregate to these ectopic sources of Duf (Ruiz-Gomez *et al.*, 2000).

The *roughest* (*rst*) gene also encodes an Ig-protein of the DM-GRASP/BEN/SC1 subfamily that is highly similar to the Ig-molecule encoded by the gene *duf* (Ramos *et al.*, 1993; Strunkelnberg *et al.*, 2001). Both proteins have five Ig domains in their extracellular fragment that are highly homologue to each other. The intracellular domains of Rst and Duf are less conserved, but harbour three highly conserved motifs: a consensus sequence for the type of autophosphorylation domain found in receptor tyrosine kinases, a candidate PDZ-domain and putative serine and tyrosine phosphorylation sites (Strunkelnberg *et al.*, 2001). Thus, Rst represents a paralogue of Duf (Strunkelnberg *et al.*, 2001). The expression pattern of *rst* and *duf* overlap to some extent during myogenesis. Both molecules are expressed by muscle founder cells, but expression of Rst is also seen in FCMs and muscle attachment sites (Strunkelnberg *et al.*, 2001). As noted above, Rst and Duf have partially redundant function during myoblast fusion. The misexpression of Rst in epidermal cells causes migration and aggregation of myoblasts to these ectopic sites as it was shown for Duf before (Ruiz-Gomez *et al.*, 2000; Strunkelnberg *et al.*, 2001). Both molecules are potentially cleaved in the course of myogenesis (Chen and Olson, 2001).

Sns and Duf interact with each other in *in-vivo* and *in-vitro* (Galletta *et al.*, 2004). In the course of myoblast fusion strong colocalisation of both molecules was shown in embryos during contact and recognition steps (Dworak *et al.*, 2001; Galletta *et al.*, 2004). The adherence between Sns or Duf expressing cells depends on the extracellular domains of both molecules, whereas the migration of FCMs additionally requires the intracellular domain of Sns (Galletta *et al.*, 2004). Therefore, migration of FCMs to muscle founder cells as well as recognition and subsequent adherence between both is regulated via the heterophilic interaction of Sns and Duf (Galletta *et al.*, 2004;

Ruiz-Gomez *et al.*, 2000). In contrast to Sns, Duf is capable of homophilic interaction as well (Dworak *et al.*, 2001; Galletta *et al.*, 2004). The binding ability of Rst to Sns or Duf is not unambiguously clarified, but appears to be similar to Duf (Dworak *et al.*, 2001; Galletta *et al.*, 2004).

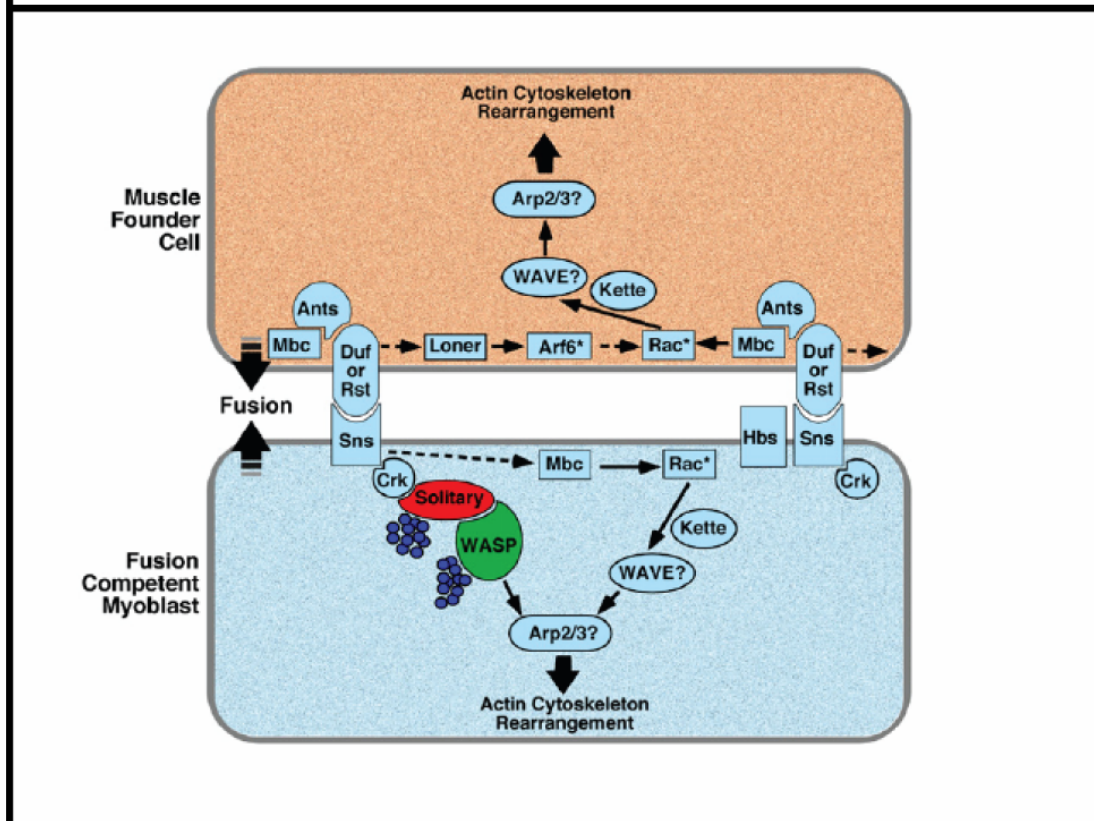
Upon contact of FCMs to muscle founder or precursor cells, Duf and Sns form a ring-shaped structure at sites of adhesion between both cell types (Galletta *et al.*, 2004; Kesper *et al.*, 2007). This structure widens during fusion and seems to serve as a docking station for a variety of different molecules involved in the rearrangement of the actin cytoskeleton (see Figure 5). Through its interaction with Duf, the large cytoplasmic protein Ants (Rols7), which is exclusively expressed in muscle founder cells and precursors, becomes localised to these adhesion sites between different myoblasts (Chen and Olson, 2001; Kesper *et al.*, 2007; Menon and Chia, 2001). Ants exhibits a putative lipolytic enzyme activity and several protein-protein interaction domains, like RING-finger motifs and ankyrin repeats, through which it recruits myoblast city (mbc) and D-Titin to the sites of adhesion between FCMs and muscle precursors (Chen and Olson, 2001; Kesper *et al.*, 2007; Menon and Chia, 2001; Rau *et al.*, 2001). Mbc is the *Drosophila* homologue of Dock180 and contains SH3 domains, two Docker (DHR1/2) domains and binding sites for the small adaptor protein D-Crk (Balagopalan *et al.*, 2006; Doberstein *et al.*, 1997; Erickson *et al.*, 1997; Galletta *et al.*, 1999; Rushton *et al.*, 1995). It is assumed that Mbc functions through the activation of the small GTPase Rac1 during muscle formation, which presumably involves a rearrangement of the cytoskeleton (Balagopalan *et al.*, 2006; Nolan *et al.*, 1998). This model is supported by the fact that Rac1 is a crucial regulator of myoblast fusion (Hakeda-Suzuki *et al.*, 2002; Luo *et al.*, 1994).

In addition, Duf recruits the Guanine nucleotide exchange factor (GEF) Loner to sites of adherence between FCMs and muscle founder/precursor cells, independent of its interaction with Ants (Chen *et al.*, 2003). Interestingly, Loner activates specifically the small GTPase Arf6, which is required for the localisation of Rac1 to the plasma membrane. Hence, two parallel pathways in muscle founder cells act together to control the activation of Rac1 at sites of adherence between myoblasts (Chen *et al.*, 2003).

In FCMs, the SH2-SH3 adaptor D-Crk is recruited to the adhesion site between myoblasts through its interaction with Sns (Kim *et al.*, 2007). D-Crk mediates a signal pathway from Sns to the cytoskeleton via direct interaction with Solitary/D-WIP (Wasp interacting protein) that in turn recruits Wasp (Kim *et al.*, 2007; Massarwa *et al.*, 2007). The complex of D-Crk, D-WIP and WASP forces the actin polymerisation at adhesion sites, which appears to be requirement for a correct membrane targeting of prefusion vesicles (Kim *et al.*, 2007). Additionally, Wasp seems to function through the Arp2/3 complex during myoblast fusion, which could implicate a more direct role of the actin cytoskeleton for the regulation of the membrane state (Massarwa *et al.*, 2007). The site of contact between FCMs and muscle founder cells/precursors attracts also the large cytoplasmic protein Blown fuse, which shows neither significant similarity to any known protein nor exhibits any conserved domains or motifs (Doberstein *et al.*, 1997). Blown fuse is solely expressed in FCMs (Kesper *et al.*, 2007) and appears in the center of the ring-shaped adhesion site between fusing myoblasts (Schroter *et al.*, 2006). Its contribution to the organisation of myoblast fusion is apparently mediated through an interaction with the WASP-regulator kette, which finally modulates the actin-cytoskeleton (Schroter *et al.*, 2004). Additionally, an interaction between Blown fuse and D-Crk has been suggested (Giot *et al.*, 2003). Mbc and D-Crk are expressed in all myoblast and are in general capable of binding to each other (Balagopalan *et al.*, 2006; Erickson *et al.*, 1997; Galletta *et al.*, 1999). Interestingly, although both mutants show severe defects in myoblast fusion, Mbc without the D-Crk binding sites is still correctly localised and still able to rescue the developmental defect of the somatic musculature in the *mbc* mutants (Balagopalan *et al.*, 2006). Thus, the mode of action of Mbc in FCMs and muscle founder cells is independent from D-Crk.

To conclude, the interaction of *duf* and *sns* provides a scaffold for signal pathways that direct actin polymerisation towards the site of contact between fusing myoblasts. The assembly of the body wall musculature is finished at 13 AEL when growth cones of motorneuron axons start to explore the surface of the myotubes and prior to the dendritic development of md-da neurons (Bate, 1993).

Figure 5. Signal transduction to the actin cytoskeleton during myoblast fusion (taken from (Kim *et al.*, 2007)). In muscle founder cells, the signal pathways Duf->Ants->Mbc and Duf->Loner->Arf6 act in parallel to activate Rac1 at sites of adherence between myoblasts. The action of Rac1 presumably leads to rearrangements of the actin cytoskeleton. In FCMs, a signal pathway from Sns to Wasp and Arp2/3, via D-Crk and Solitary, causes also a rearrangement of the actin cytoskeleton. Hbs is the paralogue of sns in *Drosophila*, which has only regulatory function during myoblast fusion (not mentioned in the text). Blown fuse is not shown here.



2.8. Scope of the project

As described above, the exploration of cellular mechanisms that govern dendrite development and differentiation are not completely understood. Hence, genetic screens are performed to find new genes that are required for the formation of specific aspects of dendrite morphology. This PhD-project aimed at identifying and subsequently characterising mutations that cause abnormal dendritic overbranching phenotypes in a subset of embryonic and larval PNS neurons of *Drosophila*.

3. Material and Methods

3.1. General fly stocks

Genotype	Source
<i>w; 109(2)80 GAL4</i>	Yuh Nung Jan; UCSF, USA
<i>w; 109(2)80 GAL4, UAS-GFP</i>	Yuh Nung Jan; UCSF, USA
<i>y w; 2-21 GAL4</i>	Yuh Nung Jan; UCSF, USA
<i>y w; 2-21 GAL4 UAS-mCD8GFP</i>	Yuh Nung Jan; UCSF, USA
<i>ppk::GFP</i>	Yuh Nung Jan; UCSF, USA
<i>MHC::tauGFP; Adv/Cyo_{am}</i>	Eric Olson; University of Texas, USA
<i>UAS-sns [FL]</i>	Susan Abmayr; Stowers Institute Kansas, USA
<i>w; sns^{z1.4}; cn[A]/Cyo</i>	Susan Abmayr; Stowers Institute Kansas, USA
<i>w; sns^{S660}/Cyo</i>	Susan Abmayr; Stowers Institute Kansas, USA
<i>Dp(?;2)bw[D], blow[1] bw[D]/Cyo</i>	Bloomington stock center; BL-4128
<i>y w; Pin/Cyo</i>	Yuh Nung Jan; UCSF, USA
<i>FRT42D</i>	Bloomington stock center; BL-1802
<i>elavGAL4 UAS-mCD8GFP hsFLP;</i> <i>FRT42D</i>	this study
<i>elavGAL4 UAS-mCD8GFP hsFLP;</i> <i>FRT42D tubGAL80/Cyo</i>	Bloomington stock center
<i>w; L Pin/CKG</i>	Yuh Nung Jan; Stanford University, USA
<i>y w hsFLP; Sp/Cyo; UAS>CD2>mCD8GFP</i>	Barry Dickson, IMP, Austria
<i>Elp/CKG; scrb e FRT80/TKG</i>	Yuh Nung Jan; UCSF, USA
<i>cmp44E[1]/CyO</i>	Bloomington stock center; BL-5494
<i>y w; P{EPgy2}cmp44E[EY09152]/CyO</i>	Bloomington stock center; BL-19884
<i>y w; Rya-r44F[16]/CyO</i>	Bloomington stock center; BL-6812
<i>y w; P{lacW}Rya-r44F[k04913]/CyO</i>	Bloomington stock center; BL-10559
<i>y w; P{lacW}Dmn[k16109]/CyO</i>	Bloomington stock center; BL-11159
<i>w; PBac{PB}sec31[c02461]/CyO</i>	Bloomington stock center; BL-10915
<i>y w; P{lacW}Ggamma1[k08017]/CyO</i>	Bloomington stock center; BL-10759
<i>cn P{PZ}(2)03996[03996]/CyO; ry[506]</i>	Bloomington stock center; BL-11361
<i>Pgi[nNC1]/SM1</i>	Bloomington stock center; BL-4007
<i>w; lin[G2]/CyO</i>	Bloomington stock center; BL-7087
<i>y w; Pin/Cyo; Dr Δ2-3/TM3 Ubx</i>	Yuh Nung Jan; UCSF, USA

3.2. Antibodies

Antibody/Antisera	Source
anti- <i>sns</i> (rabbit)	Karl-Friedrich Fischbach, University of Freiburg, Germany
6D4	DSHB, University of Iowa, USA
anti- <i>CD8</i> (rat)	Calteg Laboratories, USA
anti-rat Alexa 488	Invitrogen, Germany
anti-rabbit Cy3	Jackson Laboratories, USA
anti-rabbit Cy5	Jackson Laboratories, USA

3.3. Instruments

Devices	Manufacturer
Leica confocal microscope SP2	Leica GmbH, Heidelberg, Germany
Leica microscope stand DM-IRE2	Leica GmbH, Heidelberg, Germany
Leica fluorescens microscope MZ-16	Leica GmbH, Heidelberg, Germany
Zeiss fluorescens microscope Axioplan2	Zeiss GmbH, Oberkochen, Germany
Zeiss microscope STEMI 2000C	Zeiss GmbH, Oberkochen, Germany
Schott light source KL 1500 LCD	Schott AG, Mainz, Germany
Bio-Rad PCR system PTC-0200	BioRad Laboratories, Hercules, USA
Eppendorf Thermomixer 5436	Eppendorf AG, Hamburg, Germany
Eppendorf Centrifuge 5415 D	Eppendorf AG, Hamburg, Germany
Sigma Centrifuge 4-15C	Sigma-Aldrich, St.Louis, USA
Amersham pharmacia biotech power supply EPS 301	Amersham pharmacia biotech, Uppsala, Sweden
Peqlab Perfect Blue Horizontal Mini Electrophoresis System	Peqlab, Erlangen, Germany
BioRad Transilluminator	BioRad Laboratories, Hercules, USA
Lauda E 200 Thermostat	Lauda GmbH, Lauda-Koenigshofen, Germany
Percival I-36NL climate chamber	Percival Scientific Inc, Perry, USA
Liebherr Comfort freezer	Liebherr, Biberach an der Riss, Germany
Liebherr Refridgerator	Liebherr, Biberach an der Riss, Germany
Pipettes	Gilson, Middleton, USA

3.4. Consumables

Consumables	Source
Forceps DuMont Nr.5	FST, Germany
Fly food bottles	Greiner Bio One, Frickenhausen, Germany
Plugs for Fly food bottles	KTK, Retzstadt, Germany
Microscope slides	Menzel Glaeser, Braunschweig, Germany
Petridishes	Greiner Bio One, Frickenhausen, Germany
PCR tubes	Eppendorf AG, Hamburg, Germany
Pipette tips	Greiner Bio One, Frickenhausen, Germany
Sieves and bucket	MPI of Neurobiology, Martinsried, Germany
Glass ware	Schott, Mainz, Germany
Gloves	Sempermed, Clearwater, Florida, USA

3.5. Solutions/Chemicals

Solution/Chemicals	Composition
PBS (10x)	100mM Na ₂ HPO ₄ , 20mM KH ₂ PO ₄ , 1.37mM NaCl, 27mMKCl
PBT	0.1%-1% Triton X-100 in 1x PBS
PBT+N	PBT + 0.05% normal donkey serum
PBS-FA	9 parts PBS + 1 part 37% Formaldehyde
Normal donkey serum	Jackson Laboratories, USA
Extraction buffer	10mM Tris-HCL; 1mM EDTA; 25mM NaCl
TAE (10x)	0.4M Tris, 0.01M EDTA, 0.2M acetic acid
NaOCl	Merck, Darmstadt, Germany
ddH ₂ O	Sigma-Aldrich, St.Louis, USA
Ethanol	Merck, Darmstadt, Germany
Methanol	Merck, Darmstadt, Germany
Formaldehyde	Polyscience, Warrington, USA
Glycerol	Merck, Darmstadt, Germany
EDTA	Merck, Darmstadt, Germany
NaCl	Merck, Darmstadt, Germany
Tris	Sigma-Aldrich, St.Louis, USA

3.6. Fly maintenance

For optimal propagation, *Drosophila melanogaster* flies were raised on a standard media (fly food) at 25C and 70% relative humidity. The used fly food had the following composition:

1L media:

yeast	15 g
agar	11.7 g
molasse	80 g
corn flour	60 g
methylparaben	2.4 g
propionic acid	6.3 ml

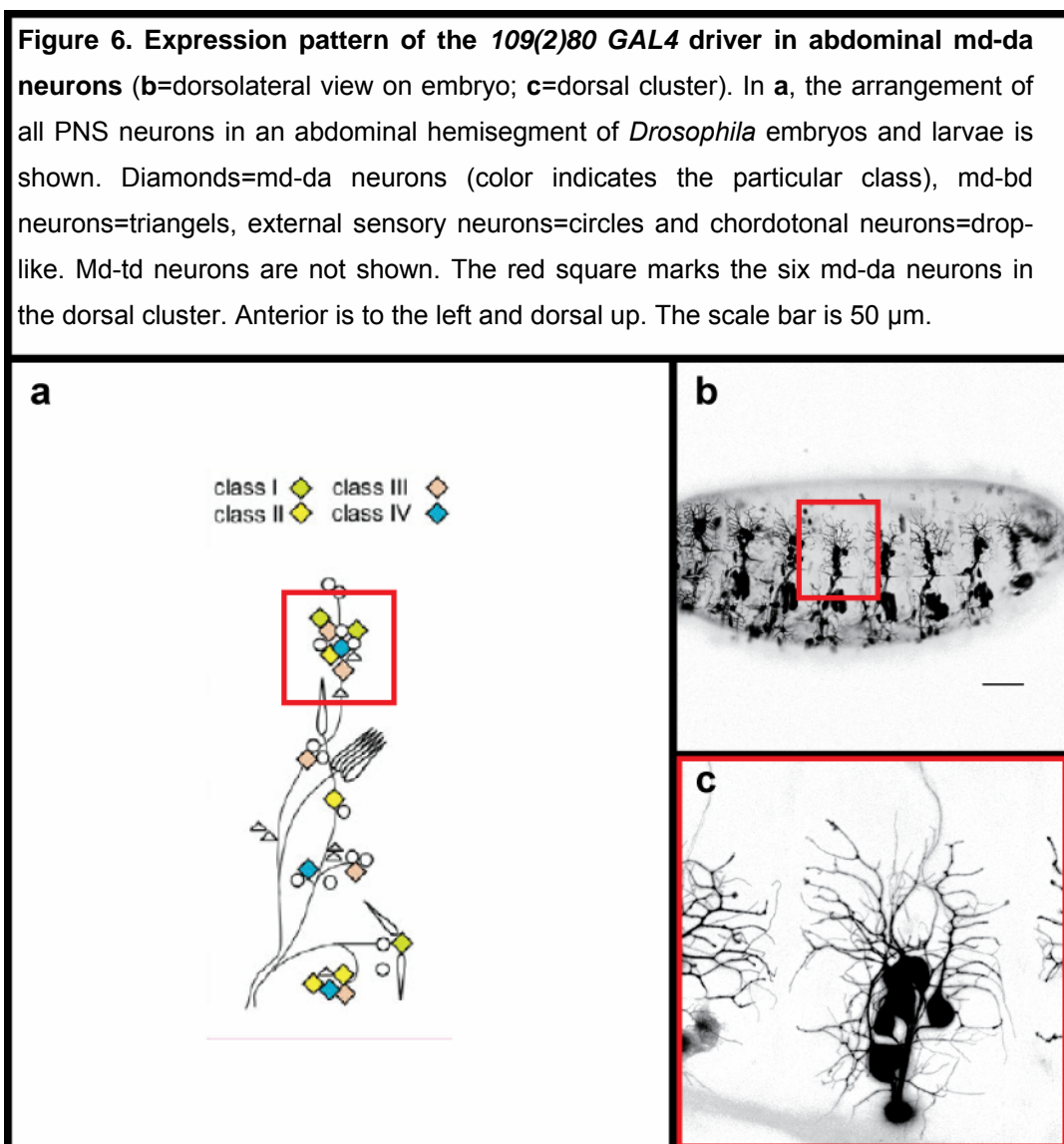
To enhance egg laying of *Drosophila* females, a paste of water-dissolved yeast granules was added to the standard media when appropriate.

3.7. Staging and collection of *Drosophila* embryos and larvae

A correct staging of *Drosophila* embryos and larvae is crucial for the study of dendrite development. For the mass collection of embryos and larvae, flies of a given genotype were kept in population cages (transparent plastic cylinders). The one end of these population cages is closed by a plastic mesh to allow air exchange, while the other end serves as connector for replaceable apple agar plates. Depending on the requirements of a given experiment, flies within a population cage were allowed to lay eggs on the surface of the apple agar for a certain period of time. Subsequently, these apple agar plates were incubated at 25C and 70% relative humidity, to allow the embryos to develop to the required stage.

3.8. Visualisation of md-da neurons

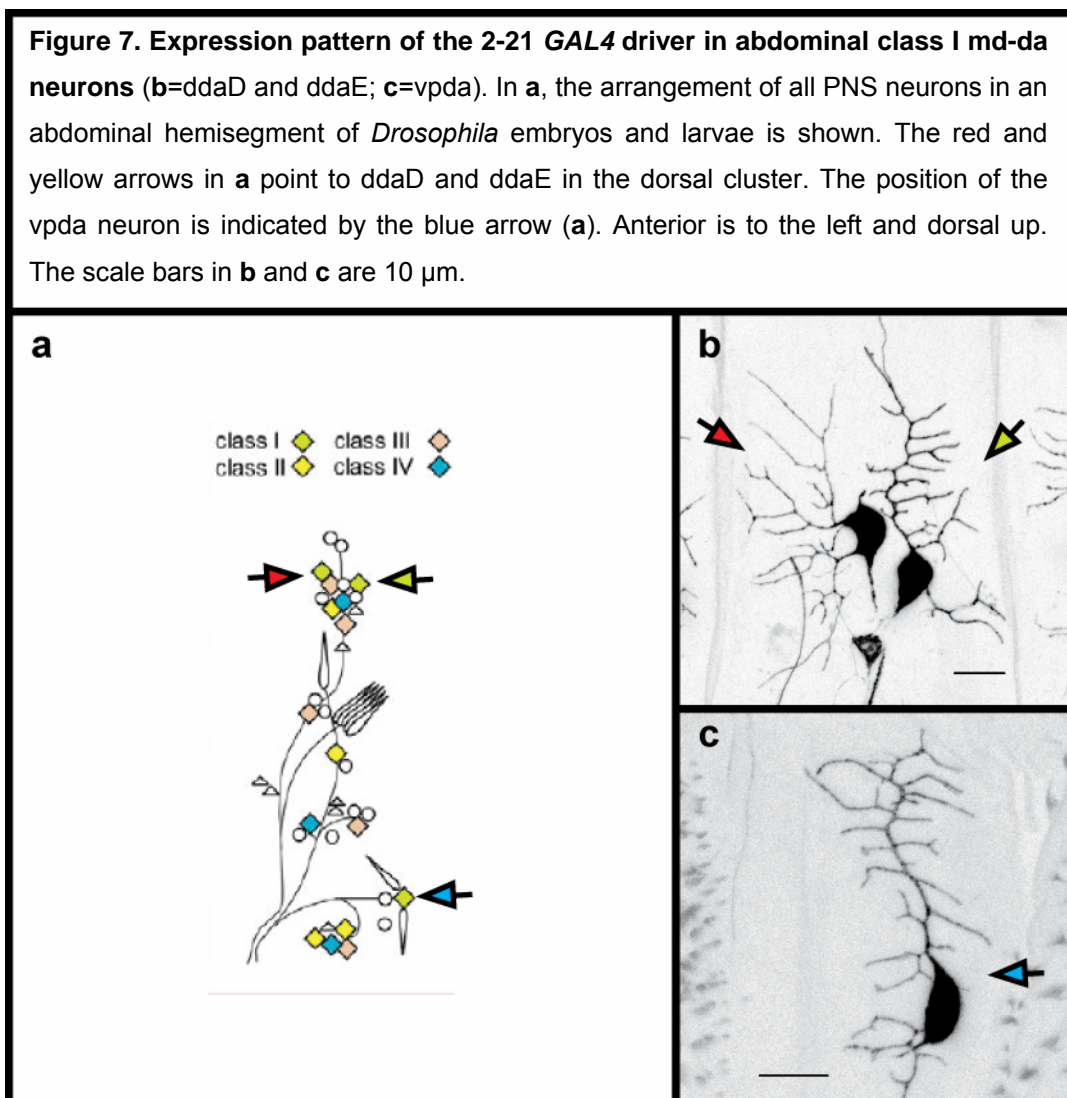
Different *GAL4* drivers were used to label all or subsets of md-da neurons with *UAS-GFP* or *UAS-mCD8GFP* reporters via the *GAL4/UAS* system (Brand and Perrimon, 1993; Yeh *et al.*, 1995). The *109(2)80 GAL4* is active in almost all PNS neurons, including all md-da neurons and a few neurons in the CNS starting from embryonic stage 15 (Gao *et al.*, 1999).



It is mainly used to study the morphology of the dendritic field that is formed by six md-da neurons in the dorsal part of an embryonic or larval

hemisegment (ddaA-F), which are called the “dorsal cluster” (Figure 6; (Gao *et al.*, 1999)). As a consequence of its expression pattern, the *109(2)80 GAL4* driver does not allow to study dendritic arbours of single md-da neurons. This *GAL4* driver was usually used with two *UAS-GFP* reporters recombined on the second chromosome. The corresponding fly line is called 80G2.

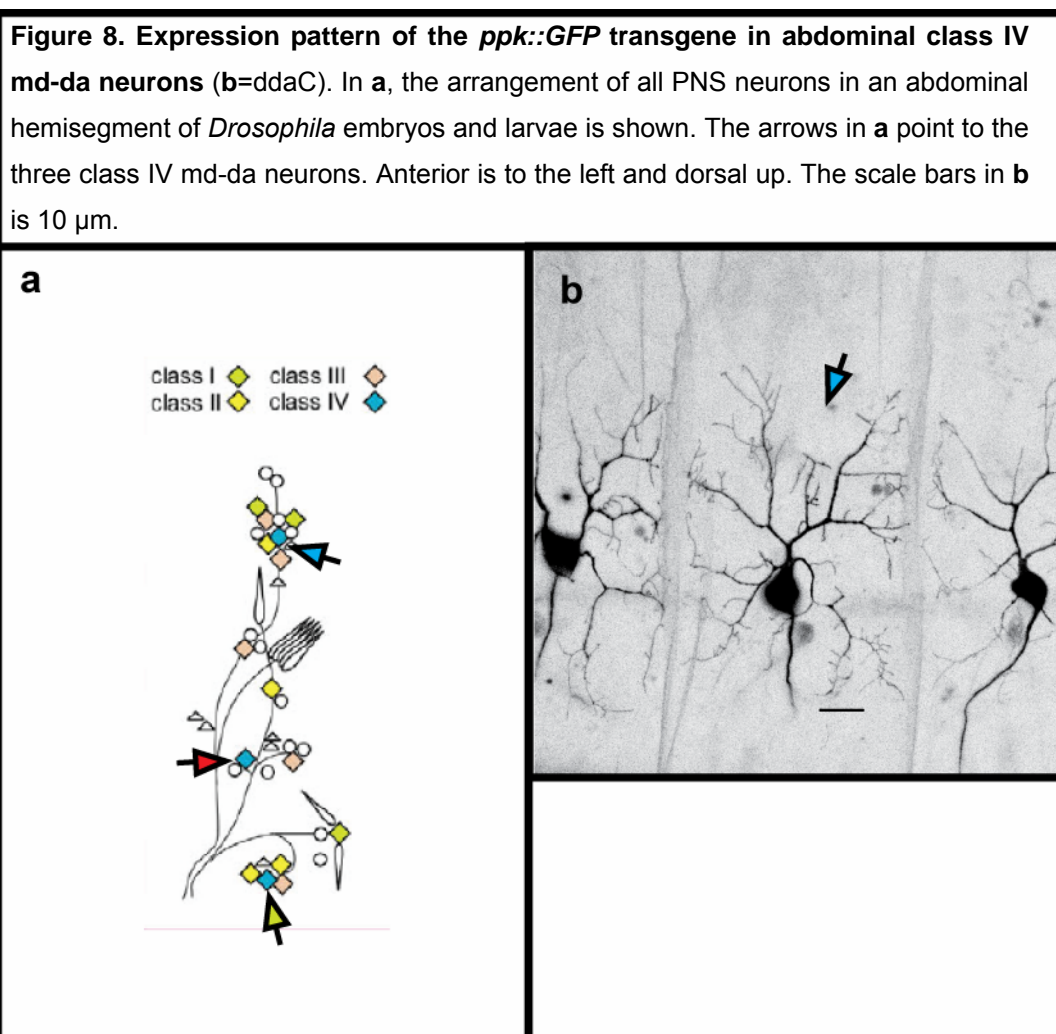
The 2-21 *GAL4* driver is active at high levels in all class I md-da neurons and to much lower extent in class IV md-da neurons (Figure 7; (Grueber *et al.*, 2003)).



It enables to study and quantify dendritic arbours of class I md-da neurons without any overlap with dendrites of neighbouring neurons. A convincing

visualization of the class I md-da neurons *ddaE* and *vpda* with this *GAL4* driver is achieved the earliest at 20-21h AEL (late stage 17). In contrast, the expression of *GAL4* in the third class I md-da neuron *ddaD* is unsteady at this stage. The 2-21 *GAL4* driver was usually combined with a *UAS-mCD8GFP* reporter and the corresponding fly line was named 2-21.

The class IV md-da neurons were visualised via a transgene that expresses *GFP* under the control of the promoter of the *pickpocket* gene (Figure 8; (Adams *et al.*, 1998; Grueber *et al.*, 2003)). An appropriate expression of *GFP* from this transgene was achieved in 21-22h old embryos.



For the FLP-out labelling of dorsal md-da neurons, the *109(2)80 GAL4* driver was crossed to *y w hsFLP; Sp/Cyo; UAS>CD2>mCD8GFP* to finally achieve

the genotype *y w hsFLP; 109(2)80 GAL4; UAS>CD2>mCD8GFP*. Eggs of these stocks were collected for 1h and incubated for 3 additional hours at 25°C (70% humidity) prior a brief heatshock for 5min at 38°C. Afterwards, eggs were allowed to develop until late embryonic stage 17 and checked for individually labelled md-da neurons under the confocal microscope.

3.9. Preparation of *Drosophila* embryos and larvae for confocal microscopy

Drosophila eggs are enveloped by a transparent vitellin membrane and additionally encased by an opaque chorion shell. To remove the chorion shell, embryos were treated with 50% NaOCl for 3 min and subsequently rinsed with ddH₂O and PBT, to remove remaining chemical. Dechorionated embryos were finally mounted in 90% glycerol on a standard microscope slide. Larvae were picked from the agar plate, briefly washed in PBS and mounted in 90% glycerol on a standard microscope slide. Cover slips on top of the larvae were attached to the slide by pieces of modelling clay, mainly to prevent the escape of the highly motile animals.

3.10. MARCM

The mosaic analysis with a repressible cell marker (MARCM) technique allows to study the cell-autonomous function of a certain gene through generation of labelled cells that are homozygous mutant for this gene in an otherwise heterozygous animal (Lee and Luo, 1999). For MARCM analysis of *sns*, a recombinant chromosome was generated that bears the *FRT42D* sequence and the *sns*^{S660} loss of function (LOF) allele. A modified protocol from Grueber *et al.* 2002 was used, to induce MARCM clones among md-da neurons. *Drosophila* eggs were collected at 25°C for 3 h and kept for additional 3 h at 25°C prior a sequence of heat shocks (45 min 38°C, 30min RT, 30min 38°C). Pictures of all MARCM clones were taken in third instar larvae.

3.11. Antibody staining in *Drosophila* embryos and third instar larvae

Antibody staining was performed on 13-15h AEL old embryos. Older embryos form a cuticle that prevents sufficient penetration of the antibody. Fixation of up to 15h old embryos was performed as follows: embryos were dechorinated in 50% NaOCl for 5min and rinsed well with ddH₂O and 0,1% PBT to remove remainings of the chemical. All dechorinated embryos were placed in a glass scintillation vial containing heptane : PBS-FA in a ration of 1:1 (Vol) and gently rotated for 30min. Subsequently, the (lower) aqueous layer with the fixative, plus all embryos that have fallen into it, was removed with a pipette. The aqueous layer was replaced with the same volume of MeOH. Embryos were separated from their vitellin membrane through vortexing for about 1 min. All embryos that have fallen to the bottom of the MeOH phase, where transferred to a fresh 1.5ml tube with a pipette and washed three times with MeOH. It is possible to store fixed embryos in MeOH at -20°C for several weeks. Prior to antibody staining, the MeOH was removed and embryos were washed three times with 0,1% PBT for 5min, incubated on a rotator for 30min in 0,1% PBT and finally rotated in 0,1% PBT+N for 30min. The primary antibody was applied in 0,1% PBT+N in a concentration of 1:20 to 1:200 and embryos were then incubated over night at 4°C. To remove the primary antibody, embryos were rinsed with 0,1% PBT four times and subsequently washed four times for 15-20min with 0,1% PBT. Prior to application of the secondary antibody, embryos were incubated on a rotator for 30min in 0,1% PBT+N. The secondary antibody was applied in 0,11% PBT+N in concentration of 1:200 to 1:500 for 90min on a rotator at RT. Finally, embryos were rinsed three times with 0,1% PBT for 5min and subsequently washed four times for 15-20 min with 0,1% PBT to remove secondary antibody. All embryos were mounted on slides in 90% glycerol.

Antibody stainings were also performed on third instar larvae. To provide optimal access for antibodies to PNS-neurons, third instar larvae were filleted

prior to fixation. Larvae were immobilised with insect pins and opened with scissors on a sylgard dish. Subsequently, fillets were fixed for 20min with 4% formaldehyd in PBS directly on the sylgard dishes. Remainings of the fixative were taken off through four washing steps with 1% PBT followed by additional 2x 30min incubation of the filets in 1% PBT and 2x 30 min incubation in 0.5% PBT on a rotator. Next, fillets were rotated in 0.5% PBT+N for 1h at 4°C. After this blocking step, primary antibodies were applied in 0.5% PBT+N in a concentration of 1:20-1:100. Larvae fillets and antibody-solution were incubated on a rotator for 2d at 4°C. Secondary antibodies were applied at concentration of 1:300 in 0.5% PBT+N, after third instar larvae fillet were separated from the primary antibody through 4x 30min washing steps in 0.5% PBT and 1x 1h blocking in 0.5% PBT+N. After 90min incubation at RT, excess of a secondary antibody was removed from the larvae fillets through four 30min washing steps in 0.5% PBT. Larvae fillets were mounted in 90% glycerol for microscopy.

3.12. Confocal microscopy and processing of images

All pictures were taken with Leica 20x or 63x glycerol immersion objectives on a Leica DM-IRE2 inverted microscope stand. A Leica SP2 confocal microscope was used. Due to a different orientation of embryos or larvae, stack size and z-step of confocal series were individually adjusted to acquire optimal visualisation of md-da neurons. Maximum projections of confocal series were calculated to show the whole dendritic arbour of md-da neurons. Photoshop (Adobe Systems, San Jose, Californien, USA) was used to enhance the contrast of images and to convert images to inverted gray scale.

3.13. Quantification of dendritic arbours of md-da neurons

Maximum-projections of confocal stacks of md-da neurons were used for the quantification of dendritic arbours. All quantifications were performed with ImageJ (<http://rsb.info.nih.gov/ij/>). Semi-automatic tracings of dendrites were generated via the ImageJ plugin NeuronJ (<http://rsb.info.nih.gov/ij/>).

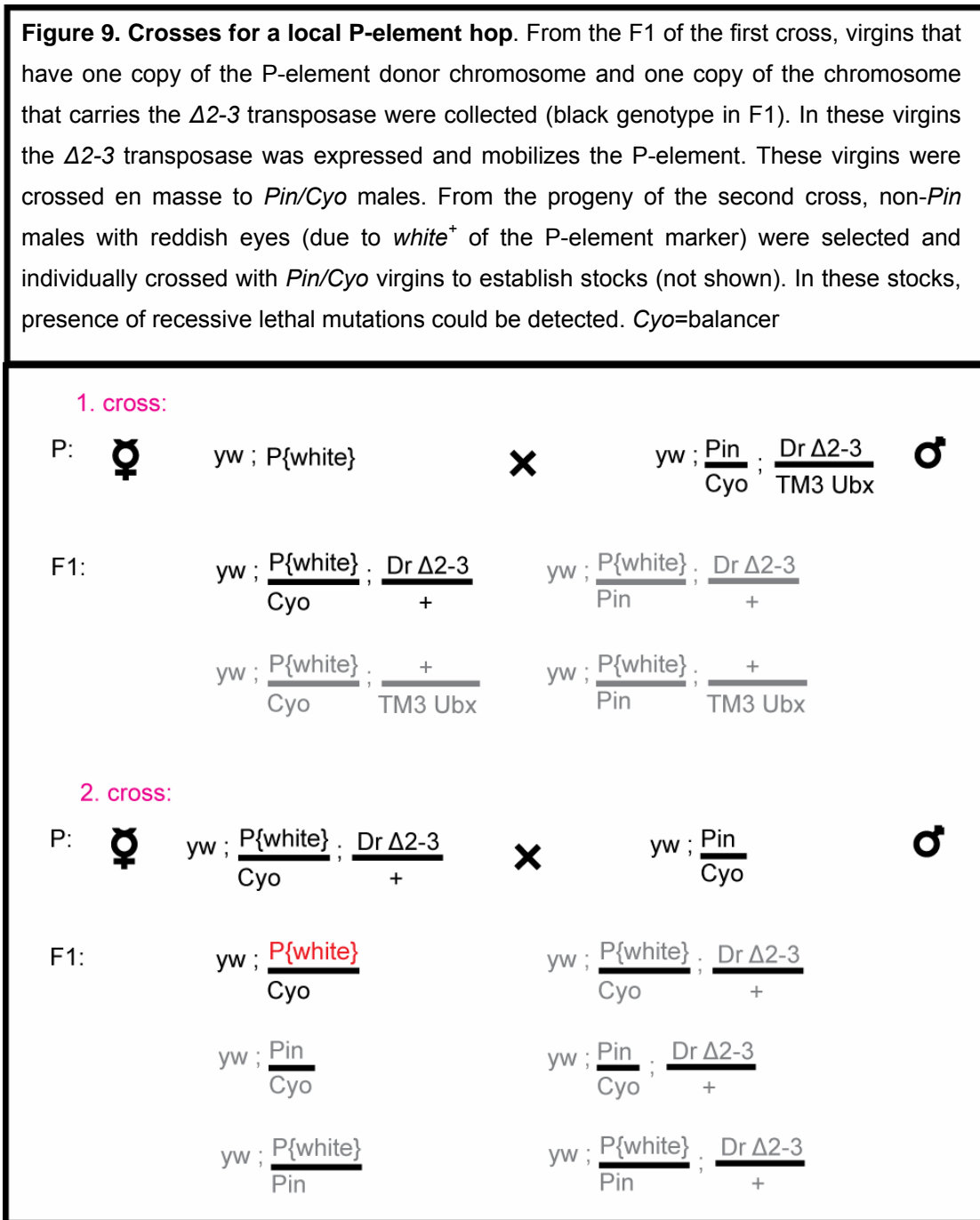
3.14. Deficiency-Mapping

The Deficiency Kit (DfKit2; stand 10/2003, Bloomington stock center; <http://flystocks.bio.indiana.edu/>) was used to roughly localize recessive lethal mutations on the second chromosome in all six mutant-lines in a range of several cytological segments. Deficiency- and mutant chromosomes are homozygous lethal and therefore are kept heterozygous over balancer-chromosomes, respectively. The corresponding Balancer-chromosomes carry usually a dominant visible and homozygous lethal marker, which allows tracing the segregation of the balancer. All deficiency lines of the DfKit2 were crossed to each of the six mutant lines, and complementation of the mutant lethality was scored by the number of flies without the dominant visible marker mutation (*Cy*, *Gla*) of the respective balancer-chromosomes in the F1 progeny. In few cases, deficiency chromosomes carry a recessive *cn* allele, which produces a visible phenotype when heterozygous over the *cn* allele on *Cy*-balancer chromosomes. Hence, animals without a *cn* or *Cy* phenotype were scored in this cases.

3.15. Local P-element hop

A local P-element hop was conducted to generate independent mutant alleles of the recessive lethal mutation in the mutant line 904. This technique is based on the mobilisation of a viable P{*white*⁺} element insertion within the chromosomal area where a recessive lethal mutation is induced in an unrelated mutant line. All flies with transposed P{*white*⁺} element were individually screened for the presence of new recessive lethal mutations. The

ones that carry such a new mutation are used for complementation test with the original mutant line. Figure 9. outlines the crosses performed for a local P-element hop. The used P-element donor chromosomes were isogenised before mobilisation.



3.16. SNP-Mapping

Single nucleotide polymorphism (SNP) mapping (Berger *et al.*, 2001; Hoskins *et al.*, 2001) was performed to map the recessive lethal mutation in the mutant line 904. This approach was based on the creation of recombinants between the mutant chromosome and two reference chromosomes, respectively.

Figure 10. SNP-mapping crosses. From the F1 of the first cross, virgins were collected that were heterozygous for the mutant and the reference chromosome (black genotype in F1). These virgins were crossed en masse to males with the chromosomal deficiency that uncovers the recessive lethal mutation on the mutant chromosome. From the progeny of the second cross, only flies that were heterozygous for the recombinant and deficiency chromosome were interesting for SNP-analysis (black genotype in the F1 progeny of the second cross). Among these flies, only those that lost the lethality and the P-element marker were used for SNP-analysis. *Cyo*=balancer chromosome.

1. cross:

P: ♀ $yw ; \frac{\text{mutant}}{\text{Cyo}}$ × $yw ; \frac{\text{reference}}{\text{Cyo}}$ ♂

F1: $yw ; \frac{\text{mutant}}{\text{reference}}$ $yw ; \frac{\text{reference}}{\text{Cyo}}$ $yw ; \frac{\text{mutant}}{\text{Cyo}}$

2. cross:

R! P: ♀ $yw ; \frac{\text{mutant}}{\text{reference}}$ × $yw ; \frac{\text{Df(2R)H3E1}}{\text{Cyo}}$ ♂

F1: $yw ; \frac{\text{mutant (reference)}}{\text{Df(2R)H3E1}}$ $yw ; \frac{\text{mutant}}{\text{Cyo}}$

$yw ; \frac{\text{mutant (reference)}}{\text{Cyo}}$ $yw ; \frac{\text{reference}}{\text{Df(2R)H3E1}}$

$yw ; \frac{\text{reference}}{\text{Cyo}}$ $yw ; \frac{\text{mutant}}{\text{Df(2R)H3E1}}$

Each reference chromosome contains a traceable $P\{yellow^+ white^+\}$ marker transgene to the left or right of the chromosomal area where the recessive lethal mutation is supposed to map. Both, reference chromosomes and the mutant chromosome were isogenized before the SNP-mapping.

Visibility of the P-element marker genes on the reference chromosomes was confirmed in heterozygous animals. The distance between the marker P-element transgenes on the two reference chromosomes is approximately 300kbp (0.3 cM). Only recombinants that lost the corresponding $P\{yellow^+ white^+\}$ marker transgene and the lethality were selected. The crosses for the SNP-mapping are presented in Figure 10.

The presence of the recessive lethal mutation in all recombinants was excluded by mating the selected virgins without balancer from the F1 of the first mapping cross to $Df(2R)H3E1$ males (see Figure 10). Because $Df(2R)H3E1$ uncovers the recessive lethal mutation, all non-balanced adults of the F1 from the second mapping cross do not contain this recessive lethal mutation anymore. For recombinations between mutant and reference chromosome with the marker P-element insertion to the right of 2R:44E3-44F7, the loss of $P\{white^+\}$ was scored to detect the desired recombinants in the progeny of the second mapping cross. In contrast, all recombinations between the mutant chromosome and the reference chromosome with the marker P-element insertion to the left of 2R:44E3-44F7 still contain the P-element transgenes of the $GAL4/UAS$ system, which expresses already $P\{white^+\}$. In this case, loss of $P\{yellow^+\}$ was scored to detect the correct recombinants. SNP-analysis with the selected recombinants was performed to map the position of the recessive lethal mutation in the mutant line 904.

For identification of sequence polymorphisms between the mutant and reference chromosomes, primer combinations were created to amplify ~1kb genomic DNA (gDNA) from intergenic regions and introns in between the two marker P-element insertions (see attached excel snp mapping.xls). All used primers were optimized for 62°C annealing temperature. PCR using these primers was performed on gDNA prepared from animals heterozygous for the mutant and a corresponding reference chromosome. Sequences of these

amplified gDNA stretches were screened for double peaks via the Seqman software (Lasergene, DNASTar, Madison USA).

3.17. Preparation of genomic DNA from adult *Drosophila*

Genomic DNA of adult *Drosophila* was prepared in two different ways. For standard PCR applications and the inverse PCR (iPCR) method that is used to determine the insertion site of P-elements, the DNAeasy Tissue Kit (Quiagen, Hilden Germany) was used to obtain gDNA from adult flies. Ten anaesthetized adult flies were placed in a 1.5 µl microcentrifuge tube and squashed in 180 µl PBS via a disposable microtube pestle. All subsequent steps followed the manufacturer instructions, starting from step2 of the protocol "Purification of Total DNA from Cultured Animal Cells", in the handbook of the DNAeasy Tissue Kit (page 24; Quiagen, Hilden Germany)). At step 7 of this protocol, elution of DNA from the column was performed only once with 100 µl H₂O. This procedure allowed large gDNA preparations with constant high quality.

A different protocol, adapted from Berger *et al.* 2001 was used to prepare gDNA from single recombinant flies for SNP-mapping in the mutant line 904 (Berger *et al.*, 2001). All recombinants were individually placed in a 96 well plate and stored at -80°C. For preparation of gDNA, single flies were squashed in 20 µl extraction buffer within the 96 well plate by using pipet tips on an Eppendorf Multipipette. Squashed flies were incubated for 5 min at 95°C in a PCR cycler and subsequently cooled down on ice. For protein digestion, 3 µl Proteinase K (20 mg/µl; NEB, USA) was added to each sample and incubated in a PCR cycler with the following program: 40 min at 37°C, 10 min at 50°C, 7 min 95°C. Afterwards, 40 µl extractionbuffer were added to each sample and the whole 96 well plate was centrifuged for 5 min at 6000 rpm. Finally the supernatant (50-60µl) was transferred to a fresh 96 well plate and stored at -20°C.

3.18. PCR

A standard 25µl PCR reaction had the following composition:

10x Reaction Buffer*	2.5µl
dNTP mix (25mM each)	2.5µl
Primer mix (10mM each)	1µl
gDNA	1µl
DNA-Polymerase**	0.5µl
H ₂ O	17.5µl

*10x ThermoPol buffer (NEB, USA) for Taq-Polymerase (NEB, USA) and Pfu 10x reaction buffer (Promega, Madison USA) for Pfu-Polymerase (Promega, Madison US)

**Taq-Polymerase or Pfu-Polymerase

All samples were set up on ice and carefully mixed before running the reaction in a PCR cycler. All standard reactions, including PCRs for SNP-mapping in the line 904, were performed with the following program for the PCR cycler:

95°C 2 min, 24(95°C 30 sec, 62°C 45 sec, 72°C 45 sec)72°C 5 min, 10°C

For all reactions that used Pfu-Polymerase, the extension time was extended, according to the expected product size. All PCR Primers were generated with the program PrimerSelect (Lasergene, DNASTar, Madison USA), according to the conditions described above.

3.19. Mapping of P-element insertions

The inverse PCR (iPCR) protocol (<http://www.fruitfly.org/>) was used to determine the position of P-element insertions. To map a P-element, the gDNA needs to be prepared from the corresponding fly line and separately digested with the restriction enzymes Sall, MspI, Sau3A I or HinP1 I (all NEB, USA). To prepare the gDNA from P-element containing fly lines, the DNAeasy Tissue Kit (Quiagen, Hilden Germany) was used. In case of recessive lethal P-element insertions, the gDNA was isolated from heterozygous adults. The used restriction enzymes cut within the P-element and additionally in the surrounding genomic sequences with high frequency, so that pieces of gDNA were generated that contain either the 3' or the 5' end of the P-element and a stretch of the corresponding flanking gDNA. These gDNA pieces were circularized through ligations at 4°C over night. Afterwards, PCRs with pairs of primers in inverted orientation were performed that used these ligated gDNA stretches as templates (see <http://www.fruitfly.org/>). The resulting PCR products were sequenced (see below) and analysed for genomic sequences that were used to determine the position of the P-element via the BLAST tool at FLYBASE (<http://flybase.bio.indiana.edu/>).

3.20. Agarose gel-electrophoresis

The standard gels, used to check the success of PCR reactions or restriction digests, had a concentration of 0.8-1 % agarose in 1xTAE-buffer. For the visualisation of DNA on the gel, ethidium bromide was added to a final concentration of 0.5 µg/ml. Gel-electrophoresis was performed in 1x TAE buffer. The ethidium bromide bound to DNA in the gel was visualised under UV-light in a BioRad Transilluminator. All gels were disposed in the according waste bins.

3.21. Sequencing of PCR products

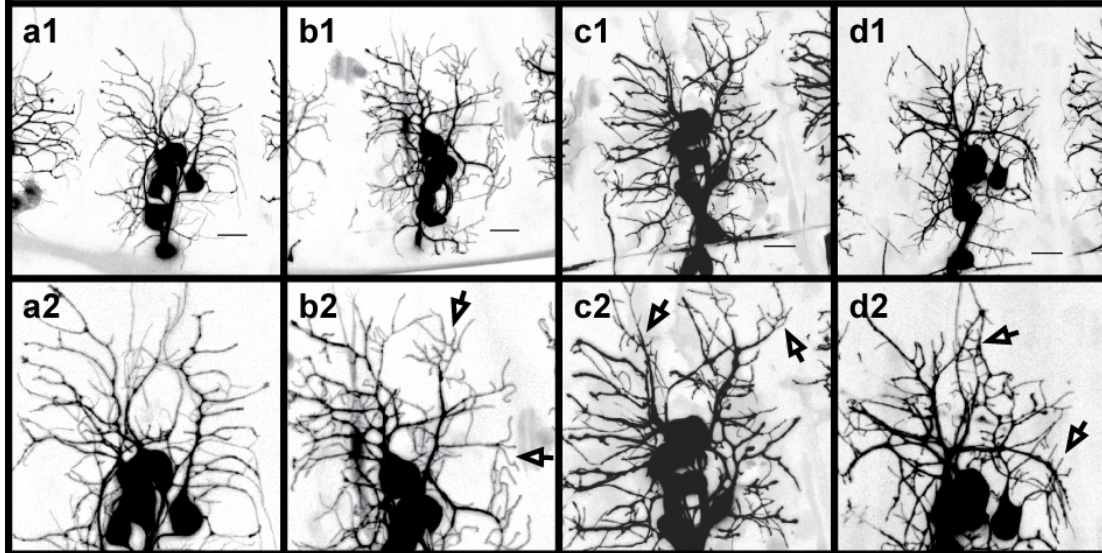
PCR products were sequenced at the DNA-Sequencing facilities of the Max-Planck Institute of Neurobiology or the Max-Planck Institute of Biochemistry. All PCR probes were treated with EXOSAP-IT (USB, Cleveland USA), according to the manufactures protocol, to remove unused primers and nucleotides from each reaction. Prior to sequencing, the sample concentration was adjusted according to the instructions of both sequencing facilities. Sequence data was aligned to the published genome of *Drosophila* via the BLAST tool at FLYBASE (<http://flybase.bio.indiana.edu/>).

4. Results

The md-da neurons of the embryonic PNS of *Drosophila* are a suitable model system to study development and differentiation of dendrites. Several *GAL4/UAS*-lines, including 80G2 (see Material and Methods page 25, (Gao *et al.*, 1999)) are available to visualize these neurons at the body wall of *Drosophila* embryos and larvae. The 80G2 flyline was used in a genetic screen that aimed at the generation of mutants on the second chromosome of *Drosophila* where dorsal cluster md-da neurons display alterations in various aspects of their dendritic morphology at embryonic stage 17 (Gao *et al.*, 1999). Ethyl methanesulfonate (EMS) was used to induce recessive lethal mutations on the second chromosome of the 80G2 fly line in a standard *Drosophila* F3 screen. This EMS-mutagenesis produced 70%-80% lethal lines, which correspond to 1-2 lethal mutations per chromosome (Gao *et al.*, 1999). Subsequently, the recessive lethal lines were screened for an abnormal dendritic phenotype of md-da neurons in the dorsal cluster at embryonic stage 17 (Gao *et al.*, 1999). In these lines, the recessive lethal mutations were mapped to identify the genes that are responsible for the dendritic phenotypes. Several genes that affect different aspects of dendritic development, like outgrowth, routing or branching, were already identified by this screen (Gao *et al.*, 1999).

This PhD project aims at the localization and characterisation of the recessive lethal mutations on the second chromosome of the mutant lines 562, 566, 774, 797, 904 and 969 that were obtained in a similar genetic screen as the one of (Gao *et al.*, 1999). The dorsal cluster md-da neurons in these six mutant lines display overbranching phenotypes at embryonic stage 17. Each of these six mutant lines represents a separate complementation group, and thus affects a distinct gene. Figure 11 shows the dendritic field formed by the md-da neurons of the dorsal cluster in 20-21h AEL old homozygous embryos of the control (Figure 11, a1 and a2) or the mutant line 969, 904 and 797 (Figure 11, b1-d2).

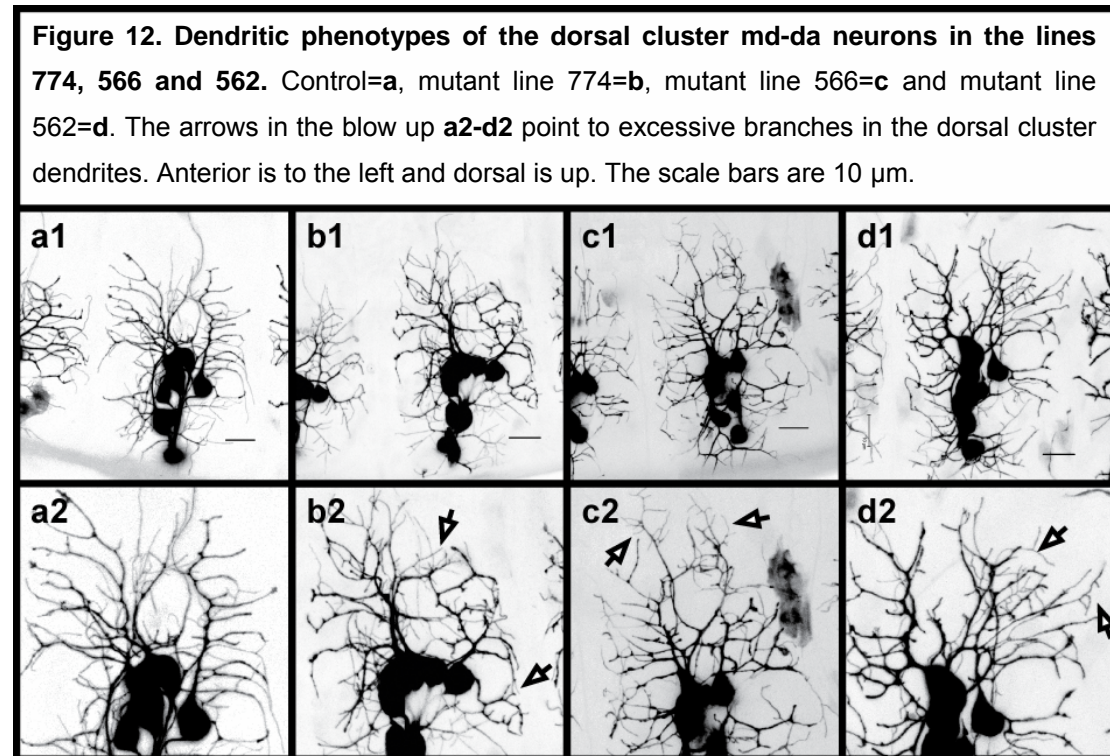
Figure 11. Dendritic phenotypes of the dorsal cluster md-da neurons in the lines 969, 904 and 797. Control=a, mutant line 969=b, mutant line 904=c and mutant line 797=d. The arrows in the blow up a2-d2 point to excessive branches in the dorsal cluster dendrites. Anterior is to the left and dorsal is up. The scale bars are 10 μ m.



The dendritic phenotypes of the dorsal cluster md-da neurons in homozygous embryos of the mutant lines 774, 566 and 562 are shown in Figure 12. To distinguish between homozygous and heterozygous embryos under the microscope, a *GFP*-labelled balancer chromosome was used in all six mutant lines (Casso *et al.*, 2000). In all six mutant lines, an increased number of dendritic termini can be detected in the periphery of the dendritic field that is formed by the six different md-da neurons in the dorsal cluster (arrows in Figure 11 and 12). Other morphological characteristics of md-da neurons are not affected. Based on the background fluorescence, gut and epidermis are normally developed in homozygous embryos (20-21h AEL) of each mutant line.

The Results part is divided into two parts. In the the first section the approaches to map the recessive lethal mutations in the six mutant lines are summarized. First, the deficiency mapping that was performed to roughly localize recessive mutations on the second chromosome in all mutant lines. Secondly, the positioning of the recessive lethal mutation in the mutant line 904 to the gene *sticks and stones (sns)*. The second section shows the initial

attempts to characterise the function of *sns* in dendrite morphogenesis of md-da neurons.



4.1. Deficiency Mapping

Via deficiency mapping it is possible to roughly localize recessive lethal mutations on a given chromosome in the range of several cytological intervals. This method utilizes chromosomal deletions (deficiencies) with known chromosomal breakpoints for complementation analysis of mutants that contain recessive lethal mutations of unknown position. If in complementation analysis, a distinct chromosomal deficiency fails to complement the lethality of a mutant, this deficiency chromosome misses the homologue WT-allele of the recessive lethal mutation on the mutant chromosome. Thus, the recessive lethal mutations in the mutant has to be localized between the two breakpoints of that deficiency.

The Bloomington stock center (<http://flybase.bio.indiana.edu/>) offers a collection of deficiency stocks for the second chromosome (DfKit2) that can be

used to roughly map recessive lethal mutations on this chromosome. All 89 chromosomal deficiencies included in the DfKit2 (stand 10/2003) uncover approximately 85% of the entire second chromosome and their breakpoints are cytologically mapped.

A summary of the deficiency mapping is available in the attached file results_dk2.xls. Each score in results_dk2.xls represents the sum of two independent crosses. Non-complementation of mutant lethality between any deficiency- and mutant chromosome was assumed, when no (or less than 10%) heteroallelic (transheterozygous) flies are seen in the F1. The deficiencies that failed to complement lethality in one of the six mutant lines are shown in Table 1. No recessive lethal mutation could be detected via deficiency mapping in the line 562. Therefore, the recessive lethal mutation in the line 562 is located outside of the area that is uncovered by the DfKit2.

Table 1. Results of the deficiency mapping. Deficiencies that uncover recessive lethal mutations on the second chromosome of the corresponding mutant lines. The stock number and the breakpoint positions of each deficiency are taken from Flybase (http://flybase.bio.indiana.edu/).			
mutant line	deficiency	stock # (BL-)	breakpoints (cytological pos.)
904	<i>Df(2R)H3E1</i>	BL-201	44D1-44F12
969	<i>Df(2R)w45-30n</i>	BL-4966	45A6-45E3
	<i>Df(2R)Np5</i>	BL-3591	44F11-45E1
	<i>Df(2L)XE-3801</i>	BL-4956	27E2-28D1
797	<i>Df(2L)net-PMF</i>	BL-3638	21A1-21B8
	<i>Df(2R)BSC11</i>	BL-6455	50E6-51E4
	<i>Df(2L)BSC30</i>	BL-6999	34A3-34B9
774	<i>Df(2L)TW161</i>	BL-167	38A6-40B1
	<i>Df(2L)JS17</i>	BL-1567	23C1-23E2
	<i>Df(2L)BSC28</i>	BL-6875	23C5-23E2
566	<i>Df(2L)FCK-20</i>	BL-5869	32D1-32F3

One to three recessive lethal mutations were localized on the second chromosome of the lines 904, 969, 774, 797 and 566 by deficiency mapping,

respectively. Thus, the number of induced recessive lethal mutations in these mutant lines corresponds to the number expected from the set up of the EMS-mutagenesis.

In the lines 969 and 774 two of the three identified deficiencies (*Df(2R)w45-30n* and *Df(2R)Np5* for the line 969; *Df(2L)JS17* and *Df(2L)BSC28* for mutant line 774) were largely overlapping as shown in Table 2 and uncover putatively the same recessive lethal mutation.

Table 2. Overlapping deficiencies in mutant lines 969 and 774. In both cases the deficiencies are largely overlapping in size and number of genes. This data was mainly gained with the CytoSearch tool at Flybase (http://flybase.bio.indiana.edu/).				
mutant line	deficiency	breakpoints (cytological position)	size overlap in %	gene overlap in %
969	<i>Df(2R)w45-30n</i>	45A6-45E3	70	66
	<i>Df(2R)Np5</i>	44F11-45E1		
774	<i>Df(2L)JS17</i>	23C1-23E2	64	59
	<i>Df(2L)BSC28</i>	23C5-23E2		

In complementation tests between balanced deficiency and mutant chromosomes, one expects a ration of 2:1 balanced to non-balanced flies in the corresponding F1. In practice, the number of balanced and non-balanced flies diverged occasionally from this theoretically expected value (see attached excel file results_dk2.xls).

Crosses between the deficiency *Df(2R)X58-12* of the stock BL-282 and any mutant line caused a general poor viability of transheterozygous animals in the F1. Consequently, no unambiguous results can be gained for the complementation analysis using this DfKit2 stock. Additionally, crosses between the DfKit2 lines BL-2471, BL-1682, BL-3133 and BL-3813 and different mutant lines were repeatedly unsuccessful (results_dk2 for details).

All deficiencies in the DfKit2 uncover large areas of the second chromosome with varying sizes. The sizes and the number of genes uncovered by the deficiencies listed in Table 1 where calculated using the Flybase CytoSearch

Tool at Flybase (<http://flybase.bio.indiana.edu/>). These results are summarized in Table 3.

Table 3. Size and gene number of the identified deficiencies. All values were acquired with the CytoSearch Tool at Flybase (http://flybase.bio.indiana.edu/). The shown values are estimates, because the breakpoints of all these deficiencies are only cytologically mapped.			
mutant line	deficiency	estimated size in kb	number of genes
904	<i>Df(2R)H3E1</i>	548	90
969	<i>Df(2R)w45-30n</i>	421	60
	<i>Df(2R)Np5</i>	554	88
	<i>Df(2L)XE-3801</i>	733	83
797	<i>Df(2L)net-PMF</i>	316	50
	<i>Df(2R)BSC11</i>	906	125
	<i>Df(2L)BSC30</i>	450	76
774	<i>Df(2L)TW161</i>	?	?
	<i>Df(2L)JS17</i>	423	56
	<i>Df(2L)BSC28</i>	268	33
566	<i>Df(2L)FCK-20</i>	587	50

By deficiency mapping, recessive lethal mutations were roughly localised on the second chromosomes of the mutant lines 566, 774, 797, 904 and 969 (see Table 1). To identify which of the roughly mapped recessive lethal mutations causes the dendritic overbranching phenotype in each line, the dendrites of the dorsal cluster md-da neuron were checked in each of these lines trans-heterozygous over the corresponding deficiencies. In transheterozygous embryos, only one copy of 80G2 is present, which is not enough to visualise dendrites of md-da neurons at embryonic stage 17. Therefore, a copy of *elavGAL4* and *UAS-mCD8GFP* on the X-chromosome was added to enhance the *GFP* expression in md-da neurons at the late embryonic stage 17. A *GFP*-labelled balancer chromosome (Casso *et al.*, 2000) was used to unequivocally identify the genotype of the analysed embryos under the microscope.

In the line 969, a verification of the dendritic phenotype for each of the two roughly mapped recessive lethal mutations was not possible due to the early lethality or severe developmental defects in the corresponding hemizygous embryos. The dendritic phenotype of the dorsal md-da neurons in embryos hemizygous for each of the identified recessive lethal hits in the lines 904, 797, 774 and 566 is illustrated in Figure 13. As control, the dendritic phenotype of dorsal md-da neurons was checked in embryos that are transheterozygous for 80G2 and each deficiency, respectively. An overbranching phenotype could be verified for only two recessive lethal mutations, in the line 904 and 797, which are uncovered by the deficiencies *Df(2R)H3E1* and *Df(2L)BSC30* respectively (see arrows in Figure 13a and 13g).

4.2. Approaches to map the recessive lethal mutation in the line 797

Altogether three recessive lethal mutations were identified on the second chromosome of the line 797 via deficiency mapping (see Table 1). An abnormal dendritic overbranching on md-da neurons could be only detected in embryos that are hemizygous for the mutant chromosome and the deficiency *Df(2L)BSC30* (see Table 1). This deficiency uncovers the cytological interval 2L:34A2-34B9. Only three deficiencies that overlap with this chromosomal segment can be used to refine the position of the recessive lethal mutation therein (see Table 4).

Figure 13. Dendritic phenotypes of dorsal cluster md-da neurons in 19-21h old embryos that are hemizygous for the recessive lethal mutations in the lines 904 (a); 797 (c, e and g); 774 (j and k); 566 (m) chromosomes (see Table 1)...The arrows in a and g point to areas with increased branch number. The pictures b-h show dorsal md-da neurons in the control embryos (80G2 chromosome over the corresponding deficiency chromosome). Anterior is to the left and dorsal is up. The scale bars are always 10 μ m. **Genotypes: a=904/ *Df(2R)H3E1*; b=80G2/ *Df(2R)H3E1*; c=797/ *Df(2R)BSC11*; d=80G2/ *Df(2R)BSC11*; e=797/ *Df(2L)net-PMF*; f=80G2/ *Df(2L)net-PMF*; g=797/ *Df(2L)BSC30*; h=80G2/ *Df(2L)BSC30*; i=774/ *Df(2L)TW161*; j=80G2/ *Df(2L)TW161*; k= 774/*Df(2L)BSC28*; l=80G2/ *Df(2L)BSC28*; m=566/ *Df(2L)FCK-20*; n=80G2/ *Df(2L)FCK-20***

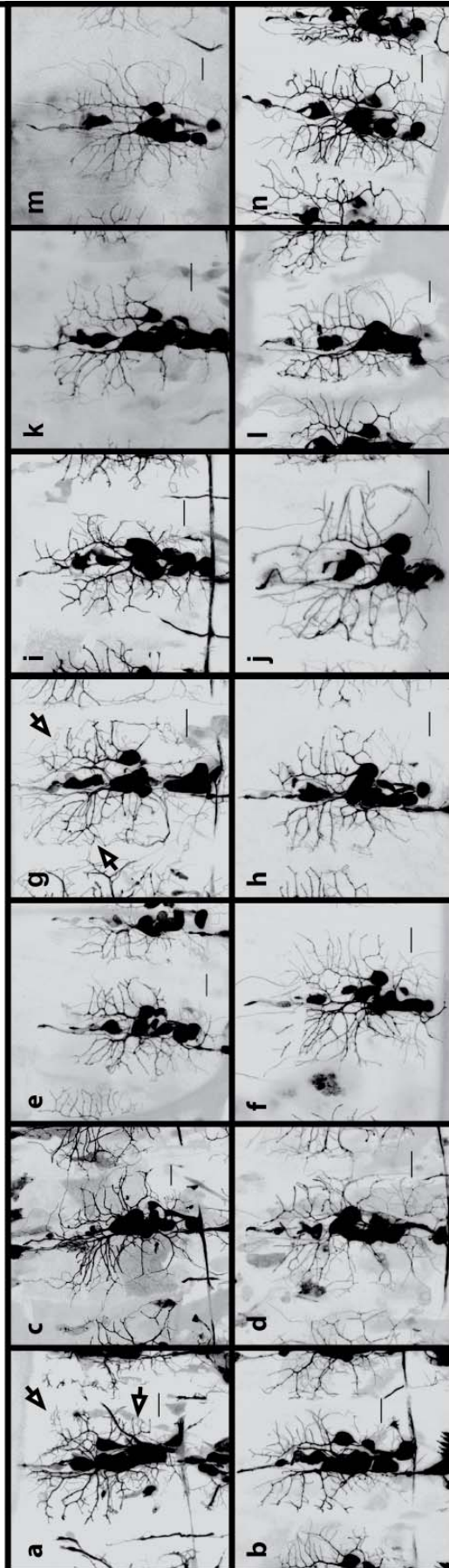
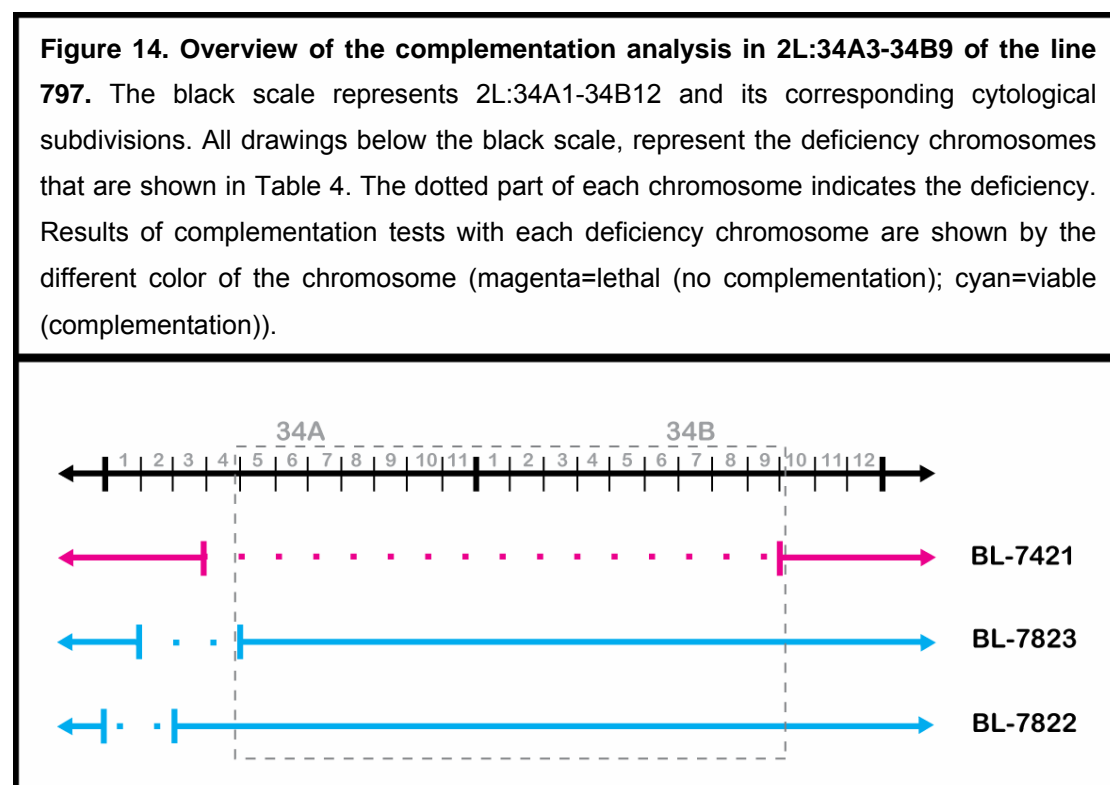


Table 4. Refined deficiency mapping of the recessive lethal hit in the line 797.
Chromosomal deficiencies used to position the recessive lethal mutation in 2L:34A3-34B9 in the line 797. Breakpoint positions are given as cytological bands and sequence region (deleted segment). The values for sequence regions are based on different releases of the *Drosophila* genome and can therefore vary.

deficiency	stock # (BL-)	breakpoints (deleted segments)	size in kb
<i>Df(2L)ED784</i>	7421	34A4-34B6 (2L:13004448..13332060)	328
<i>Df(2L)Exel7055</i>	7823	34A2-34A7 (2L:12912530..13176783)	264
<i>Df(2L)Exel8028</i>	7822	34A1-34A2 (2L:12818930..12822787)	110

The result of the complementation analysis with the deficiencies in Table 4 is shown in Figure 14. Based on these data, the recessive lethal mutation is localised in the chromosomal interval 2L:34A7-34B8, which includes 58 genes.



Since additional chromosomal deficiencies or recessive lethal P-element insertions were not available, the mapping of the recessive lethal mutation in this target area could not be proceeded.

4.3. Mapping of the recessive lethal mutation in the line 904

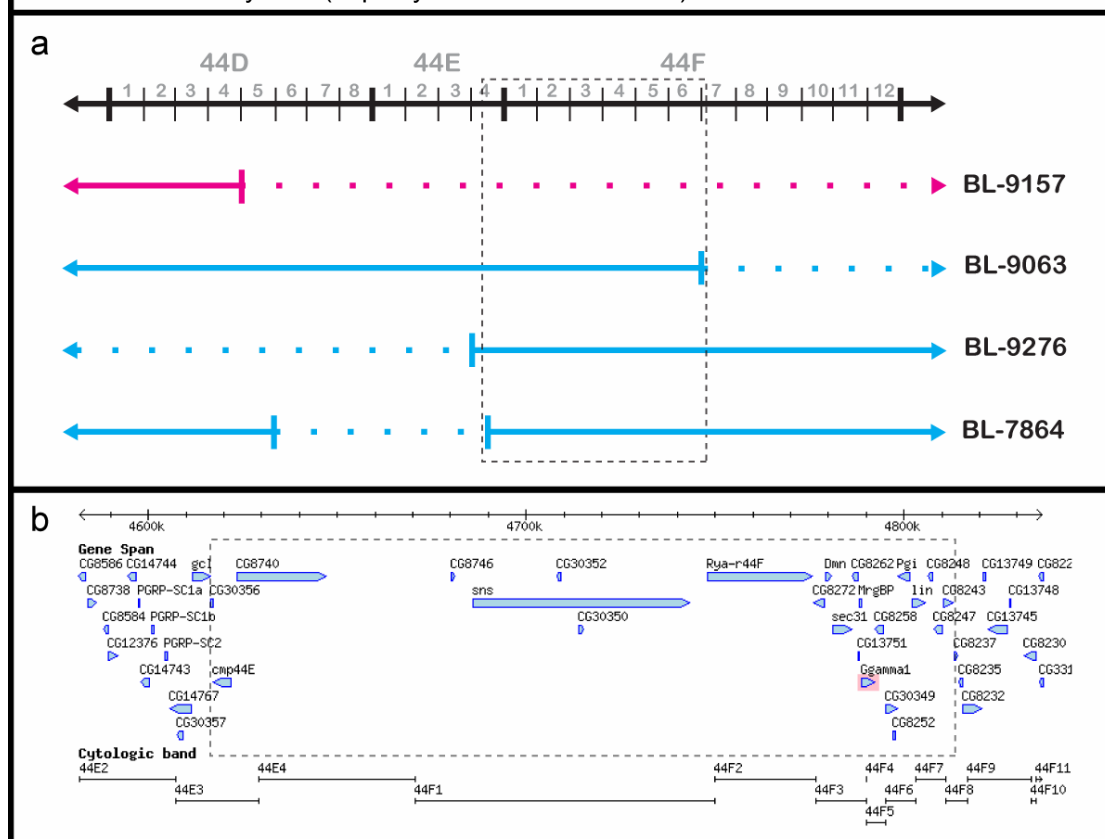
The Deficiency Mapping on the second chromosome of the line 904 identified a recessive lethal mutation within the cytological interval 2R:44D1-44F12. To refine this mapping, complementation analysis with additional overlapping deficiencies was performed. Table 5 introduces the deficiencies that were used for this approach.

Table 5. Refined deficiency mapping of the recessive lethal mutation in the line 904.			
Chromosomal deficiencies used to narrow down the recessive lethal mutation on the second chromosome of the mutant line 904. Breakpoint positions are given as cytological bands and sequence region (deleted segment). The values for sequence regions are based on different releases of the <i>Drosophila</i> genome and can therefore vary.			
deficiency	stock # (BL-)	breakpoints (deleted segments)	size in kb
<i>Df(2R)ED1770</i>	9157	44D5-45B4 (2R:4167442..4719354)	552
<i>Df(2R)ED1791</i>	9063	44F7-45F1 (2R:4434543..5065065)	631
<i>Df(2R)ED1742</i>	9276	44B9-44E3 (2R:3685981..4235942)	550
<i>Df(2R)Exel7098</i>	7864	44D5-44E3	80

Figure 15 summarizes schematically the complementation analysis performed with the deficiencies shown in Table 5. Based on these data, a recessive lethal mutation is localized between 2R:44E3-44F7, which is indicated by a dashed rectangular in Figure 15 panel a. The deficiency *Df(2R)Exel7098* in BL-7864 uncovers the genes *CG30356*, *gcl*, *CG14767* and *CG30357* in 2R:44E3 (<http://flybase.bio.indiana.edu/>).

The area that was defined by complementation analysis with overlapping deficiencies (see Table 5, Figure 15) is approx. 195kbp large and contains 22 genes, which are grouped inside the dashed rectangular in Figure 15 (panel b). An obvious candidate with a known and well described function in the nervous system is not present among these 22 genes. For the genes *cmp44E*, *Rya-r44F*, *Dmn*, *sec31*, *Ggamma1*, *CG8258*, *Pgi* and *lin*, recessive lethal mutations are available at the Bloomington stock center (stand 04/2007).

Figure 15. Overview of the complementation analysis in 2R:44D1-44F12 of line 904. The black scale in Panel a represents 2R:44D1-44F12 and its corresponding cytological subdivisions. All drawings below the black scale represent the deficiency chromosomes that are shown in Table 5. The dotted part of each chromosome indicates the deleted segment. Results of complementation tests with each deficiency chromosome are shown by the different color of the chromosome (magenta=lethal (no complementation); cyan=viable (complementation)). This complementation analysis positioned a recessive lethal mutation to 2R:44E3-44F7 (dashed rectangular). Panel b shows the genes that are located within 2R:44E3-44F7 (dashed rectangular; source: Gbrowse tool at Flybase (<http://flybase.bio.indiana.edu/>)).



All tested mutant alleles for these eight genes were able to complement the lethality of the mutant line 904, which indicates that none of these genes is affected in this mutant line.

Because, it was impossible to map the recessive lethal mutation in the line 904 by the means of overlapping deficiencies or available mutant alleles of candidate genes, two approaches were chosen to finally map the mutation within the 195kbp large cytological intervall 2R:44E3-44F7. First, a local P-element hop was conducted to create an independent allele of the recessive lethal mutation in the mutant line 904, which would be easily localizable via iPCR. Secondly, a modified SNP-mapping was performed, which enables precise mapping of recessive lethal mutations with the highest resolution. Both attempts would provide the possibility to gain an allele of the recessive lethal mutation in the mutant line 904 without 80G2 on the same chromosome (see below).

4.4. Local P-element hop in the line 904

This technique is based on the bias of the *Drosophila* P-element transposons to integrate into the 5'UTR or the first exons of target genes that are located in the proximity of their original place of insertion (Liao *et al.*, 2000; Spradling *et al.*, 1995; Tower *et al.*, 1993). Due to the P-element integration, target genes are frequently disrupted (Spradling *et al.*, 1995). Therefore, the mobilisation of a known P-element is likely to generate random recessive lethal mutations nearby its original insertion site. Hence, recessive lethal insertions obtained through the mobilisation of a P-element that is originally localised within the cytological interval to which the lethal hit in the line 904 was mapped, could be used for complementation analysis with this line.

The aim of this approach was to generate independent P-element allele of the recessive lethal mutation in the line 904, which can be easily mapped via the well established iPCR protocol. Consequently, through identification of the P-element position, the EMS-mutation is mapped as well.

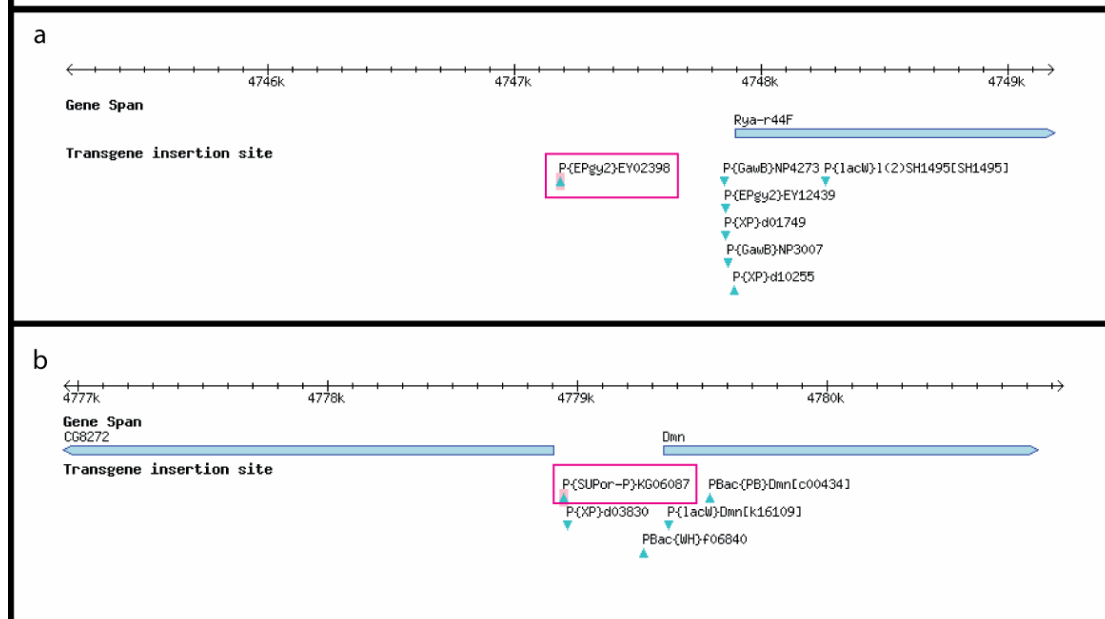
However, a major drawback of a local P-element hop are the unknown background mutations that might originate from imprecise excisions or

multiple insertions on the donor chromosome. The frequency of P-element transposition depends on the used source of P-element transposase, which catalyses the excision and integration of P-elements. Moreover, different type of P-elements transpose with varying efficiency (Bellen *et al.*, 2004).

stock # (BL-)	P-element	position
15867	<i>y w; P{EPgy2}EY02398</i>	2R:44F1 (2R:4371494..4371494)
14021	<i>y w; P{SUPor-P}KG06087</i>	2R:44F3 (2R:4403252..4403252)

Two different P-element lines were selected for the local P-element hop, which are introduced in Table 6. Since *P{EPgy2}* and *P{SUPor-P}* elements transpose with higher efficiency, insertions of these two kinds of P-elements were preferred (Bellen *et al.*, 2004).

Figure 16. Positions of the P-elements *P{EPgy2}EY02398* (a) and *P{SUPor-P}KG06087* (b) in 2R:44F. *P{EPgy2}EY02398* is inserted upstream of the gene *Rya-r44F*. *P{SUPor-P}KG06087* is inserted between the genes *CG8272* and *Dmn*. Source: Gbrowse tool at Flybase (<http://flybase.bio.indiana.edu/>).



Since, the local P-element hop aimed at generating recessive lethal mutations, viable P-element insertions were selected to distinguish between successful and unsuccessful mobilization. Figure 16 shows the positions of the P-element insertions in BL-15687 and BL-14021, respectively. *P{EPgy2}EY02398* is inserted approx. 750bp from the transcription start of the gene *Rya-r44F* and *P{SUPor-P}KG06087* is inserted in a approx. 500bp gap between *CG8272* and *Dmn*. Both P-elements carry *white*⁺ alleles as insertional markers. The lethality of the mutant line 904 was complemented by both P-element lines.

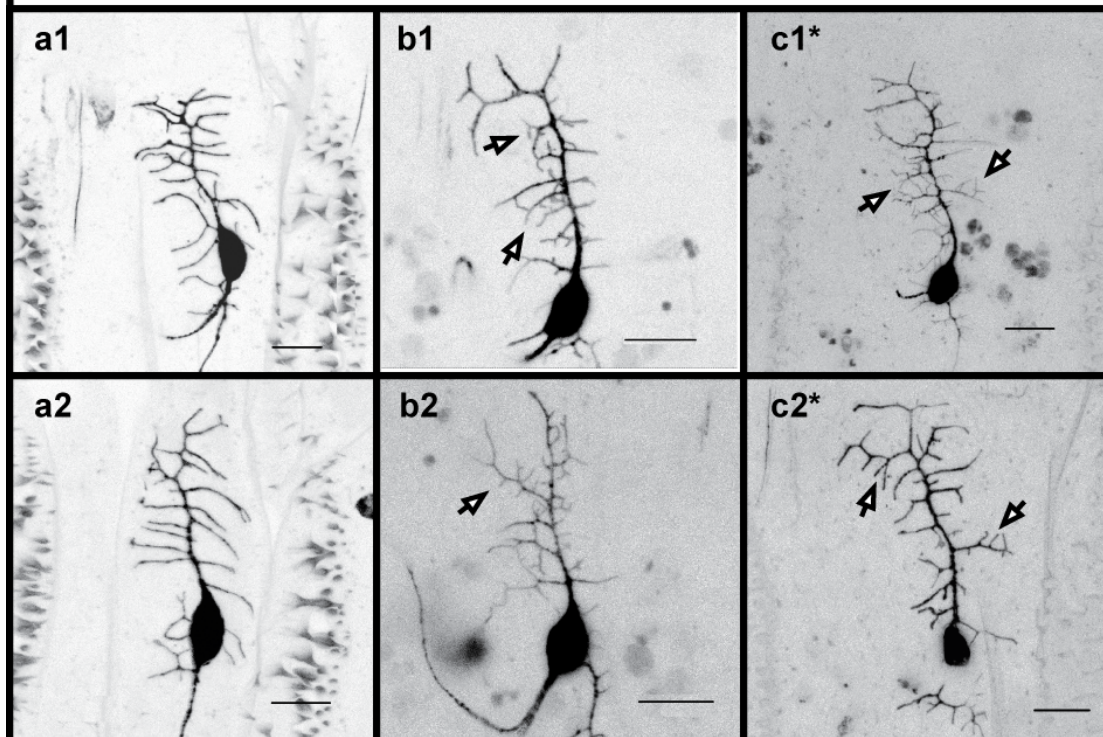
For the description of the local P-element hop see Material and Methods (page 31). Among the progeny of the second cross (Figure 9), males were chosen that show expression from the *P{white*⁺*}* marker. Each *P{white*⁺*}* positive male was crossed to *y w; Pin/Cyo* virgins to establish a balanced stock that was checked for the presence of a recessive lethal mutation on its second chromosome. Finally, all generated recessive lethal mutations, were checked for their ability to complement the lethality of the mutant line 904. The results of the local P-element hop are summarized in Table 7.

P-element	# of hops	# of viable insertions	# of lethal insertion	# of insertions lethal to 904
<i>P{EPgy2}EY02398</i>	54	50	4	1
<i>P{SUPorP}KG06087</i>	67	67	0	0

The mobilization of the *P{SUPorP}KG06087* element did not produce any recessive lethal mutation. Among the *P{EPgy2}EY02398* hops four recessive lethal mutations could be detected.

Figure 17. Phenotype of the class I md-da neuron vpda in the line P66. The vpda neuron in all shown genotypes was visualized in the 2-21 GAL4 UAS-mCD8GFP background. Panel **a1** and **a2** display vpda neurons in control animals. In contrast, vpda neurons in the line P66 (panel **b1**, **b2**) form more high order branches. Panel **c1** and **c2** show vpda neurons in line 904(3)* that display a similar overbranching phenotype than the vpda neurons in the line P66.

* The line 904(3) was generated at a later time point; during SNP-mapping in the line 904 (see section bla). Scale bar are 10 μ m. Dorsal is up and anterior to the left.

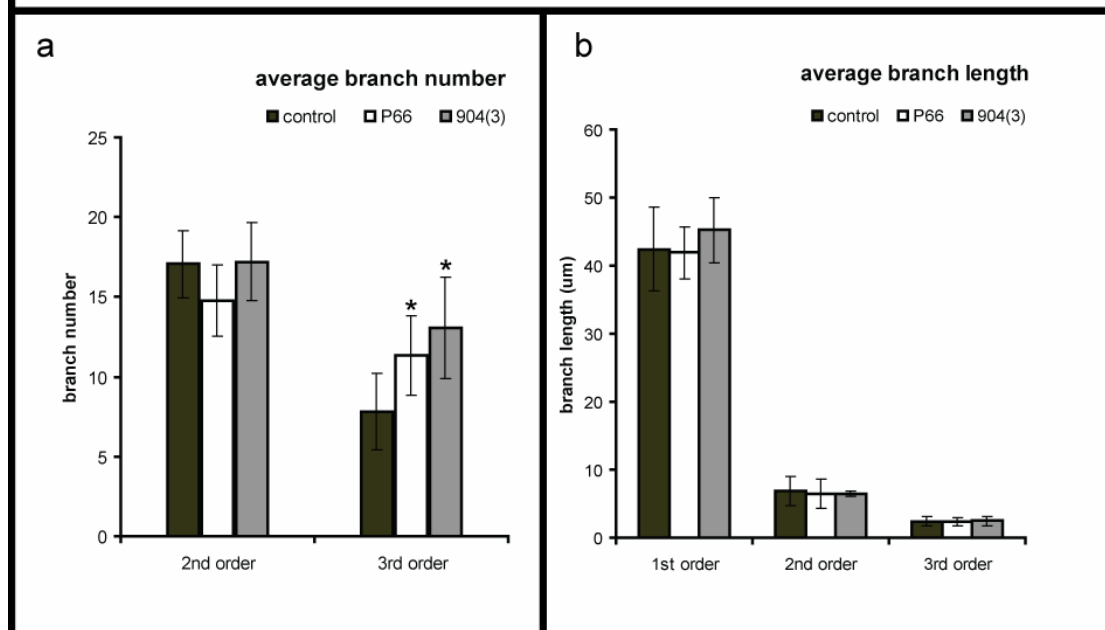


One of these four recessive lethal insertions failed to complement the lethality of the mutant line 904. This insertion was named P66. The dendritic morphology of the class I md-da neuron vpda in this P66 line was analyzed in 2-21 (see Figure 17).

At the same developmental stage, the vpda neurons in the mutant line P66 produced significantly more third order branches compared to the controls (control=7.83 n=27(18), P66=11.34 n=40(23) $p=5,3 \times 10^{-5}$, 904(3)=13.04 n=26(14) $p=3,4 \times 10^{-5}$), whereas the number of second order branches was not altered (Figure 18).

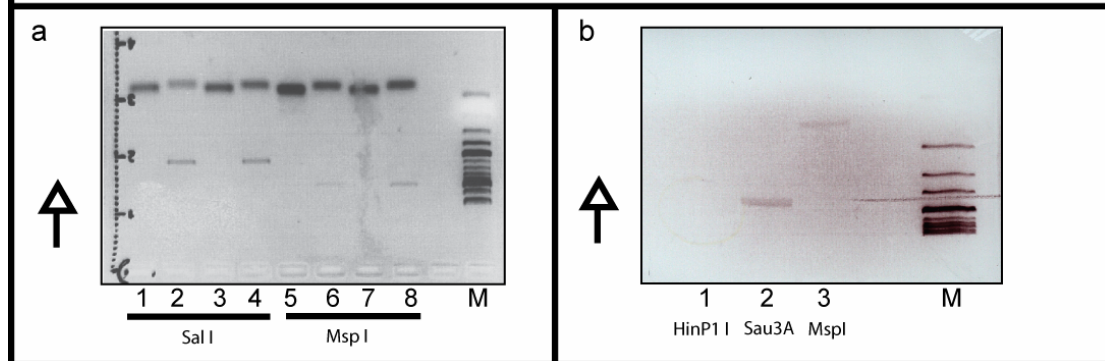
Figure 18. Quantification of the dendritic morphology of the class I md-da neuron vpda in line P66. Panel a shows the average branch number for vpda neurons in the three tested genotypes. In both mutants, vpda neurons have a significantly higher number of third order branches (control=7.83 n=27(18), P66; 2-21=11.34 n=40(23), 904(3); 2-21=13.04 n=26(14)). Branch length is not altered in all three genotypes (see Panel b).

* Mutant line 904(3) contains the recessive lethal mutation of the line 904 but without 80G2. This line is a side product of the SNP-Mapping in the mutant line 904 that was performed at a later time point.



The iPCR (see Material and Methods page 37) from *MspI* and *Sall* digests of total P66 gDNA resulted in the amplification of one band from the 3' end of the P-element insertion (see Figure 19). The sequence of this band aligned to the 5'UTR of the gene *cmp44E* in 2R:44E. Surprisingly, two independent *cmp44E* LOF alleles, *cmp44E[1]* and *cmp44E^{EY09152}* (BL-5454 and BL-19885, respectively), did not complement the lethality of the mutant line P66.

Figure 19. Gel picture of the iPCR in the mutant line P66. Panel **a** shows the gel picture of the iPCR from the 3'end of the P66 insertion. *Sal*I (lanes 1-4) and *Msp*I (5-8) digest of P66 gDNA were used as templates. The 550bp bands in lane 2 and 4 as well as the 1kb bands in lane 6 and 7 represent the same reactions from two independent gDNA preparations/digests. M labels the 100bp DNA ladder. Panel **b** shows the gel picture of the iPCR from the 5'end of the P66 insertion. *Hin*PI (lane 1), *Sau*3A (lane 2) and *Msp*I (lane 3) digests of P66 gDNA were used as a template. M labels the 1kb DNA ladder.



Additionally, no nucleotide exchange could be detected in the genomic sequence (+1kb upstream or downstream) of *cmp44E*. Both *cmp44E* (LOF) alleles complemented the lethality of the mutant line 904, which means that the line 904 does not possess a LOF mutation in *cmp44E* (see page 49). The iPCR from the 5'end of the P-element insertion in P66, revealed a flanking sequence that anneals to a genomic sequence approx. 750bp upstream of the gene *Rya-r44F*. This position represents the place of the original insertion of the *P{EPgy2}EY02398* in BL-15867. Assuming a recessive lethal mutation in the gene *Rya-r44F*, complementation tests were performed between P66, 904 and the two LOF alleles *Rya-r44F*^{K04913} and *Rya-r44F*[16]. Both LOF alleles of *Rya-r44F* complemented the lethality of the line 904 (see page 49) and P66. Therefore, no recessive lethal mutation in the gene *Rya-r44F* is present in the lines 904 and P66.

The P-element position in mutant line 904 could thus not be conclusively determined by iPCR. Thus, *in-situ* hybridization of *P{EP}*-elements was performed, to localize the recessive lethal P-element insertion on the second chromosome of the mutant line P66 (Anna Cyrklaff; EMBL-Heidelberg Germany). In the stock BL-15867 that provided the donor P-element, two

P{EP}-insertion could be localized in 2L:30A1-A5 and 2R:44F1-3. Hence, beside the one in 2R:44F1-3, BL-15867 contains another P-element on the left arm of the second chromosome, which was not declared in the genotype of that stock. In contrast, one *P{EP}*-element could be localised in 2R:44F1-3 on the second chromosome of the line P66. Apparently, the P-element insertion in 2R:44F1-3 in BL-15867 was not moved or moved within 44F1-3 during the P-element local hop. The second, unknown insertion in 2L:30A1-5 became probably excised without subsequent reintegration.

To summarize, this approach generated a recessive lethal P-element insertion that failed to complement the lethality in the mutant line 904. Additionally, *vpda* neurons in this mutant produced an overbranching phenotype similar to the one observed on the *vpda* neurons in the mutant line 904. Unfortunately, this P-element insertion could not be unambiguously localized via the iPCR technique. This is most likely due to a second unknown P-element insertion in the donor stock. Flanking sequences from both ends of a P-element in P66 do not align to the same position on the second chromosome. The two associated genes, *cmp44E* and *Rya-r44F*, are not mutated in the lines P66 or 904.

4.5. SNP-Mapping in the line 904

Sequence polymorphisms such as single-nucleotide polymorphisms (SNP) or nucleotide insertions and deletions are used as genetic markers for mapping mutations via meiotic recombination in *S.cerevisiae* (Winzeler *et al.*, 1998), *A.thaliana* (Cho *et al.*, 1999), *C.elegans* (Koch *et al.*, 2000) and *Drosophila* (Hoskins *et al.*, 2001). As genetic markers, sequence polymorphisms link directly the genetic and physical map of a chromosome. They are highly abundant and genetically inert in most cases, which allows precise mapping of mutations with highest resolution. Dense maps of sequence polymorphisms are already generated for the second and third chromosomes of common *Drosophila* laboratory strains (Berger *et al.*, 2001; Hoskins *et al.*, 2001; Martin *et al.*, 2001; Nairz *et al.*, 2002). Also, strategies to use these maps for positioning of mutations already exist (Berger *et al.*, 2001; Hoskins *et al.*,

2001; Martin *et al.*, 2001; Nairz *et al.*, 2002). Berger *et al.* 2001 created the so far most comprehensive maps of sequence polymorphisms for the second and third chromosomes of unrelated *Drosophila FRT* and *EP* strains. Based on this work, the average frequency of sequence polymorphisms between any pair of strains is at least one polymorphism per kb (Berger *et al.*, 2001). This data supported the idea that it is feasible to find enough SNPs in 2R:44E3-44F7 between reference and mutant chromosomes, to perform SNP-mapping of the recessive lethal mutation in the line 904 in a reasonable amount of time.

The SNP-mapping approach in line 904 was based on a recombination between the mutant and reference chromosomes, which carry traceable $P\{yellow^+ white^+\}$ transgenes either to the left or right of 2R:44E3-44F7. Among all generated recombinants, only those that lost both lethality and the $P\{yellow^+ white^+\}$ marker transgenes were chosen. This procedure ensures that for the subsequent SNP-analysis only those recombinant chromosomes are used, where the chromosomal exchange has occurred between the unknown position of the recessive lethal mutation and the respective $P\{yellow^+ white^+\}$ marker transgenes to the left or right of it.

To find appropriate reference chromosomes, nine Bloomington stocks that carry $P\{yellow^+ white^+\}$ transgenes on the left or right side of 2R:44E3-44F7 were selected, which could potentially serve as recombination marker. All nine selected $P\{yellow^+ white^+\}$ stocks are introduced in Table 8. Five published SNP-markers in 2R:44 that distinguish between *FRT* and *EP* chromosomes were used to assess the presence and frequency of SNPs between mutant and $P\{yellow^+ white^+\}$ chromosomes (Berger *et al.*, 2001). The attached Excel file snp mapping.xls shows all the features of the chosen SNP-marker and the results of the performed analysis.

Based on these data, BL-19704 and BL-15750 were selected as a source for a reference chromosome for SNP-mapping of the recessive lethal mutation from the left side and right side of 2R:44E3-44F7, respectively. The outline of all mapping crosses is given in Material & Methods page 33 (Figure 10).

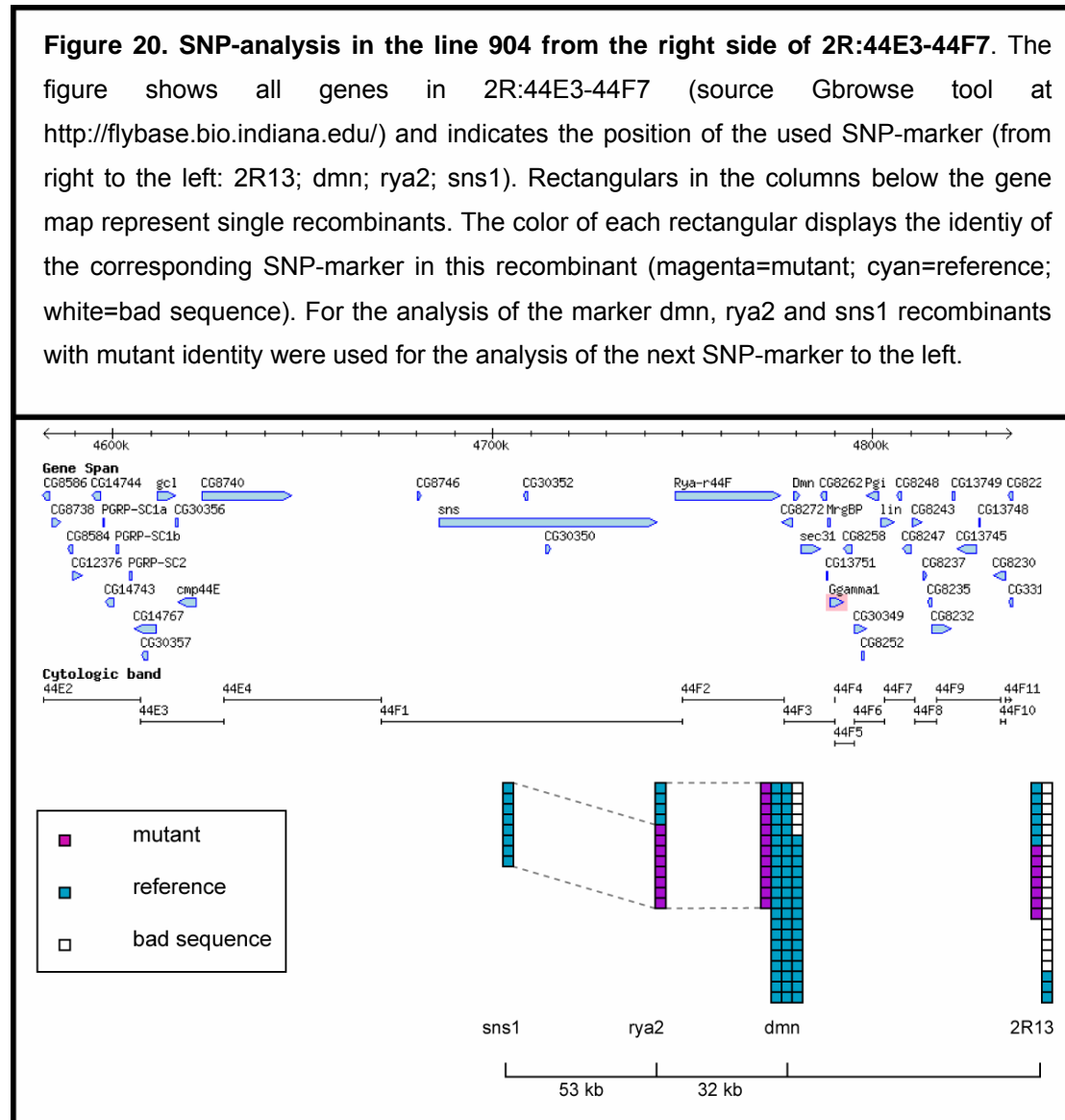
Table 8. Potential reference chromosomes for SNP-mapping in 2R:44E3-44F7 of mutant line 904.		
stock # (BL-)	P-element	P-element position (associated gene)
13212	$P\{y[+mDint2] w[BR.E.BR]=SUPor-P\}$	44B3 (<i>Pabp2</i>)
21364	$P\{w[+mC] y[+mDint2]=EPgy2\}$	44B7 (<i>CG8707, CG30373</i>)
14354	$P\{y[+mDint2] w[BR.E.BR]=SUPor-P\}$	44C2 (<i>pnut</i>)
14992	$P\{y[+mDint2] w[BR.E.BR]=SUPor-P\}$	44C4 (intergenic region)
17553	$P\{w[+mC] y[+mDint2]=EPgy2\}$	44D1 (<i>Cyp4e2</i>)
19704	$P\{w[+mC] y[+mDint2]=EPgy2\}$	44D4 (<i>rgr</i>)
15750	$P\{w[+mC] y[+mDint2]=EPgy2\}$	45A2 (<i>CG13741</i>)
13166	$P\{y[+mDint2] w[BR.E.BR]=SUPor-P\}$	45A8 (<i>Phax</i>)
15992	$P\{w[+mC] y[+mDint2]=EPgy2\}$	45A9 (<i>CG11784</i>)

For identification of sequence polymorphisms between mutant and reference chromosomes, 20 1kbp stretches within 2R:44E3-44F7 were screened for sequence polymorphisms. Nine of these PCR products contained useful sequence alteration. These results are summarized in the attached excel file *snp mapping.xls*.

Altogether 720 bottles with approximately 200 flies per bottle were screened for recombinants between the mutant and reference chromosomes. Out of these flies, 58 and 72 recombinants, respectively to the left and right side of the recessive lethal mutation, were isolated for SNP-analysis. This finding corresponds to a frequency of recombination between the recessive lethal mutation and the respective marker P-element transgenes of 0.08% for the left side and 0.1% for the right side.

Figure 20 illustrates the results of SNP-analysis from the right side of the recessive lethal mutation in 2R:44E3-44F7. The presence of recombinants with mutant identity for a given marker indicates that the recessive lethal mutation is localized to the left of this marker. Among the first 32 recombinants, seven were found with mutant and nine with reference identity for the right most marker 2R13. Next, all 72 recombinants were gradually tested for the *dmn* marker, which is located about 66kbp to the left of 2R13.

Only 12 of them were still mutant for that position. Hence, the 66kbp between 2R13 and *dmn* do not contain the recessive lethal mutation.



The 12 remaining recombinants with mutant identity for the marker *dmn*, were tested for the marker *rya2* in between the genes *sticks and stones* (*sns*) and *Ryanodine receptor 44F* (*Rya-r44F*). Since eight of these 12 recombinants were mutant for the marker *rya2*, the recessive lethal mutation did not affect *Rya-r44F* or *CG8272*. All eight remaining recombinants had reference identity for the marker *sns1* to the left of *Rya-r44F*. Consequently, the recessive lethal

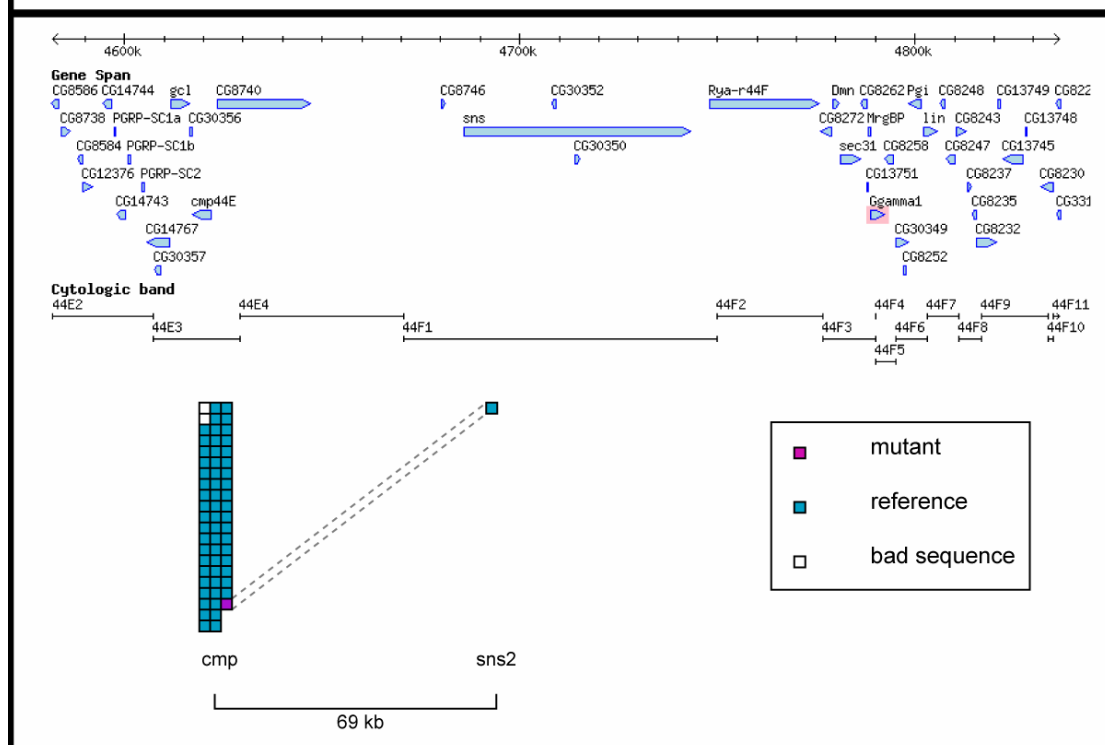
mutation in the mutant line 904 must be inserted to the left (upstream) of the marker *rya2*.

The results of the SNP-analysis from the left side of the recessive lethal mutation in 2R:44E3-44F7 are shown in Figure 21. In this case, the presence of recombinants with mutant identity at a given marker position indicates that the recessive lethal mutation is positioned to the right of this marker. Gradually, all 58 recombinants, generated from the left side of the recessive lethal mutation, were tested to finally identify one recombinant with mutant identity for the most left marker *cmp* in 2R:44E3-44F7. Hence, the gene *cmp44E* does not contain the recessive lethal mutation in the line 904, which confirms the results of the complementation test with known recessive lethal alleles of this gene (see page 49). The remaining recombinant, which was mutant for the marker *cmp*, had a reference identity for the marker *sns2*.

Concluding, the SNP-mapping approach in 2R:44E3-44F7 of the line 904 positioned the recessive lethal mutation among the genes *CG8740*, *CG8746*, *sns*, *CG30352* and *CG30350*, which confirms the complementation data that was gained with chromosomal deficiencies or known recessive lethal alleles of candidate genes so far. Finally, this approach could show that it is feasible to perform SNP-mapping with reasonable resolution within a small chromosomal area, provided that appropriate reference chromosomes are available.

By recombination between the mutant chromosome and the reference chromosome with the *P{yellow⁺ white⁺}* transgene to the right of the recessive lethal mutation, special recombinants were created that still carry the lethality but lost 80G2. In these recombinants, the whole left arm of the second chromosome and parts in proximity to the right side of the centromere were exchanged from the mutagenized second chromosome of the mutant line 904. Thus, these recombinant chromosomes were partially cleaned and could be combined with different *GAL4/UAS* lines to visualize md-da neurons. Altogether, two of these recombinants, 904(2) and 904(3), were selected for the future experiments. The presence of the recessive lethal mutation in these two recombinants was verified by complementation analysis with the mutant line 904 and *Df(2R)H3E1*.

Figure 21. SNP-analysis in the line 904 from the left side of 2R:44E3-44F7. The figure shows all genes in 2R:44E3-44F7 (source Gbrowse tool at <http://flybase.bio.indiana.edu/>) and indicates the position of the used SNP-marker (from left to the right: *cmp* and *sns2*). Rectangulars in the columns below the gene map represent single recombinants. The color of each rectangular displays the identity of the corresponding SNP-marker in this recombinant (magenta=mutant; cyan=reference; white=bad sequence). For the analysis of the two marker *cmp* and *sns2*, recombinants with mutant identity were used for the analysis of the next SNP-marker to the right.

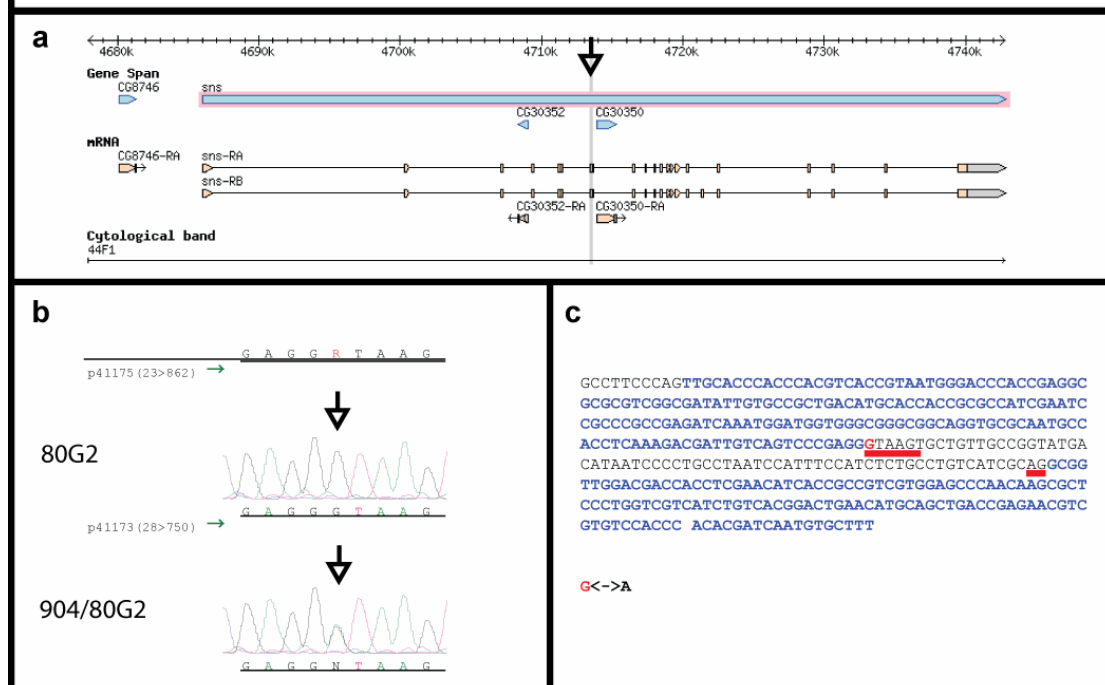


4.6. Sequencing of the remaining candidate genes

To detect a nucleotide exchange the complete coding sequence of the genes *CG8746*, *CG30352* and *CG30350* was sequenced. Due to dimensions of the gene *sns*, only its 5'UTR, all exons, 3'UTR as well as 1kb up and downstream of the open reading were sequenced. While no modification was detected in the other genes, in *sns* a reproducible nucleotide exchange from guanine to adenine was found at the position 2R:4713580. This transition affects the splice

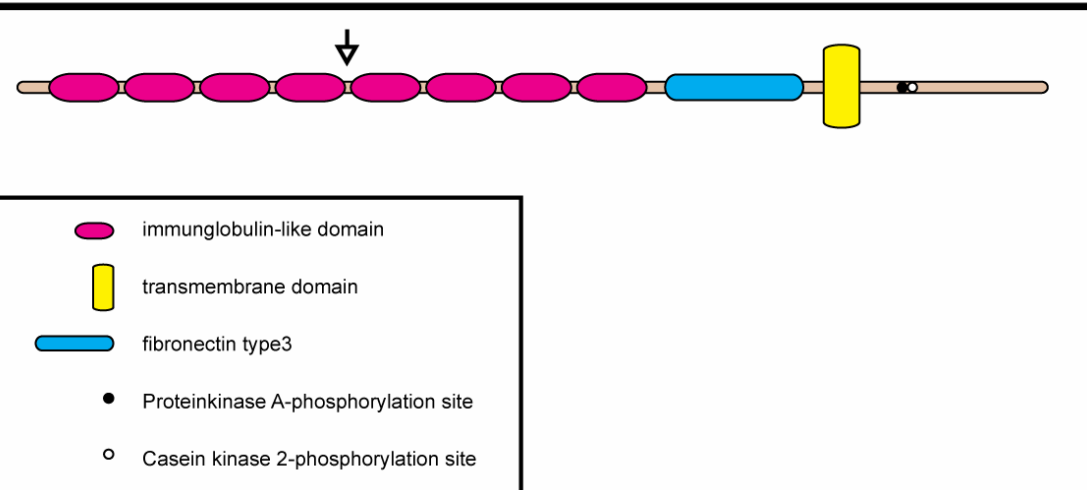
donor consensus sequence between the 7th and the 8th exons of *sns* (see Figure 22).

Figure 22. Sequence analysis of the genes *sns*. Panel **a** shows the predicted genes and the corresponding mRNAs between 2R:4677910..4742797. The black arrow in Panel **a** marks the position of the detected mutation in *sns*. Panel **b** and **c** show the nucleotide exchange that was found at position 2R:4713580. Original sequence data are displayed in Panel **b**. This mutation affects the consensus sequence of the splice donor site between the 7th and 8th exons of *sns* as depicted in Panel **c** (exon sequence=blue letters; intron sequence=black letters; consensus sequences of splice sites are underlined in red). The red letter in Panel **c** is mutated in the line 904.



As a consequence of a splice failure at this site, all subsequent open reading frames (ORFs) are expected to be by STOP codons within a few hundred bp. The *sns* protein in the line 904 would be disrupted between the fourth and fifth immunoglobulin-like domains in the extracellular part of the molecule (see arrow in Figure 23).

Figure 23. Schematic overview of the structural domains of the Sns protein (based on (Artero *et al.*, 2001; Bour *et al.*, 2000)). The entire protein consists of 1549 amino acids. Eight immunoglobulin-like domains and one type3 fibronectin domain were detected in the extracellular part of *sns*. The intracellular tail contains no conserved domains but a PKA and a CK2 phosphorylation site. The arrow points to the site where the Sns protein should be disrupted in the line 904.

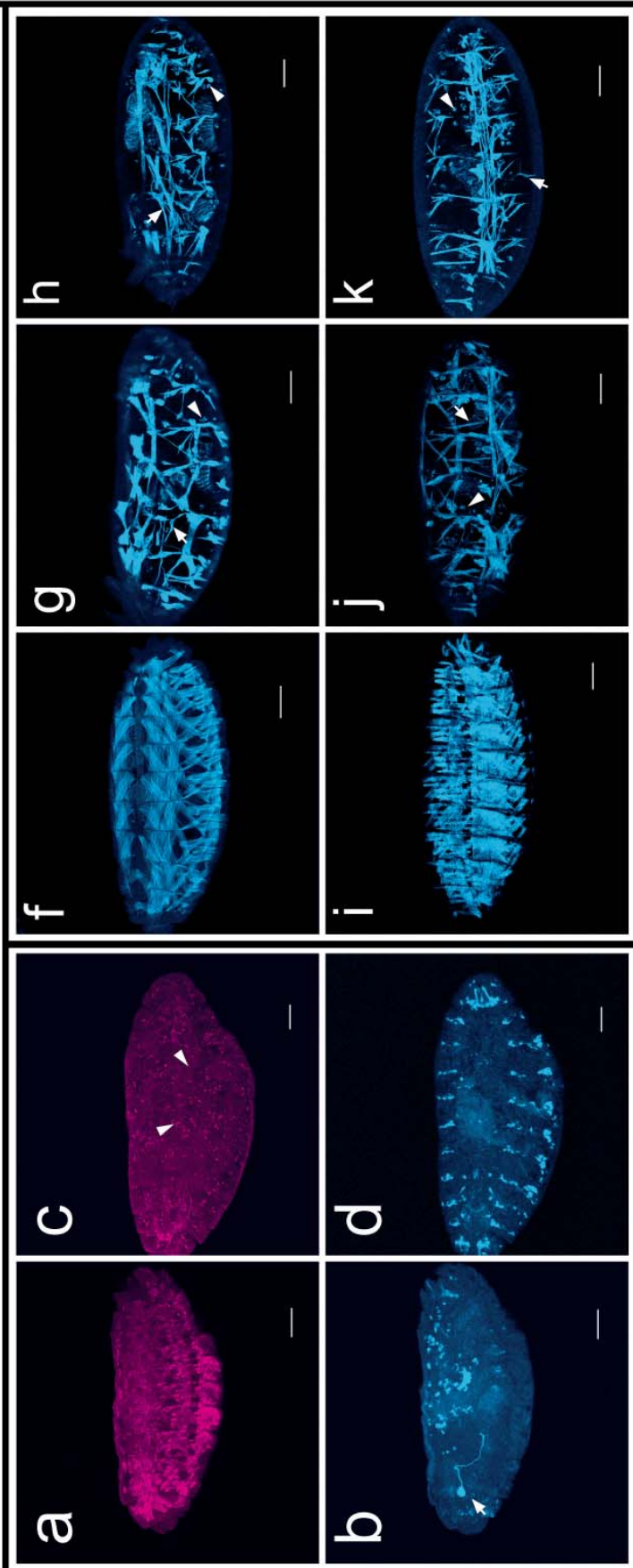


4.7. Verification of the mapping result

To confirm that the line 904 contains a recessive lethal mutation in the gene *sns*, complementation analysis was performed with two independent recessive lethal null alleles of *sns*, *sns*^{S660} and *sns*^{zf1.4} (kindly provided by Prof S. Abmayr). Both, *sns*^{S660} and *sns*^{zf1.4}, failed to complement the lethality of the line 904, which proves that the line 904 harbours a new recessive lethal allele of the gene *sns*.

It is shown that *sns* null mutants fail to form somatic body wall musculature during embryogenesis, which finally causes lethality of these animals (Bour *et al.*, 2000). Therefore, the status of the body wall musculature in the mutant lines 904 and *sns*^{S660} was examined through visualization of all muscles via immunostaining or through a *MHC::tauGFP* transgene (kindly provided by Prof Eric Olson; ((Chen and Olson, 2001), Figure 24).

Figure 24. Examination of the somatic musculature in line 904. Panels **a-c** show immunostaining with a muscle-specific antiserum (DHSB) on heterozygous (**a** and **b**) or homozygous (**c** and **d**) stage 16 embryos. The CKG balancer stains the Bolwig organ of heterozygous embryos (arrow in **b**), whereas 80G2 on the mutant chromosome is only visible in homozygous embryos (**d**). In heterozygous embryos, the body wall musculature is visible. (**a**). This staining is completely missing in homozygous embryos (**c**). Only a dotted staining, which might represent unfused myoblasts (arrowheads in **c**) is detectable. The panels **f-g** and **h**= dorsolateral view; **l,j** and **k**= ventrolateral view), visualised by a *MHC::tauGFP* transgene. Control embryos with normal musculature are shown in panels **f** and **i**. In both *sns* mutants (*sns*^{S660}=**g** and **j**; 904(3)=**h** and **k**) a body wall musculature is not formed. Instead, mononucleated mini muscles can be seen (arrows in **g-k**). Also, a few unfused myoblasts can be seen in both mutants (arrowheads in **g-k**). Scale bars are 50µm. Anterior is to the left and dorsal up.



As shown in Figure 24 c and g-k, the formation of the body wall musculature in the line 904 and *sns*^{S660} embryos is severely impaired. The Hybridoma antisera 6D4 staining resulted in a punctuated staining in the homozygous 904 mutants, which most likely marks unfused myoblasts, and fails to detect any muscle fiber as seen in the heterozygous siblings.

A qualitatively better view of the muscle phenotype was provided by the *MHC::tauGFP* transgene (see Figure 24 f-k). Similar to the immunostaining, no multinucleated muscle fiber could be detected in both mutant line 904 and *sns*^{S660}. Instead, small and apparently mononucleated muscle fibers are detectable that are reminiscent to mini muscles as described in different mutants with comparable phenotypes of the body wall musculature, like *rolling pebbles* or *blown fuse* ((Chen and Olson, 2001; Schroter *et al.*, 2004); arrows in Figure 24 g-k). Unfused myoblasts seem to be visualized by the *MHC::tauGFP* transgene as well as indicated by dotted GFP stainings in both mutant line 904 and *sns*^{S660} (arrowheads in Figure 24 g-k). Muscle attachment sites or the dorsal vessel seem not to be affected in both mutants.

To summarize, in both the lines 904 and *sns*^{S660}, multinucleated muscle fibers are almost completely missing as it is already described for *sns* null mutants (Bour *et al.*, 2000). No difference in the severity of the musculature phenotype is visible between the line 904 and *sns*^{S660}.

Hence, based on the complementation data and the mutant phenotype of the body wall musculature, the recessive lethal mutation in the mutant line 904 represents a LOF allele of *sns*, which is called *sns*⁹⁰⁴ from now on.

4.8. Expression of *sns* in md-da neurons of the line 904 rescues the dendritic phenotype

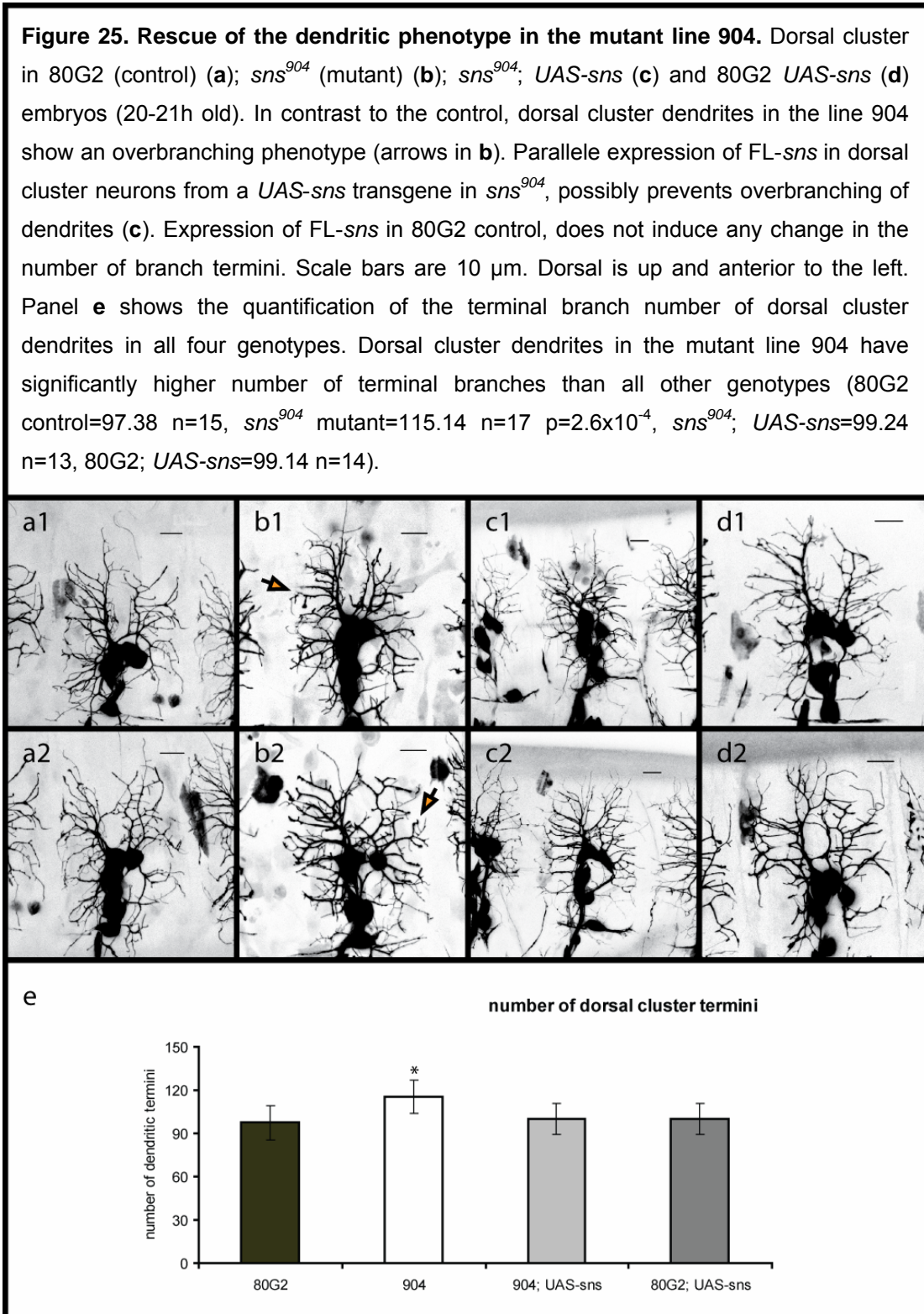
Is the mutation of *sns* responsible for the dendritic phenotype in md-da neurons of mutant line *sns*⁹⁰⁴ at late embryonic stage 17 (20-21 AEL)? To answer this question, full-length *sns* (FL-*sns*) was expressed under the control of the *109(2)80GAL4 driver* from a *UAS*-transgene (kindly provided by Prof Susan Abmayr) in parallel to *GFP* in the line *sns*⁹⁰⁴. Under the control of the mesoderm-specific *GAL4*-driver *24B*, this *UAS-sns* transgene is able to

rescue the loss of the body wall musculature in the *sns* mutants (Bour *et al.*, 2000). To assess the dendritic phenotypes in these genotypes, the number of dendritic termini in the dorsal cluster was ascertained for each tested genotype.

As shown in Figure 25, the *UAS-sns* transgene is able to convert the overbranching phenotype of dorsal cluster dendrites in the line 904 back to the control level (80G2 (control)=97.38 n=15, *sns*⁹⁰⁴ (mutant)=115.14 n=17 p=2,6x10⁻⁴, *sns*⁹⁰⁴ *UAS-sns* (rescue)=99.24 n=13, 80G2 *UAS-sns* (GOF)=99.14 n=14). Thus, this experiment indicates, that a mutation of *sns* in the line 904 is responsible for the abnormal dendritic phenotype. Furthermore, it supports that *sns* controls branch formation of dorsal cluster md-da neurons cell-autonomously. No change in the number of dendritic termini could be observed in the flies of the genotype 80G2; *UAS-sns*, which would represent a gain-of-function (GOF) of *sns* in the dorsal cluster neurons.

4.9. Expression analysis of *sns* in *Drosophila* embryos and larvae

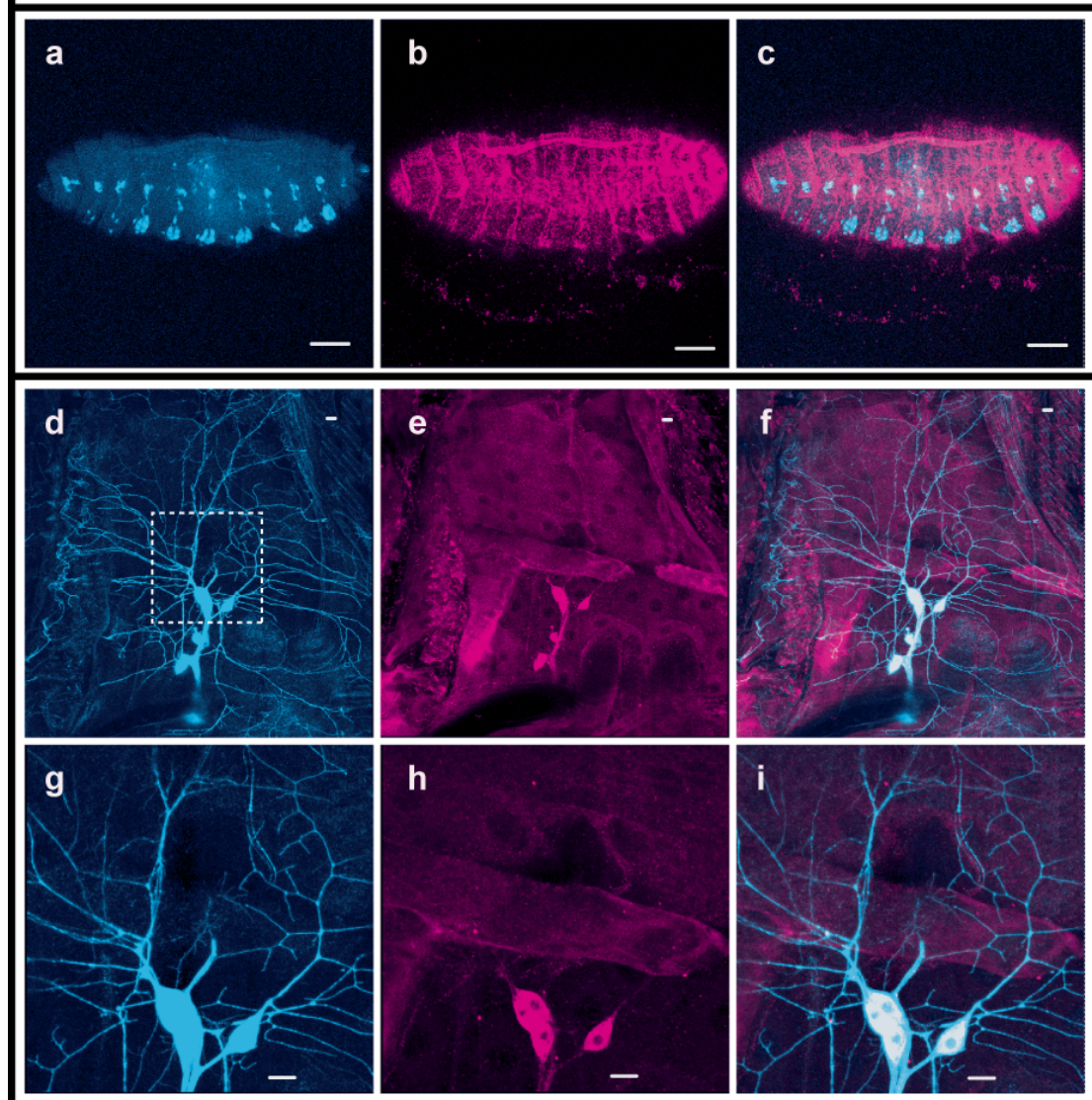
A prerequisite for a putative cell-autonomous function of Sns in dendrite morphogenesis of md-da neurons is its presence in these cells. During embryogenesis, the expression of *sns* starts in the visceral and somatic mesoderm prior onset of myoblast fusion at embryonic stage 11, reaches its peak at stage 14 and declines until stage 17 (Bour *et al.*, 2000). In the somatic mesoderm, Sns is exclusively expressed in the fusion-competent-myoblasts (FCMs; (Bour *et al.*, 2000)). In addition, a weak expression of *sns* is also detectable in the muscle attachment sites at early stage 17 (Bour *et al.*, 2000). An expression in the PNS up to early embryonic stage 17 could not be detected (Bour *et al.*, 2000), but at the final embryonic stages and all larval stages, when the dendritic morphology of md-da neurons is usually studied, the expression pattern of *sns* is not known.



Therefore, a staining with a monoclonal antibody against the *sns* protein (kindly provided by Prof Karl-Friedrich Fischbach) was performed in the embryos (15-16h AEL) and third instar larvae fillet. As shown in Figure 26, *sns*

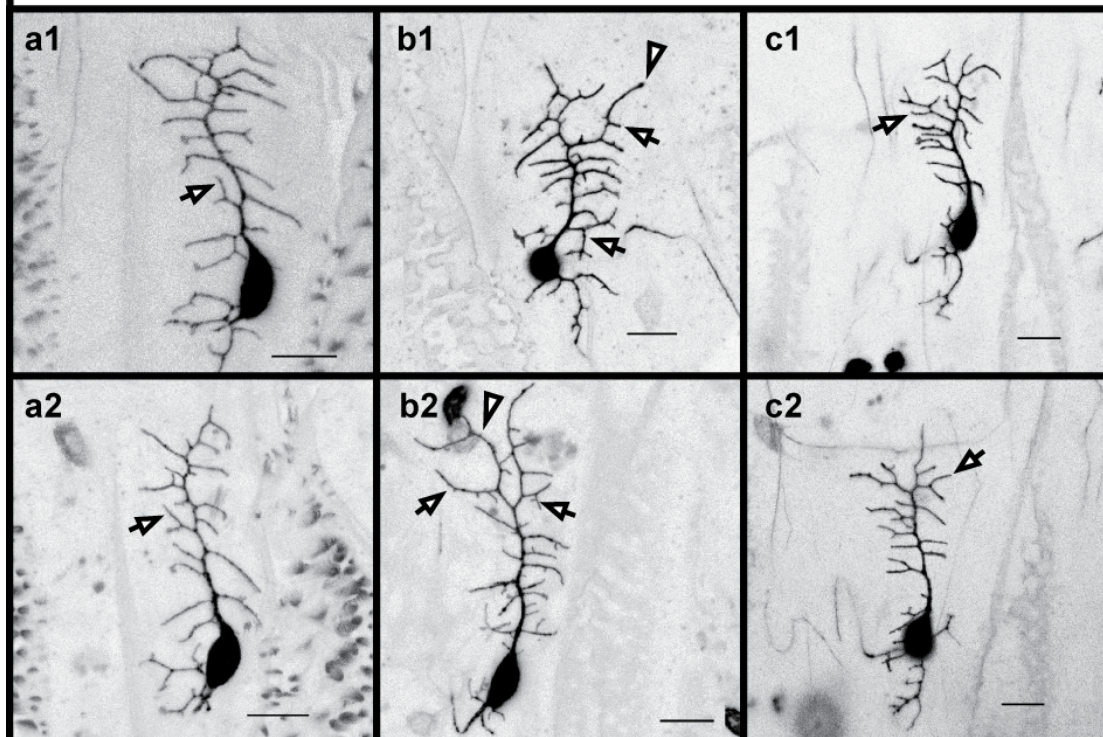
expression in the 15-16h AEL old embryos is detected at the muscle attachment sites, but not in the md-da neurons of the PNS (Figure 26 a-c), which agrees with previous findings (Bour *et al.*, 2000).

Figure 26. Anti-sns staining in the 15-16h old embryos (a-c) and third instar larvae filet (d-f). In embryos, anti-sns stains muscle attachment sites but not md-da neurons (a=109(2)80 GAL4 UAS-GFP; b=anti-Sns; c=overlay of a and b). In the third instar larvae, sns expression was detected in the epidermis, the body wall musculature and in soma, axons and proximal dendrites of all md-da neurons (d=109(2)80 GAL4; UAS-mCD8GFP; e=anti-sns; f=overlay). Anterior is to the left and dorsal is up. The scale bars are 50 μ m.



In the third instar larvae, *sns* is expressed in the epidermal cells, the body wall musculature and all md-da neurons of the PNS (Figure 26 d-i). The anti-*sns* staining appeared in the soma, axons and most proximal dendrites of md-da neurons. *Sns* could not be detected in more distal dendrites. Thus, *sns* is expressed in md-da neurons at the late larval stages.

Figure 27. Dendritic morphology of the class I md-da neuron vpda in *sns* mutant embryos (20-21h old). 2-21 was used to visualize the vpda neurons. Vpda neurons in embryos of the mutant lines *sns*⁹⁰⁴⁽³⁾ (b) and *sns*^{S660} (c) produce more third order branches than controls (a). The arrows in b and c mark excessive branches. Additionally, a long second order dendrite can be seen frequently in *sns* mutants (arrowheads in b and c), which did not significantly differ in length from the longest second order dendrite in the controls. Scale bars are 10 μ m. Dorsal is up and anterior to the left.

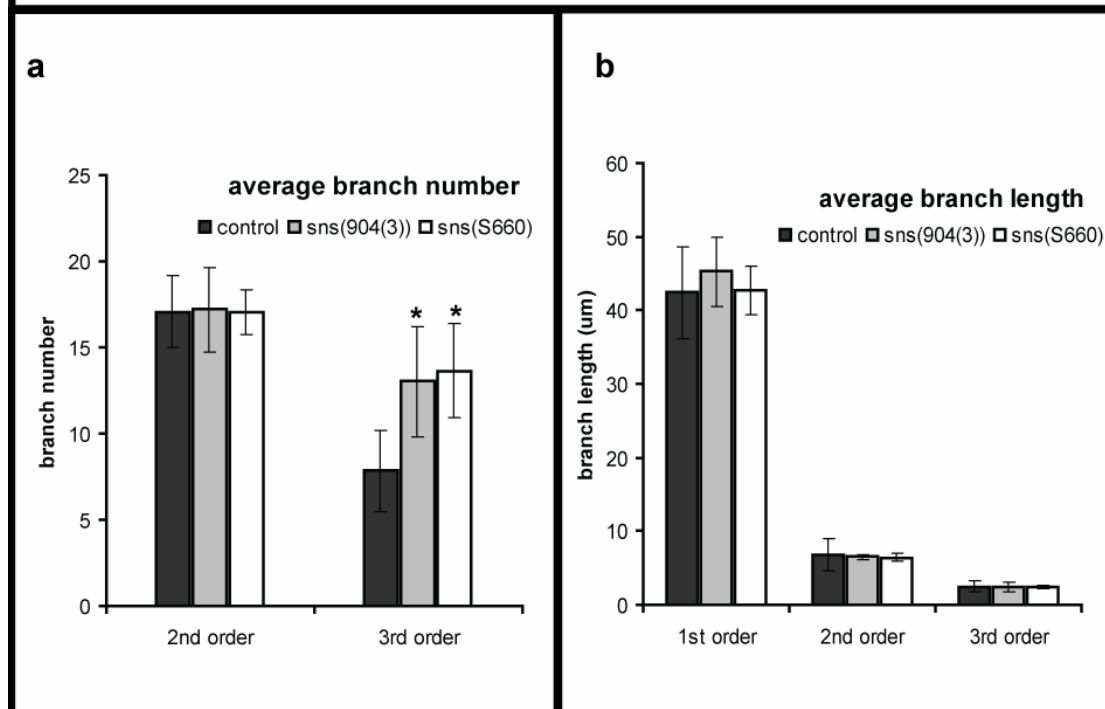


4.10. Analysis of dendrite morphology of class I and class IV md-da neurons in *sns* mutants

Mutant line *sns*⁹⁰⁴ was isolated based on the presence of the overbranching phenotype in the dorsal cluster dendrites that are formed by six different md-

da neurons. Which md-da neurons are responsible for this alteration of dendritic morphology? The presence of the *109(2)80 GAL4* driver and the *UAS-GFP* reporter on the second chromosome of the line 904 do not allow to study dendrite morphology in the individual md-da neurons. Therefore, mutant line *sns*⁹⁰⁴⁽³⁾ and *sns*^{S660}, which do not bear 80G2, were combined with the *2-21 GAL4* and a *UAS-mCD8GFP* or the *ppk::GFP* transgene to check the dendritic phenotypes of class I or class IV md-da neurons, respectively. Figure 27 shows the results of the analysis of the ventrally located class I md-da neuron (*vpda*) in both *sns* mutants. The quantifications of the dendritic phenotypes are shown in Figure 28.

Figure 28. Quantifications of the dendritic phenotype of *vpda* neurons in *sns* mutant embryos. Panel **a** shows a significant difference in the number of third order branches between control and *sns* mutants (2-21 (control)=7.83 n=18; *sns*⁹⁰⁴⁽³⁾ (mutant)=13.04 n=14 p=3.4x10⁻⁵; *sns*^{S660} (mutant)=13.65 n=14 p=2.3x10⁻⁶). Panel **b** shows the average branch length of *vpda* neurons in all three genotypes. No difference in branch length could be observed.



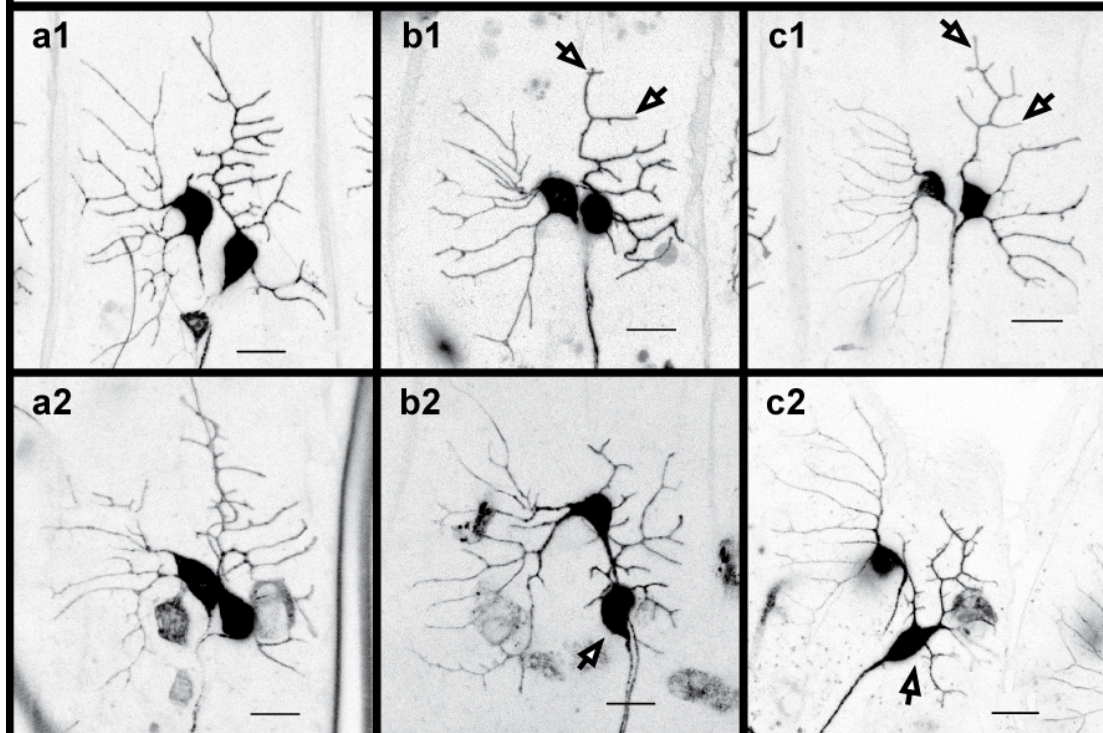
The *vpda* neurons in embryos (20-21h AEL) of the three tested genotypes have one primary dendrite, which grows in the dorsal direction. It produces

the same number of second order dendrites that grow in anterior or posterior direction (Figure 27). In comparison to the control, the vpda neurons of *sns* mutant embryos show a significantly higher number of the third order branches (arrows in Figure 27 and quantifications in Figure 28; 2-21 (control)=7.83 n=18; *sns*⁹⁰⁴⁽³⁾ (mutant)=13.04 n=14 p=3,4x10⁻⁵; *sns*^{S660} (mutant)=13.65 n=14 p=2,3x10⁻⁶).

No difference in the average length of first, second or third order dendrites could be detected between control and both mutants (Figure 28), which also indicates that the developmental time frame of vpda neurons is not obviously altered in the embryos without body wall musculature. Surprisingly, one seemingly longer second order branch could be occasionally detected at the distal end of the primary dendrites in both *sns* mutants. Sometimes it gives the impression that the growth cone of the primary dendrites split to produce two new branches (arrowhead in Figure 27 b and c). To confirm this observation, the average length of the longest second order dendrite was calculated for all three genotypes, but no significant difference could be detected between them (2-21 control=13.31 n=18; *sns*⁹⁰⁴⁽³⁾=14.75 n=14; *sns*^{S660}=14.71 n=14). Therefore, a specific overbranching phenotype could be consistently observed in vpda neurons in the mutant lines *sns*⁹⁰⁴⁽³⁾ and *sns*^{S660}.

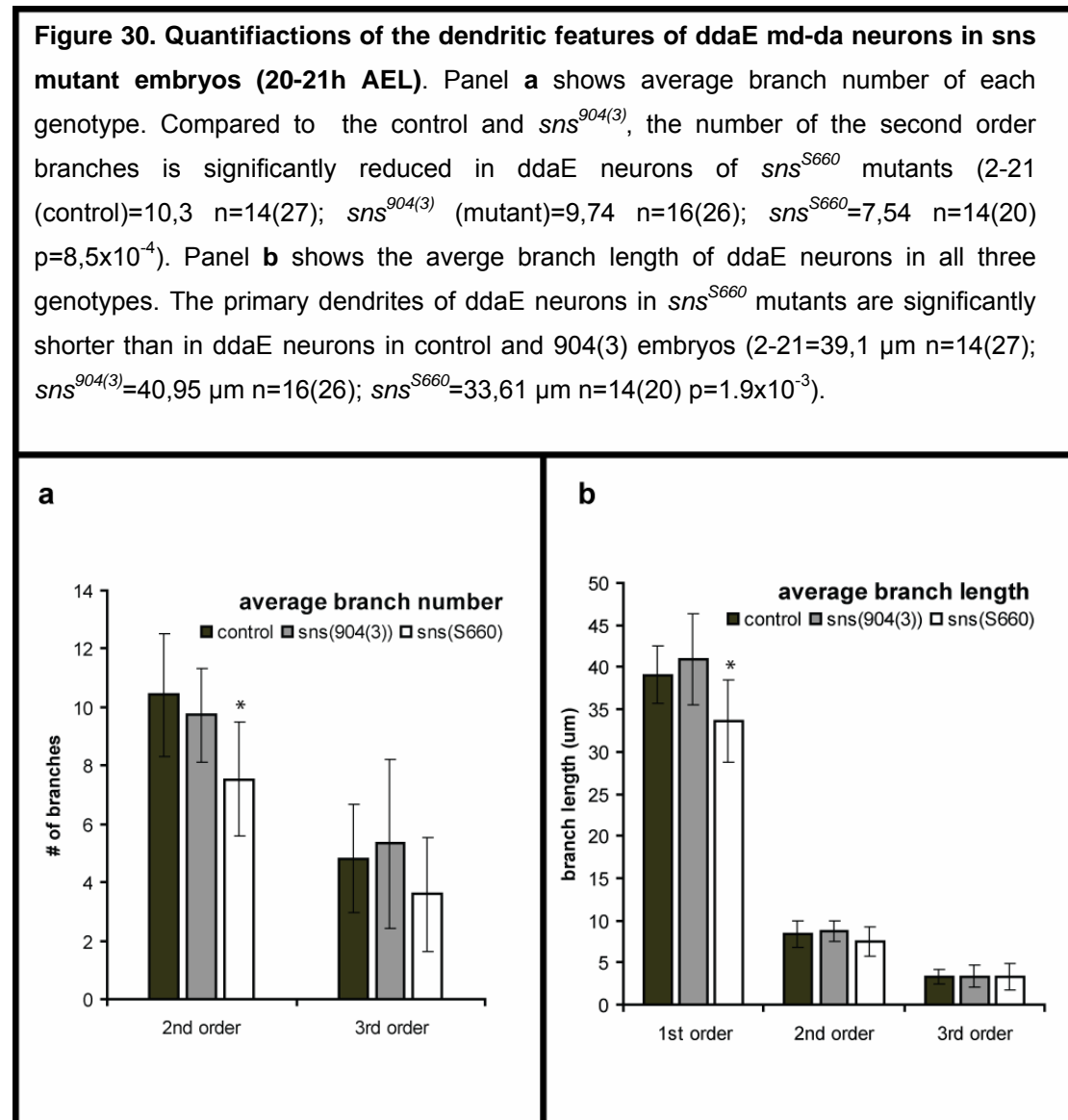
In addition, the dendritic phenotypes of the dorsal cluster class I neurons, ddaD and ddaE, in the lines *sns*⁹⁰⁴⁽³⁾ and *sns*^{S660} was examined in the 2-21 background. Figure 29 presents examples of these two neurons in the embryos of both the control and the two mutants in late stage 17 (20-21h AEL). The *GFP* expression in the ddaD neurons appears often weaker than in the ddaE neurons. In about one third of all tested embryos, the dendrites of the ddaD neuron were undetectable. Therefore, only the arbour characteristics of the ddaE neuron could be quantified to assess differences among the three tested genotypes.

Figure 29. Dendritic morphology of the class I *ddaE* md-da neuron in *sns* mutant embryos (20-21h AEL). 2-21 was used to visualize the *vpda* neurons (a). A variety of abnormal dendritic phenotypes appear in *ddaE* (the right neuron) neurons in *sns*⁹⁰⁴⁽³⁾ (b) and *sns*^{S660} (c) mutants that are never present in the controls. Often, *ddaE* neurons have reduced dendritic arbours due to shorter primary dendrites and less secondary dendrites (b1 and c1) in both *sns* mutants. Finally, *ddaE* neurons change slightly their position relative to the control (a, b2 and c2). The scale bars are 10 μ m. Dorsal is up and anterior to the left.



Surprisingly, *ddaE* neurons in both *sns* mutants display a variety of different phenotypes. As shown in Figure 29, *ddaE* neurons in the control animals have one dorsally oriented first order dendrite with a stereotyped length that produces repeatedly second order branches. The majority of these second order branches grows towards the posterior end of the respective hemisegment, and only a low number also to the anterior end. In both mutants, the dendrites of *ddaE* neurons show qualitatively similar mutant phenotypes. Often, dendrites of the *ddaE* neurons have shorter primary dendrites and less second order dendrites (arrows in Figure 29 b1 and c1). Thus, the complexity of the *ddaE* arbours appears to be reduced. Also, a slight change of the soma position is sporadically observed in both mutants

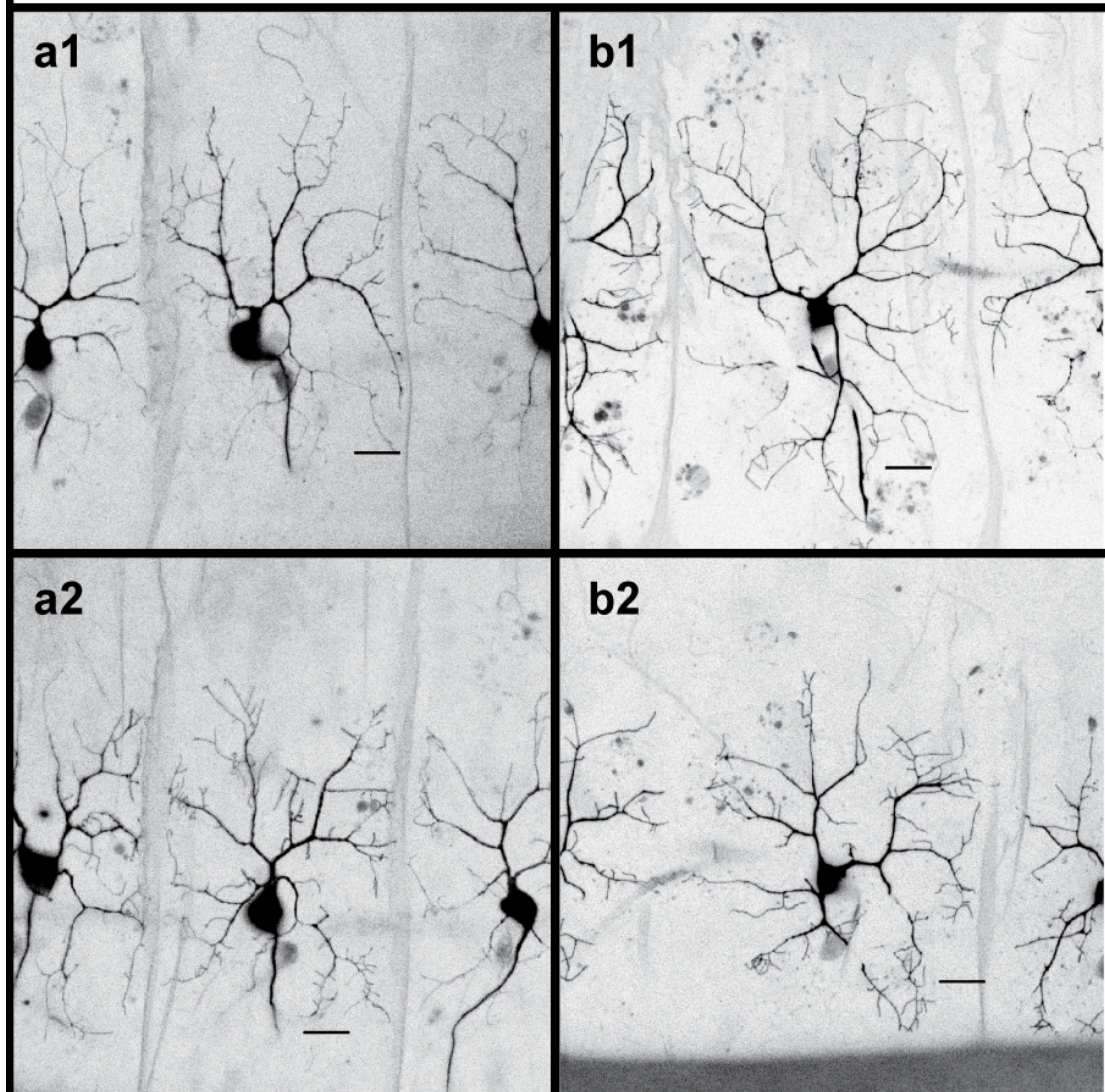
(arrows in Figure 29 b2 and c2). These phenotypes or the combination of both, are more frequent in the *sns*^{S660} mutant (28/30; 93%) than in the mutant line *sns*⁹⁰⁴⁽³⁾ (20/28; 71%). Figure 30 shows quantifications of the arbour characteristics of *ddaE* neurons, averaged from all animals per genotype regardless of their *ddaE* phenotypes.



No difference in terms of dendritic branch number or length could be detected between the *ddaE* neurons of line *sns*⁹⁰⁴⁽³⁾ and control. Unexpectedly, *ddaE* neurons of the mutant line *sns*^{S660} have significantly less second order branches (Figure 30a; 2-21 (control)=10.43 n=27(14); *sns*⁹⁰⁴⁽³⁾=9.74 n=26(16);

$sns^{S660}=7.54$ $n=20(14)$ $p=8,5 \times 10^{-4}$) than the control or the line $sns^{904(3)}$. Additionally, primary dendrites of *ddaE* neurons in sns^{S660} are significantly shorter (Figure 30b; 2-21 (control)=39.11 $n=27(14)$; $sns^{904(3)}=40.95$ $n=26(16)$; $sns^{S660}=33.61$ $n=20(14)$ $p=1,9 \times 10^{-3}$) than in control and the mutant line $sns^{904(3)}$. An overbranching phenotype could not be observed in *ddaE* neurons in neither of the two mutants.

Figure 31. The dendritic phenotype of the class IV md-da neuron *ddaC* in control and sns^{S660} embryos (21-22h AEL). In both cases, *ddaC* neurons are visualised by a *ppk::GFP* transgene. No obvious difference is detectable between both genotypes. Scale bars are 10 μ m. Dorsal is up and anterior to the left.

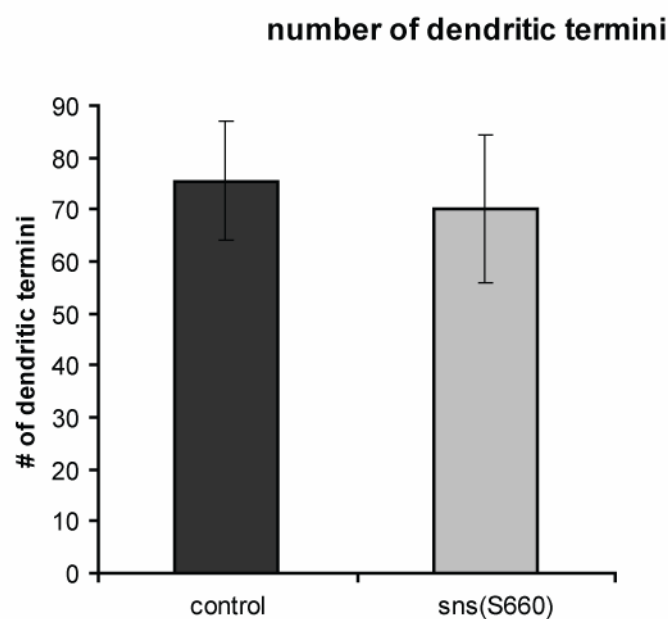


Hence, *ddaE* neurons do not contribute to the higher number of dendritic termini in the dorsal cluster of the mutant line *sns*^{S660}. The qualitatively similar phenotypes of *ddaE* neurons in both mutants could not be quantitatively confirmed.

The dorsal cluster contains the class IV md-da neuron *ddaC*. To gain an insight into the dendritic phenotype of *ddaC* neurons in *sns*^{S660} mutants, the *ppk::GFP* transgene, which expresses *GFP* exclusively in class IV neurons, was combined with this line. Due to the weaker activity of the *ppk::GFP* transgene during embryogenesis, the dendritic phenotype of *ddaC* neurons was investigated in 21-22h old embryos. The dendritic morphology of *ddaC* neurons in the mutant line *sns*^{S660} and control embryos is shown in Figure 31.

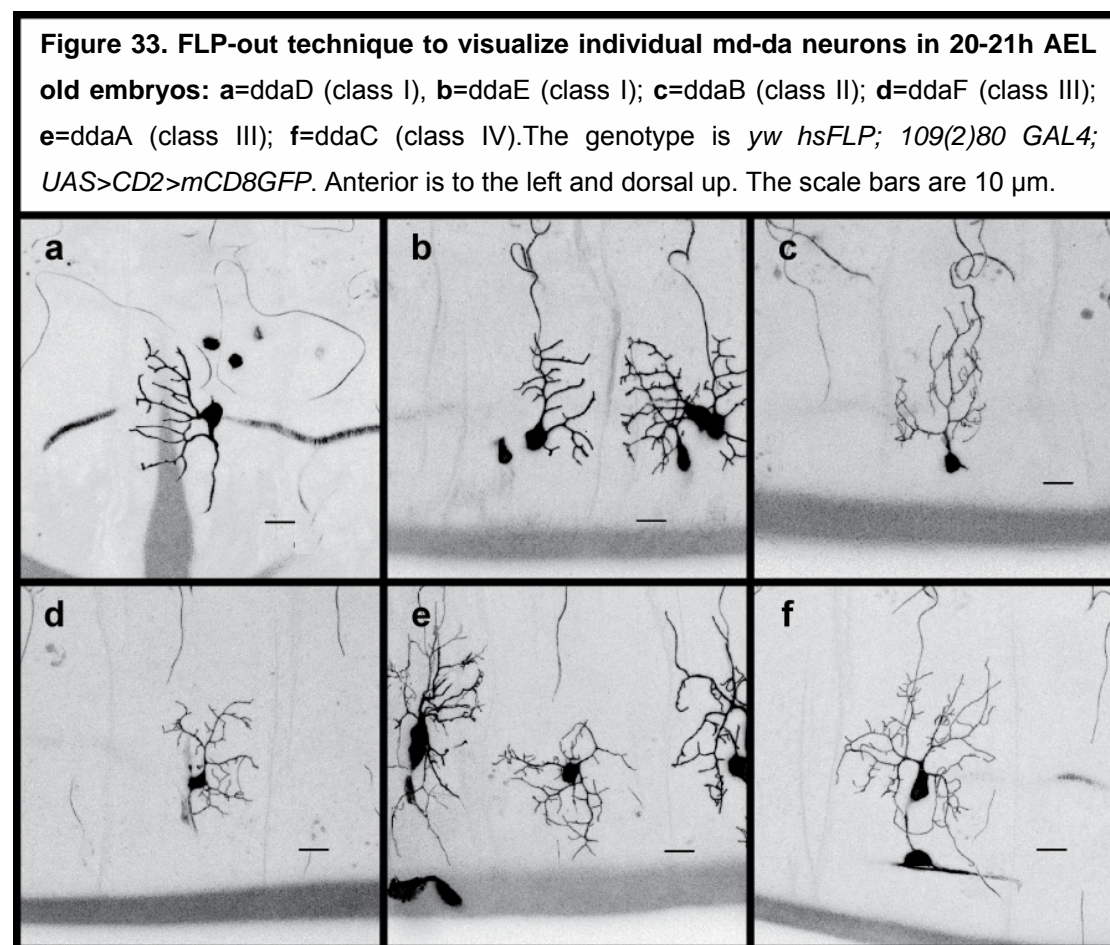
Neither differences in the dendritic morphology nor differences in the number of dendritic termini could be detected between *ddaC* neurons in the control and mutant embryos (see Figure 32). Consequently, loss of function of *sns* does not affect dendritic morphology of *ddaC* neurons in 21-22h old embryos.

Figure 32. Quantifications of dendritic termini in the class IV md-da neuron *ddaC* in control and *sns*^{S660} embryos (21-22h AEL). At this developmental stage, no difference could be observed in the number of dendritic termini in control and mutant.



4.11. An approach to analyse dendritic morphology of the remaining md-da neurons

The dendrites of class I and class IV md-da neurons in the dorsal cluster of the mutant line *sns*⁹⁰⁴⁽³⁾ or *sns*^{S660} mutants do not show any obvious overbranching phenotype. Therefore, the dorsally located class II and/or class III md-da neurons are potentially responsible for the dendritic phenotype of the dorsal cluster md-da neurons in the line 904.



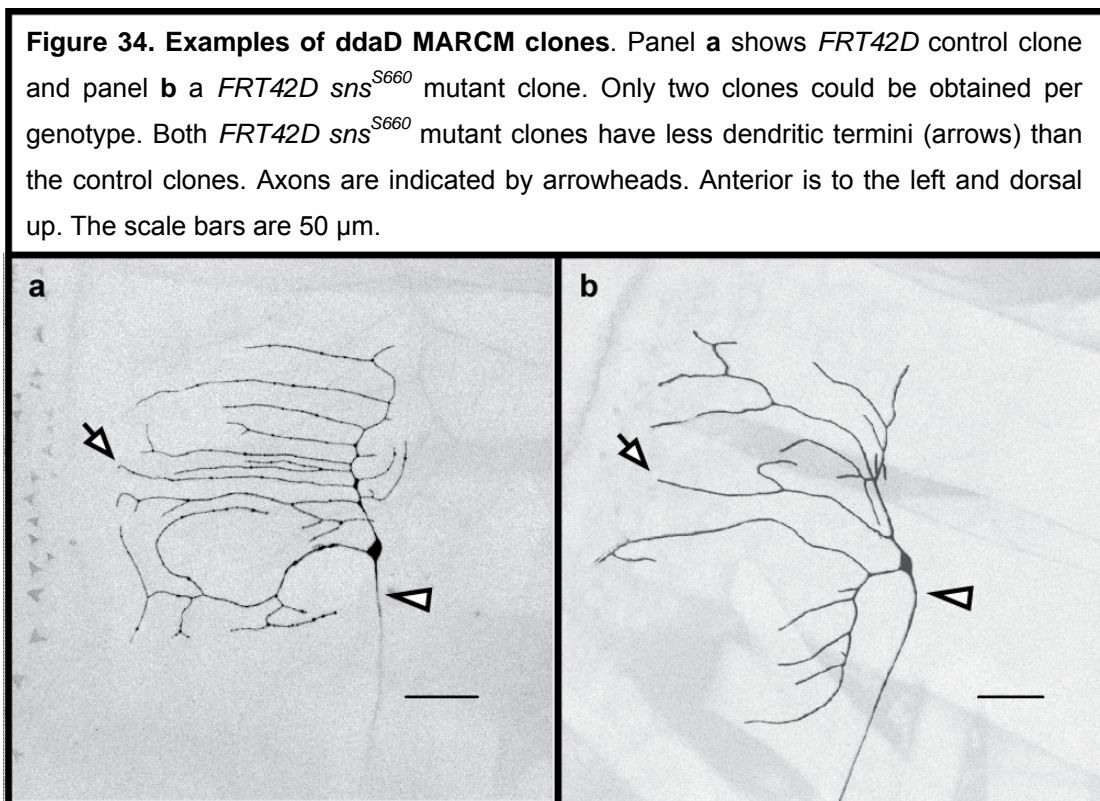
Unfortunately, there are no available *GAL4* lines with specific expression pattern exclusively in class II or class III md-da neurons in *Drosophila* embryos. Thus, a FLP-out approach was tested to label individual dorsal md-da neuron (see Material and Methods page 27). Figure 33 shows the dendrites of each single md-da neuron of the dorsal cluster. The best

frequency of singly labelled cells was achieved with a brief heat shock of 5min. So, it is possible to mark individual md-da neurons in 20-21h AEL old embryos via the FLP-out technique. In the future, this method can be used also in a *sns* mutant background.

4.12. MARCM of *sns* in md-da neurons of the dorsal cluster

The data obtained up to this point, indicate that mutations in the *sns* gene cause dendritic alterations. These phenotypes can be cell-autonomously rescued in the md-da neurons (see Figure 25). MARCM can provide an additional lines of evidence that the phenotype is due to a cell-autonomous requirement of *sns* in the md-da neurons. As described in Material and Methods page 28, MARCM enables the generation of *GFP*-labelled and homozygous mutant md-da neurons in an otherwise heterozygous and unlabeled background. Hence, this genetic technique allows to study individual *sns*^{S660} mutant md-da neurons and to verify a possible cell-autonomous function of *sns* in dendrite morphogenesis.

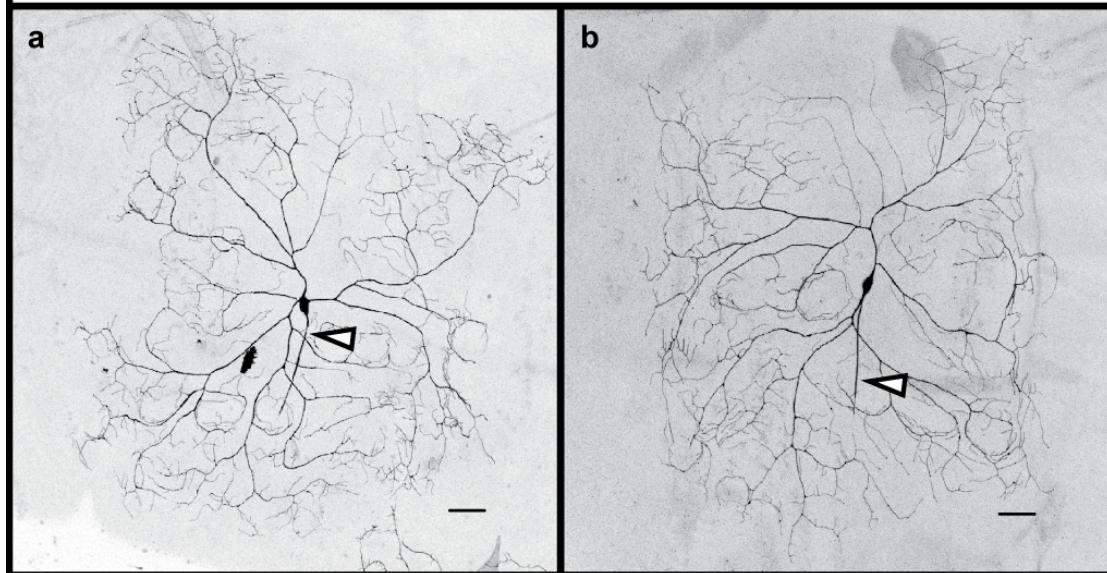
For MARCM analysis of *sns* in md-da neurons, a recombinant chromosome was created that bears the *FRT42D* transgene and the *sns*^{S660} LOF mutation. The original *FRT42D* chromosome was used for the generation of control MARCM clones. Unfortunately, the frequency of MARCM clones was very low with both, the *FRT42D sns*^{S660} and the original *FRT42D* chromosome, due to an unspecified problem with the used *FRT42D tubGal80* chromosome.



Similarly, only few clones of the dorsal md-da neurons were generated. Low numbers of clones exclude a quantitative MARCM analysis. Therefore, only ddaD and ddaC MARCM clones can be presented here. Figure 34 shows examples of the obtained ddaD MARCM clones.

Two ddaD MARCM control clones and two *sns^{S660}* mutant clones could be induced. In both mutant clones the number of the dendritic termini was reduced compared to the controls (*FRT42D*: 25 n=2; *FRT42D sns^{S660}*: 16 n=2), which suggests a cell-autonomous function of *sns* in branch formation in these neurons. Examples of the produced ddaC control and *sns^{S660}* mutant MARCM clones are shown in Figure 35.

Figure 35. Examples of *ddaC* MARCM clones. Panel **a** shows a *FRT42D* control clone and panel **b** a *FRT42D sns*^{S660} mutant clone. Only three control clones and seven *sns*^{S660} mutant clones could be induced. No difference of the dendrite morphology control or mutant *ddaC* clones could be detected. Axons are indicated by arrowheads. Anterior is to the left and dorsal up. The scale bars are 50 μ m.



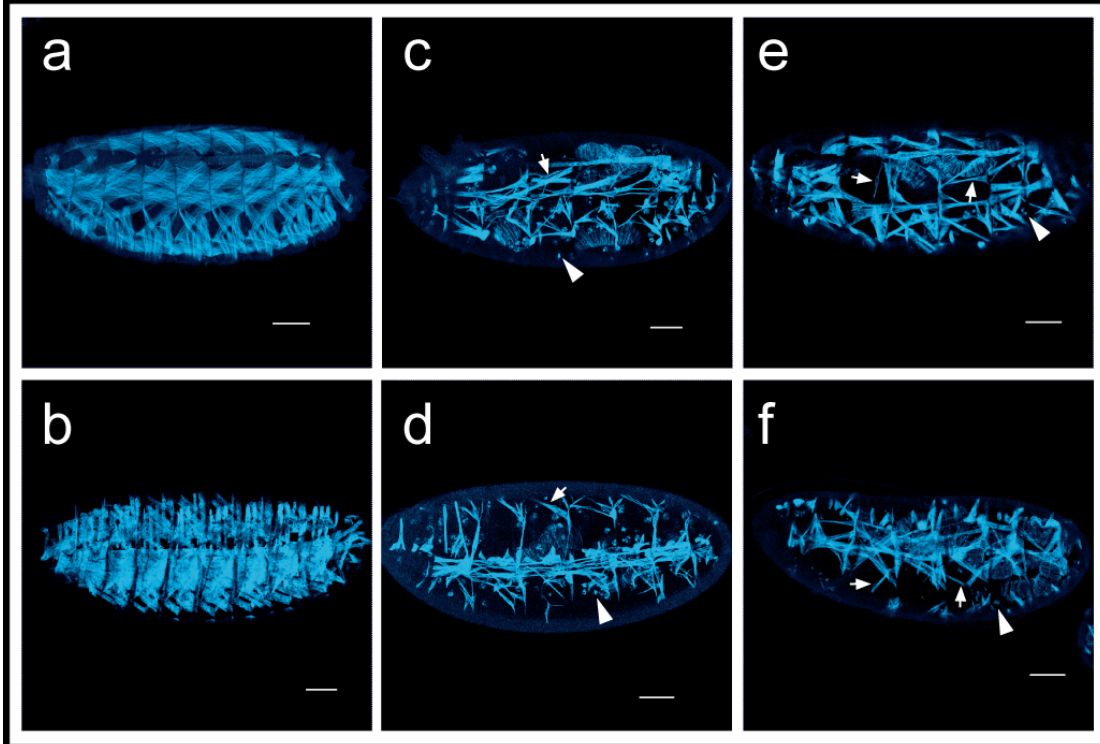
The dendritic morphology of the control and mutant *ddaC* MARCM clones did not show major differences. Hence, *sns* seems not to affect cell-autonomously the dendritic differentiation of class IV md-da neurons.

4.13. Analysis of dendritic morphology of md-da neurons in a *blown-fuse* mutant

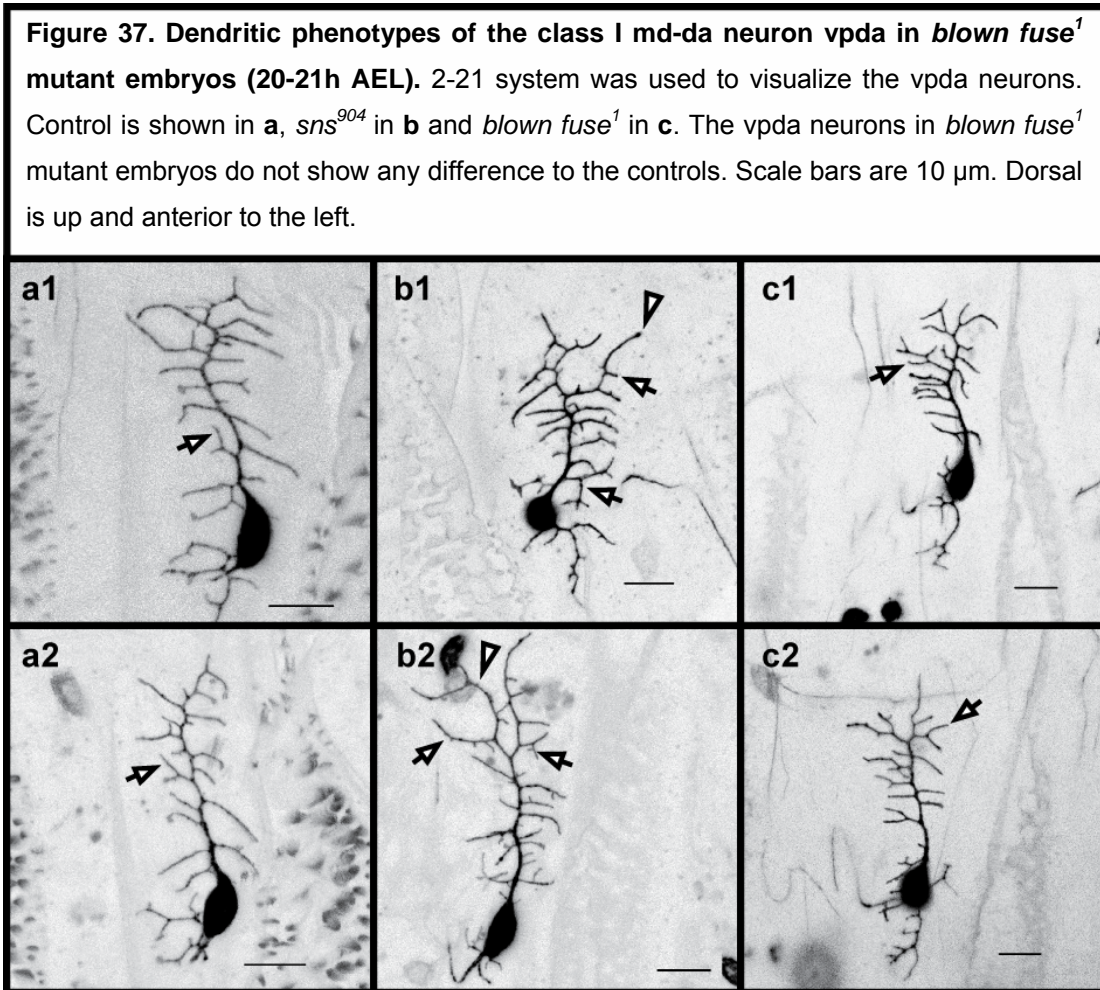
All md-da neurons develop their dendrites in a layer between the epidermis and the body wall musculature (Gao *et al.*, 1999). An interaction between the musculature and md-da neurons is conceivable, because of the tight proximity of these cells. Therefore, it is possible that the dendritic phenotype of md-da neurons in *sns* mutants could be caused by the loss of the body wall musculature. This would mean that the dendritic phenotype in *sns* mutant is not due to a direct action of this gene in md-da neurons. For example, the loss of body wall musculature in the *sns* mutants might delay the embryonic

development and consequently affect dendritic development of md-da neurons indirectly.

Figure 36. The body wall musculature in *blown fuse*¹ mutant embryos (20-21h AEL). Control is shown in **a** and **b**, *sns*⁹⁰⁴ in **c** and **d** and *blown fuse*¹ in **e** and **f**. Panels **a,c** and **e** show dorsolateral view, whereas panels **b, d** and **f** show ventrolateral view, respectively. In *sns*⁹⁰⁴ and *blown fuse*¹ mutants, the somatic musculature is not normally formed. Instead, small and often mononucleated muscles (arrows in **c, d, e** and **f**) are seen in both mutants. Also, unfused myoblasts can be observed in both mutants (arrowheads in **c,d,e** and **f**). Scale bars are 50 μ m. Dorsal is up and anterior to the left.



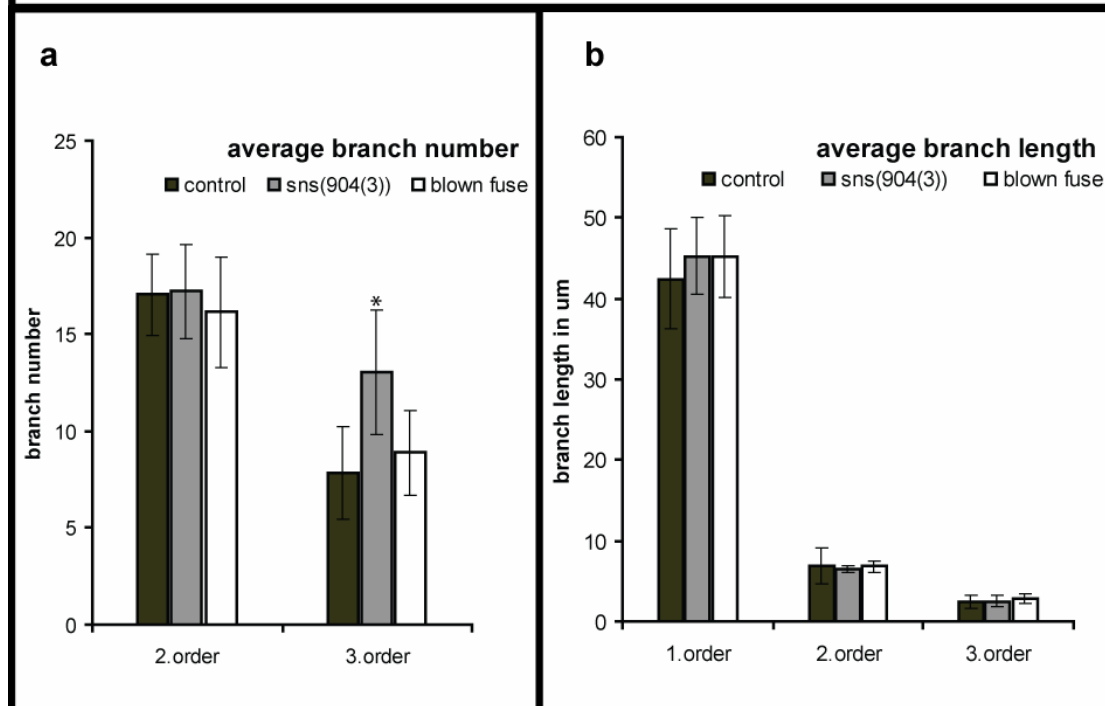
If this holds true, the dendritic morphology of md-da neurons should be affected in a similar way in all mutants, where formation of the body wall musculature is prevented during embryogenesis. In *blown fuse*¹ mutant embryos, fusion of myoblasts is inhibited and the body wall musculature consequently fails to form (Figure 36, (Doberstein *et al.*, 1997; Paululat *et al.*, 1999)). Only mononucleated remnants of muscles (mini-muscles) and few unfused myoblasts can be observed in both genotypes.



Hence, the musculature phenotypes in *blown fuse* and *sns* mutants appear very similar. In both mutants, the dendritic phenotype of class I md-da neurons was examined in the 2-21 background (see Figure 37). The vpda neurons in *blown fuse*¹ mutants do not show any obvious alterations of their dendritic arbours in comparison to the controls. No significant changes in the number of branches or length of branches could be observed in the vpda neurons in the *blown fuse*¹ mutant embryos (see Figure 38).

The dendrites of the class I md-da neuron vpda in the *blown fuse*¹ mutant do not show an overbranching phenotype as in the *sns*⁹⁰⁴ mutants. Moreover, in both mutants, number and length of primary and secondary branches of vpda neurons are not altered in comparison to the control neurons.

Figure 38. Quantifications of the dendritic phenotype of the class I md-da neuron vpda in *blown fuse*¹ mutant embryos (20-21h AEL). Panel a shows quantifications of vpda dendrites in control, *sns*⁹⁰⁴ and *blown fuse*¹ mutant embryos (20-21h old). The number of third order dendrites is not altered in the *blown fuse*¹ mutants (control=7.83 n=18(27), *sns*⁹⁰⁴=13,04 n=14(26), *blown fuse*¹=8,88 n=16(28)). There is no difference in the branch length among the three tested genotypes (panel b).



Thus, it seems that the loss of the body wall musculature has no significant impact on the development of the vpda neuron. This excludes also a delay of neuronal development due to a possible restriction of the embryonic development in the *sns* or *blown fuse* mutants, since overall dendritic features of vpda neurons are not altered in these mutants. This observation suggests that *sns* has a direct effect on the dendrite development in *Drosophila* embryos, independent of the dramatic muscle phenotype. Taken together with the cell-autonomous rescue of the dendritic phenotype (Figure 25 on page 67), and with the presence of Sns in the md-da neurons at the larval stages (Figure 26 on page 68), these data suggest that *sns* acts within the md-da neurons to modulate dendritic morphology.

5. Discussion

5.1. Summary of the results

This project used the md-da neurons of the embryonic and larval PNS of *Drosophila* to identify and characterise genes that are involved in the regulation of branch formation in dendrites. Thus, the aim of this project was to map recessive lethal mutations on the second chromosome of six mutant lines that showed an abnormal dendritic overbranching in the dorsal group of md-da neurons at embryonic stage 17. In one of these mutant lines, namely the mutant line 904, a recessive lethal mutation was mapped to the gene *sticks and stones (sns)* that encodes a transmembrane molecule of the Ig-superfamily, which is required for myoblast fusion during the formation of the body wall musculature in *Drosophila*. A rescue of the overbranching phenotype in the dendrites of dorsal md-da neurons of the line 904, through expression of *sns* exclusively in these neurons, proved that the dendritic phenotype is due to a mutation in *sns* and suggests that this molecule acts cell-autonomously to control the formation of dendritic branches in md-da neurons. Moreover, *sns* expression could be detected in md-da neurons at larval stages, which further supports a cell-autonomous function of this molecule.

The dendrites of class I md-da neurons show opposite dendritic phenotypes in *sns* mutants. In contrast to the vpda neuron that showed a mild overbranching phenotype, the dendritic complexity of the dorsal class I md-da neuron ddaE was somewhat reduced. Furthermore, no dendritic phenotype could be seen in the dorsal class IV neuron ddaC. Interestingly, the increased number of high order branches of the vpda neuron in *sns* mutants was not seen in a *blown fuse* mutant, which also lacks a somatic body wall musculature.

5.2. A genetic screen to identify new genes involved in dendrite morphogenesis of md-da neurons

All sensory neurons of the embryonic and larval PNS of *Drosophila* are located at the body wall, between the epidermis and the somatic musculature (reference Bodmer and Jan (Gao *et al.*, 1999)). The md-da neurons develop their complex dendritic arbours directly underneath the epidermis in an almost two-dimensional fashion (Gao *et al.*, 1999). Several *GAL4* driver lines are available that allow to label these neurons in living animals, via the cell-specific expression of fluorophores. The embryonic development of md-da neurons has been studied by using a *GAL4* driver, which is active in all md-da neurons (Gao *et al.*, 1999). At the late embryonic stage 17, the md-da neurons of the dorsal cluster generate a dendritic field with a reproducible morphology ((Gao *et al.*, 1999), Figure 6 on page 25). Thus, this system allows screening for recessive lethal mutations that affect the differentiation of these dorsal cluster dendrites. Such an attempt was performed by the group of Prof Y.-N. Jan, via EMS-mutagenesis of a fly line that harbours the pan md-da *GAL4* driver *109(2)80* (Gao *et al.*, 1999). Several new genes that influence diverse aspects of dendrite differentiation, like: outgrowth, branching and routing, were already identified in that screen (Gao *et al.*, 1999). The success of this attempt was also based upon the availability of genetic tools in *Drosophila* that allow to map and characterize recessive lethal mutations in a reasonable amount of time.

5.3. Limitations of the screen

A drawback of this model system is the relative insensitivity of the readout. The expression pattern of the used *GAL4* driver line makes it difficult to analyse dendritic arbours of individual md-da neurons. A complete structural stereotypy of the dorsal cluster dendrites is not achieved at the late embryonic stage 17, as all md-da neurons continue to differentiate their dendritic arbours until early larval stages (Sugimura *et al.*, 2003). Therefore, mutants with more

subtly altered dendritic morphologies need to be carefully analysed to exclude false-positive phenotypes.

EMS mutagenesis produces many non-lethal mutations beside the few recessive lethal ones. Since the dendritic phenotype might be due to such a non-lethal mutation, the mapping of recessive lethal mutations was started with all six mutant lines that share a common overbranching phenotype, to increase the chance that at least one of these mutations is responsible for the dendritic phenotype.

The production of false-positive phenotypes in the dendrites of md-da neurons may occur changing the normal developmental time frame of the embryos. Examination of epidermal structures or gut characteristics, which is possible through the autofluorescence of these tissues, as well as the onset of muscle contractions in late embryonic stages can help to determine the developmental stage of the embryo. Moreover, the generated mutants might have defects in non-neuronal tissues that affect indirectly the dendritic architecture of md-da neurons. This possibility can only be ruled out through appropriate analysis, after localisation of the mutations that causes the dendritic phenotype in md-da neurons of such mutants.

5.4. The dendritic phenotype of md-da neurons in the six mutant lines

The dendrites of the dorsal cluster md-da neurons in all six mutant lines generate a higher number of termini than in the controls, whereas other arbours characteristics are not changed. Differences of the dendritic phenotype between individual mutants are not reproducible, due to variations in the degree of the dendrite overbranching among individuals of the same genotype. To analyse and quantify the phenotype of single md-da neurons in a mutant line, the mutation that produces the phenotype needs to be separated from the 80G2, which is only possible after its mapping.

5.5. Approaches to map recessive lethal mutations in *Drosophila*

In general, recessive lethal mutations are mapped in a two-step process. First, the mutation is roughly localised to approximately 100-200kbp large interval on the mutant chromosome via deficiency mapping (see Material and Methods page 31; Results page 41). Subsequently, the mutation becomes positioned to a single gene within this defined chromosomal area. Several techniques are available for this second mapping step. A technically easy possibility is to use additional deficiencies that overlap in the chromosomal intervals that contain recessive lethal mutations. Through complementation analysis with these deficiencies it is feasible to narrow down successively to the area where a recessive lethal mutation is induced. The combination of these deficiencies with recessive lethal transposon insertions can provide the chance to enhance the resolution of such a mapping attempt to single genes (Bellen *et al.*, 2004).

The specificity of such an approach depends on the availability of sufficient chromosomal deficiencies and recessive lethal transposon insertions in the chromosomal interval of interest. Furthermore, the breakpoints of chromosomal deficiencies should be molecularly mapped, which allows precise and reliable analysis of the complementation data. Collections of recessive lethal transposon insertions and deficiencies with molecularly mapped breakpoints are being constantly expanded, but are often still not sufficient to provide an adequate resolution (Parks *et al.*, 2004; Ryder *et al.*, 2004).

The huge number of available P-element insertions provides several additional possibilities to map recessive lethal mutations (Chen *et al.*, 1998; Zhai *et al.*, 2003). First, the feature of the P-element transposase to induce site-specific recombination between sister chromosomes, instead of a P-element transposition, can be used to map recessive lethal mutations, despite the low frequency of this recombination event (Chen *et al.*, 1998). Secondly, the large number of available P-element insertions can be utilized as molecular markers for classical meiotic recombination mapping (Zhai *et al.*, 2003). Due to the presence of the *GAL4* and *UAS* insertions on the

mutagenized chromosomes, the first technique was not applicable for the mapping of recessive lethal mutations in the six mutant lines. The 80G2 line includes three P-element transgenes per chromosome (1x*GAL4* driver and 2x*UAS-GFP*), which would interfere with the procedure of the site-specific recombination. Similarly, the presence of three P-element insertions on the mutant chromosomes limits also the practicability of the second technique, because the transposon marker *white*⁺ is already present in the six mutant lines. The usage of a different P-element marker, like *yellow*⁺, is conceivable but more demanding, since P-element insertions with other markers than *white*⁺ are rarer.

A powerful but also tedious and technically challenging approach is SNP-mapping. Nevertheless, several groups have proven the applicability of this technique, where SNPs are used as molecular markers for meiotic recombination mapping (Berger *et al.*, 2001; Hoskins *et al.*, 2001). High resolution maps of SNPs were already generated for distinct pairs of chromosomes, which showed an abundant availability of these molecular markers along the major chromosomes. A comparable SNP map does not exist between the mutagenized chromosomes of the six mutant lines and corresponding reference chromosomes. Therefore, a first step is to find appropriate reference chromosomes that can be used to create sufficient local SNP markers for mapping of recessive lethal mutations on the second chromosome of the six mutant lines in a high resolution. Moreover, alternative markers for the P-elements, rather than *white*⁺, would be also required for SNP-mapping as well, to limit the area, where the meiotic recombination between a mutant and a reference chromosome would take place.

The number of applicable methods to localise recessive lethal mutations in the six mutant lines is therefore rather limited. Hence, successful mapping depends on the availability of deficiencies and P-element insertions in the chromosomal area of interest. The resolution of this approach needs to be high enough, to identify the recessive lethal mutation via direct sequencing of the remaining candidate genes.

5.6. Deficiency mapping of recessive lethal mutations

Via deficiency mapping, recessive lethal mutations could be localised on the second chromosome in five of the six mutant lines (see Table 1 page 42). In the mutant lines 969, 797 and 774 more than one recessive lethal mutation was mapped (see Table 1 page 42). The mutation that causes lethality of homozygous animals in the mutant line 562 is most likely not uncovered by the used collection of chromosomal deficiencies and could therefore not be identified. Since the second chromosome of these mutant lines contain a variety of different mutations, the complementation analysis with chromosomal deficiencies might produce a decreased viability of transheterozygous animals, although recessive lethal mutations are not uncovered. Such effects could cause ambiguous results of complementation tests and could undermine the efforts to map recessive lethal mutations, as it is the case for *Df(2R)X58-12* (BL-282), which caused a general poor viability in almost all transheterozygous animals (see Results page 43). For this reasons, it is recommendable to verify the complementation data with independent and smaller deficiencies that overlap within the identified area.

An EMS mutagenesis is usually set to produce a small number of recessive lethal mutations. Thereby, many other, non-lethal mutations are induced on the same chromosome that could be also responsible for the dendritic phenotype. Also synergetic effects of different mutations on the mutant chromosomes might cause the overbranching of the md-da neurons. To prevent such a possibility, the dendritic phenotype of md-da neurons was re-examined in transheterozygous animals for each identified deficiency that uncovers a recessive lethal mutation in the lines 904, 797, 774 and 566 (see Figure 13). An overbranching phenotype in the md-da neurons was confirmed for the recessive lethal mutation in the line 904 (uncovered by *Df(2R)H3E1*) and for one of the three recessive lethal mutations in the line 797 (uncovered by *Df(2L)BSC30*). These results suggest that these two recessive lethal mutations produce the dendritic phenotype in the lines 904 and 797, respectively.

Frequently, the viability of transheterozygous embryos was impaired. Many embryos showed unspecific defects of neuronal morphology or were obviously delayed in their development. Due to such limitations, the recessive lethal mutations in the mutant line 969 could not be reliably examined. The corresponding control embryos did not show these problems in a comparable frequency. Hence, the presence of two recessive lethal mutations could cause the poor viability of transheterozygous embryos. A solution for this situation could be the separation of the two recessive lethal mutations by meiotic recombination. In such recombinants, each mutation could be examined individually. Otherwise, different and smaller deficiencies could be tested for their compatibility with the mutant chromosome of the mutant line 969.

5.7. Mapping of the recessive lethal mutation in the line 797

Three deficiencies with molecularly mapped breakpoints were used to minimize the number of candidate genes from 76 to 58 in the chromosomal interval that is uncovered by *Df(2L)BSC30* (see Results Table 4 and Figure 14). Thus, the resolution of the deficiency mapping is not high enough to start the sequencing of candidate genes. To complete the mapping, a set of small chromosomal deficiencies within the target area could be created for complementation analysis with line 797 (Huet *et al.*, 2002; Parks *et al.*, 2004; Ryder *et al.*, 2004). In addition, the set of available *UAS-RNAi* lines could be used to successively knock down candidate genes in the 80G2 fly line (Dietzl *et al.*, 2007).

5.8. Mapping of the recessive lethal mutation in the line 904

In the mutant line 904, a recessive lethal mutation was localised to the chromosomal interval 2R:44D1-44F12 via deficiency mapping. Four additional deficiencies that overlap in this area were used for further complementation analysis (see Results Table 5 and Figure 15). Since the breakpoints of these four deficiencies are molecularly mapped, it was possible to determine the number of remaining candidate genes for the recessive lethal mutation in the

mutant line 904. Eight of these 22 remaining genes were excluded by complementation analysis with available recessive lethal P-element insertions.

Two approaches were started to map the recessive lethal mutation in the remaining 200kbp. First, a local P-element hop was conducted to generate recessive lethal mutations in an independent fly line that could be used for a complementation analysis with the mutant line 904 (see Results page 50). Thus, in the best case, this technique would create independent alleles of the recessive lethal mutation in a comparatively clean background. This allele could be immediately combined with different *GAL4* drivers to examine the dendritic phenotype specifically in class I or class IV md-da neurons. Furthermore, the possibility to precisely excise this P-element again, would allow to control that the insertion is responsible for the phenotype.

Secondly, despite the technical concerns, a SNP-mapping approach was conducted to position the recessive lethal mutation within 2R:44D1-44F12, because of the following reasons. Due to the position of the recessive lethal mutation to the right side of the P-elements present in 80G2, it was possible to use the easily scoreable *white*⁺ as P-element marker to the right side of the recessive lethal mutation. For the SNP-mapping from the left side of the recessive lethal mutation, *yellow*⁺ was chosen as a P-element marker. More important, it turned out to be unexpectedly easy to identify adequate reference chromosomes with a sufficient number of SNPs that distinguish them from the mutant chromosomes.

5.9. Local P-element hop

Two different types of P-elements were used for this approach in the mutant line 904 (see Results Table 6). The mobilisation of the *P{SUPor-P}* element from BL-14021 generated no recessive lethal insertion among the 67 selected lines (see Results Table 7). After mobilisation of the *P{EPgy2}* element in BL-15867, 54 individual lines were isolated (see Results Table 7). Among all these lines, four carried recessive lethal insertions and one of them did not complement the lethality of the mutant line 904. This insertion line was named

P66. Interestingly, the analysis of the *vpda* neuron in P66 revealed an overbranching phenotype that was similar to the one seen in *vpda* neurons of mutant 904(3) at a later time point of this project (see Results Figure 17 and 18). The iPCR protocol, which was performed to determine the new position of the P-element in P66, returned two different flanking genomic sequences from the 5' and 3' ends of this P-element insertion, respectively. The sequence from the 5' end of the insertion anneals to the original position close to the gene *Rya-r44F*, whereas the sequence from the 3' end anneals to the 5'UTR of the gene *cmp44E*, which is several kbp upstream of *Rya-r44F*. Independent recessive lethal alleles of *Rya-r44F* and *cmp44E* complemented the lethality of the lines P66 and 904. Hence, these two genes are not affected in both mutants. An *in-situ* hybridisation of the *P{EPgy2}* element on polytene chromosomes of the original BL-15867 line and of the P66 mutant confirmed the presence of the P-element upstream of the gene *Rya-r44F* in both lines. Moreover, another P-element insertion was detected in BL-15867 on the left arm of the second chromosome in 2L:30A1-A5, which was absent in P66. This second P-element insertion in BL-15867 was not declared in the genotype of this stock.

The complementation data and the similar dendritic phenotype of the *vpda* neuron in the mutant line P66 and 904 suggests that P66 contains a recessive lethal allele of *sns*. But at the time point when this local P-element hop was performed, this conclusion was not possible, due to the confusing data from the iPCR and the *in-situ* hybridisations of *P{EPgy2}* elements in P66 and BL-15867. How is it possible that the iPCR reveals flanking sequences in *Rya-r44F* and *cmp44E*, although both genes are quite far away from each other and additionally are not affected in the mutant line P66? The explanation that the P-element upstream of *Rya-r44F* moves several times and fakes the iPCR results through the transportation of gDNA stretches from imprecise excisions is not likely, because these excised gDNA pieces should cause severe deletion mutations in *cmp44E* or *Rya-r44F*. How did *sns* become mutated in the P66 line? It is conceivable that the second and undeclared P-element insertion in BL-15867 produced this mutation through its insertion in *sns*. How could this fit to the data of the *in-situ* hybridisation? Either the two P-element

insertions in *sns* and *Rya-r44F* are too close to each other so that they could not be distinguished anymore by this technique, or this P-element became again imprecisely excised and left a deletion in *sns*, but did not reinsert.

Hence, the stocks that are used as P-element donors should be accurately analysed before their usage in a local P-element hop. Multiple transposon insertion in a jumpstarter stock are likely to cause ambiguous results as presented here. Furthermore, the dimensions of this approach were much too small. It would be advantageous to use four or five independent donor P-elements. To increase the number of new recessive lethal P-element mutations, many more individual transpositions should have been screened. The work on the P66 line was stopped due to the confusing mapping data.

5.10. SNP-Mapping

The performed SNP-mapping positioned the recessive lethal mutation in the mutant line 904 among five genes in 2R:44E3-44F7 (see Results Figure 20 and 21). This result confirmed the data of the complementation analysis with overlapping deficiencies and recessive lethal P-element insertions (see Results Figure 15) and could exclude ten more candidate genes. It could be shown that *yellow*⁺ can be used as a P-element marker for SNP-mapping instead of *white*⁺, although it is comparatively more tedious. Moreover, only six single SNP markers were enough to exclude the majority of the remaining candidate genes in 2R:44E3-44F7. Therefore, SNP-mapping is a powerful approach, which is even applicable without an already established map of SNP-markers. The only limiting factor appears to be the time consuming generation of a sufficient number of recombinants to perform SNP-mapping with highest resolution.

5.11. Mapping of the recessive lethal mutation to the gene *sns*

The SNP-mapping localised the recessive lethal mutation to five genes in 2R:44E3-44F7. Among these genes, a reproducible nucleotide exchange was identified in *sns* at the position 2R:4713580. This mutation alters the

consensus sequence of the splice donor site between the seventh and eighth exon in *sns* (see Results Figure 22). Hence, it is likely that splicing is not initiated at this site. In this case all subsequent ORFs are shifted and terminated by irregular STOP codons. Two independent null alleles of *sns* did not complement the lethality of the mutant line 904. Thus, the line 904 contains a *sns* LOF allele.

In *sns* mutant embryos, myoblast fusion is prevented and the body wall musculature consequently fails to form (Bour *et al.*, 2000). For this reason, the state of the body wall musculature in the mutant line 904 was examined by antibody stainings and a *MHC::tauGFP* transgene (see Results Figure 24). As in the *sns*^{S660} mutant embryos, a normal somatic musculature is not present in embryos of the mutant line 904. Instead of large and precisely arranged myotubes, only small and elongated fibers that resemble differentiated but unfused muscle precursors are visible (“mini-muscles”; (Chen and Olson, 2001; Schroter *et al.*, 2004)). Also, unfused and undifferentiated myoblasts were detected. The phenotypes of the somatic musculature in the mutant line 904 and *sns*^{S660} are virtually the same. Thus, the sequence analysis, the complementation data and the phenotype of the musculature show that the line 904 contains a LOF mutation in the gene *sns*, which was therefore named *sns*⁹⁰⁴.

5.12. Does *sns* affect the dendrite differentiation of md-da neurons directly?

Mutant line *sns*⁹⁰⁴ contains a recessive lethal mutation in the gene *sns* that inhibits the development of the larval body wall musculature (Bour *et al.*, 2000). In addition, *sns* is not known to be expressed in the neuronal tissue during the first phase of the embryonic development, when the somatic musculature is formed (Bour *et al.*, 2000). This raises the question, how is the dendritic phenotype of the dorsal md-da neurons produced in the line *sns*⁹⁰⁴? Could it be due to a specific function of *sns* or a secondary effect that is caused by the loss of the body wall musculature?

Taking into account the function and the published expression pattern of *sns* (see Introduction page 16; (Bour *et al.*, 2000)) it is likely that the dendritic phenotype of md-da neurons in the mutant line 904 is an indirect effect due to the loss of the body wall musculature. Nevertheless, a direct function of *sns* can not be completely excluded. The expression pattern of *sns* during late embryonic or larval stages is not known, but dendrites of md-da neurons show massive growth and differentiation, especially in the late embryonic stage 16 and 17 (Gao *et al.*, 1999). In addition, there are no indications for a correlation between specific defects of the musculature or epidermis and specific changes of dendritic morphology of md-da neurons (Parrish *et al.*, 2006).

Hence, a *UAS*-transgene that allows expressing full-length (FL) *sns* under *GAL4* control was used to rescue the dendritic phenotype in the dorsal md-da neurons in the mutant line 904 at embryonic stage 17. To obtain a quantifiable readout, the number of termini of the dendritic field that is formed by the dorsal md-da neurons was counted. In line *sns*⁹⁰⁴, a significantly higher number of dendritic termini was detected in comparison to the control (see Results Figure 25). Moreover, the expression of FL-*sns* under the control of the *109(2)80 GAL4* driver reduced the number of dendritic termini in line *sns*⁹⁰⁴ to control levels. This indicates that the dendritic phenotype in md-da neurons of line *sns*⁹⁰⁴ is due to the loss of *sns* specifically in md-da neurons at late embryonic stage 17. The expression pattern of the *109(2)80 GAL4* driver is very restricted to the nervous system so that a leakage of *sns* expression in the musculature or epidermis can be excluded (Gao *et al.*, 1999). Furthermore, the lethality of line *sns*⁹⁰⁴ was not rescued by the expression of *sns* under the control of the *109(2)80 GAL4*. The blockage of the somatic musculature was still present in this genotype, which further supports the specificity of this experiment.

The rescue experiment implies that *sns* might be expressed in the md-da neurons at the late embryonic or larval stages. Unfortunately, it is technically difficult to perform an antibody staining in embryos that are older than 16h AEL (see Material and Methods page 29). But in the third instar larvae fillets, expression of Sns was detected in the musculature, epidermis and all md-da neurons. This indicates that *sns* expression is not completely abolished after

formation of the somatic body wall musculature during embryonic and larval development.

In *sns* mutants, the class I md-da neuron vpda showed an overbranching phenotype in 20-21h old embryos (see Results Figure 27 and 28). This reproducible readout offers the possibility to examine the dendritic phenotype of the vpda in different muscle mutants, like *blown fuse*¹ (Doberstein *et al.*, 1997), in which *sns* is normally expressed. The loss of *blown fuse* prevents the formation of the body wall musculature in a comparable way as in *sns* mutants (see Figure 36; (Doberstein *et al.*, 1997)). Interestingly, the vpda neuron in *blown fuse*¹ mutants did not show any alteration in the branch number or length in 20-21h old embryos (see Results Figure 37 and 38). Thus, a loss of the somatic musculature does not affect the dendritic differentiation of vpda, which consequently means that the body wall musculature has no impact on dendrite development of this class I md-da neuron at the late embryonic stage 17. In addition, the loss of the body wall musculature does not seem to delay the general development of the vpda neuron, which could indirectly cause such an overbranching phenotype as the one observed for the vpda neurons in *sns* mutants.

According to the rescue experiment, the dendritic phenotype in the dorsal cluster md-da neurons of the line *sns*⁹⁰⁴ is a consequence of the loss of *sns* in these neurons. Furthermore, the phenotype of the vpda neuron in *blown fuse*¹ mutants suggests that the body wall musculature does not contribute to the dendritic differentiation of this neuron at the embryonic stage 17.

5.13. Does *sns* have a cell-autonomous function in the dendrite morphogenesis of md-da neurons?

The rescue of the dendritic overbranching phenotype of the dorsal cluster md-da neurons through specific expression of a *UAS-sns* transgene in these neurons implies that *sns* has an cell-autonomous function. This is supported by the finding that *sns* is expressed in md-da neurons at least at later larval stages. To obtain a confirmation for these findings, a MARCM was initiated, which could not be finished in time, due to technical problems. Otherwise, a

class-specific knock down of *sns* expression through *UAS-RNAi* could be performed to prove a cell-autonomous function of *sns*. With MARCM the dendritic phenotype of individual *sns* mutant md-da could be studied in an otherwise heterozygous background. Thus, it would provide useful information that could help to understand the role of Sns during dendrite morphogenesis of md-da neurons.

5.14. What is the role of *sns* in the dendritic development of md-da neurons?

In the line *sns*⁹⁰⁴, a LOF mutation of the gene *sns* produced a dendritic overbranching phenotype of the dorsal md-da neurons. Due to the expression pattern of the *109(2)80 GAL4* driver, it was not possible to study the dendritic phenotype of individual md-da neurons in the line *sns*⁹⁰⁴. Thus, the mutant lines *sns*⁹⁰⁴⁽³⁾ and *sns*^{S660} were combined with the *2-21* or the *ppk::GFP* transgene to label specifically class I or class IV md-da neurons (see Material and Methods page 25).

As already mentioned above, the vpda neurons in both *sns* mutants showed a significantly increased number of the third order dendrites in comparison to the control (see Results Figure 27 and 28), whereas other features of the dendritic arbours were not changed. The normal length of the primary and secondary dendrites of the vpda neuron in both *sns* mutants indicates that the increased number of third order branches was not due to a developmental delay. In contrast, the dendritic arbours of the dorsal class I md-da neuron ddaE looked somewhat reduced or were slightly shifted in their positions in the line *sns*⁹⁰⁴⁽³⁾ and *sns*^{S660}. This phenotype was more penetrant in the *sns*^{S660} mutant. The quantifications of the dendritic arbour characteristics of the ddaE in the *sns*^{S660} mutant revealed a significantly reduced length of the primary dendrite and a reduced number of secondary dendrites in comparison with the control. No quantitative alterations of the ddaE dendrites could be detected in the line *sns*⁹⁰⁴⁽³⁾. What might be the reason for the variations of the dendritic phenotype in the ddaE neuron between line *sns*⁹⁰⁴⁽³⁾ and *sns*^{S660}? The loss of Sns could be compensated by a partially redundant

signal pathway during the development of the ddaE md-da neuron. Hence, in 20-21h AEL old embryos, the loss of *sns* expression would not produce the LOF phenotype of the dendrites with a constant high penetrance.

However, the dendritic phenotypes in the class I md-da neurons vpda and ddaE were opposite. The dendrites of the vpda neurons were mildly overbranched in both *sns* mutants, whereas the dendritic arbours complexity of the ddaE neuron was subtly reduced in the *sns*^{S660} mutant. Thus, a general definition of the role of the gene *sns* for the dendrite development of class I md-da neurons can not be formulated at the moment. What could be an explanation for this finding? Assuming that *sns* has a cell-autonomous function in class I md-da neurons, it could potentially affect different intracellular signal pathways in vpda and ddaE neurons, which are responsible for the distinct functions of *sns* in both neurons. This would require the assumption that the ddaE and the vpda neurons vary in their expression profiles, which is supported by the different proneuronal origin of both cells (Jarman *et al.*, 1993).

Although, it could be shown in this study that the loss of the body wall musculature in *blown fuse*¹ mutants did not change the dendritic morphology of the vpda neuron, it does not consequently mean that the same is true for the ddaE neuron. Despite the low chance for such a case, it is conceivable that the development of the ddaE neurons is indirectly modified by the loss of the musculature. How could this fit to the rescue experiment in the dorsal cluster of the line *sns*⁹⁰⁴, were the overbranching phenotype of the md-da neurons was converted to control level by the expression FL-*sns* specifically in this neurons? The dendrites of the ddaE neurons were not overbranched in *sns* mutants, which means that this neuron did not contribute to the phenotype of the dorsal cluster dendrites in the line *sns*⁹⁰⁴. Furthermore, a rescue of the ddaE neuron would not be detectable in this experimental setup, since the expression pattern of the *109(2)80 GAL4* driver impedes the study of the dendritic morphology of individual md-da neurons.

As already mentioned above, the dendrites of the dorsal class I md-da neuron ddaE did not show an overbranching phenotype. In addition, the

dendrites of the dorsal class IV md-da neurons were not altered in both *sns* mutants. Thus, the dorsal class I and class IV md-da neurons are not responsible for the increased number of termini in the dendritic field of the dorsal cluster md-da neurons in the line *sns*⁹⁰⁴. Consequently, the overbranching phenotype in this line must be due to an abnormal branch formation in the dendrites of the dorsal class II or class III md-da neurons. Up to date, there are no *GAL4* driver that allow to label specifically these md-da neurons during embryonic stages. For this reason, a FLP-out technique was successfully tested for its ability to label individual md-da neurons in the dorsal cluster. By using this approach, it is possible to examine the dendritic phenotype of single md-da neurons in a *sns* mutant at the embryonic stage 17.

In a complementary approach, MARCM analysis would be helpful to find the md-da neurons that are responsible for the overbranching of the dorsal cluster dendrites in the line *sns*⁹⁰⁴ and to clarify the discrepancy between the dendritic phenotypes of the *ddaE* and *vpda* neurons. Both techniques should allow to define the mode of action of *Sns* during dendrite morphogenesis of the md-da neurons.

5.15. The role of *Sns* during the formation of dendrites

Based on its mutant phenotype, *Sns* is required for the first steps of myoblast fusion in *Drosophila* (Bour *et al.*, 2000). Through its interaction with *Duf* or *Rst*, *Sns* mediates the initial attraction (Ruiz-Gomez *et al.*, 2000; Strunkelnberg *et al.*, 2001) and adherence (Galletta *et al.*, 2004) between the two different myoblast types at the onset of muscle formation during the embryonic development. The interaction between *Sns* and *Duf* (Galletta *et al.*, 2004; Kesper *et al.*, 2007) recruits molecules to the site of the myoblast fusion in FCMs (Kim *et al.*, 2007; Massarwa *et al.*, 2007) and muscle founder cells (Chen *et al.*, 2006; Chen and Olson, 2001; Menon and Chia, 2001) that are involved in the modulation of the actin-cytoskeleton. In FCMs, *Sns* binds to the SH2-SH3 adaptor protein *D-Crk* that in turn recruits *Solitary*, a Wasp interaction protein, and the Wasp/Arp2-3 complex (Kim *et al.*, 2007;

Massarwa *et al.*, 2007). Solitary and Wasp are needed for the localised induction of actin polymerisation at the sites of myoblast fusion (Kim *et al.*, 2007). Moreover, this actin-polymerisation is essential for the directed transport of exocytotic vesicles towards the area between aligned myoblasts that is defined by the interaction of Sns and Duf (Kim *et al.*, 2007). Hence, Sns provides a positional cue for actin polymerisation and consequently the transport of secretory vesicles. Similarly, the vertebrate homologue of Sns, named Nephtrin (Bour *et al.*, 2000; Putaala *et al.*, 2001), binds the SH2-SH3 adaptor protein Nck that is known to modulate the actin cytoskeleton through its association with Wasp (Buday *et al.*, 2002; Jones *et al.*, 2006). Nephtrin is expressed in kidney, pancreas and the brain, where it is localised in the cerebellum and the mesencephalon (Putaala *et al.*, 2001). The polymerisation of the actin cytoskeleton upon interaction of Nephtrin and Nck is crucial for the maintenance of the podocyte cellular junction, and has been shown to induce process formation in HEK-293T cells (Jones *et al.*, 2006; Li *et al.*, 2006).

Furthermore, the binding of Nck to Nephtrin and the resulting actin polymerisation depends on a Tyrosin phosphorylation of the cytoplasmic tail of Nephtrin through the Src-family kinase Fyn (Jones *et al.*, 2006; Li *et al.*, 2006). Interestingly, Fyn is required for different aspects of neuronal development, like the semaphorin dependent formation of dendritic branches and spine maturation in hippocampal cells (Morita *et al.*, 2006) or axon guidance through phosphorylation of the Netrin receptor DCC (Meriane *et al.*, 2004). Although an interaction of Sns with a member of the Src kinase family has not been shown so far, the presence of two putative kinase recognition sites (Artero *et al.*, 2001) suggest that the Sns function might be also controlled by phosphorylation of its cytoplasmic tail, which could be provided by Src kinases.

During myoblast fusion in *Drosophila*, the function of Sns depends on its interaction with two other transmembrane molecules of the Ig-superfamily, which are called Duf and Rst (Galletta *et al.*, 2004; Ruiz-Gomez *et al.*, 2000; Strunkelberg *et al.*, 2001). A broad functional diversity has been reported for Rst in *Drosophila*, where it is essential for axon guidance in the visual system (Ramos *et al.*, 1993; Schneider *et al.*, 1995) and formation of the complex eye

(Reiter *et al.*, 1996). Could the function of Sns during dendrite morphogenesis be also affected by these two molecules? In vertebrates, Nephrin interacts with Neph1 and Neph2, which represent homologues of roughest (Gerke *et al.*, 2003). Both Neph proteins are expressed in kidney and the brain, specifically in dendrites and synapses of Purkinje cells (Gerke *et al.*, 2006). A direct interaction between Nephrin and Neph1 has not been shown so far, but appears very likely due to a similar expression pattern. What could be the function of an interaction between Sns and Rst? As mentioned above, Rst is involved in the guidance of axons in the visual system of *Drosophila* (Schneider *et al.*, 1995). Moreover, the homologue of Rst in *C.elegans*, SYG-1, is expressed in specific motorneurons and controls the positioning of synapses through its interaction with an unknown ligand expressed by epidermal guidepost cells (Shen and Bargmann, 2003). Hence, Rst seems to be involved in targeting events within the nervous system and could serve as an extrinsic cue for Sns that might control the spatiotemporal formation of dendritic branches.

It seems that the members of the Nephrin subfamily of transmembrane adhesion molecules organise the actin polymerisation machinery to specific sites, through interaction with SH2-SH3 adaptor proteins that in turn activate asp A possible function of Sns in the nervous system is supported by the expression pattern of vertebrate Nephrins. The ability of the Nephrin-Nck complex to induce “spikey” protrusion in HEK-293T cells shows that the rearrangement of the actin cytoskeleton through Nephrin can cause morphological changes of cells (Li *et al.*, 2006). Thus, Sns might regulate the branching of dendrites through a targeted polymerisation of the actin cytoskeleton. It could serve as a positional cue that determines where new branches would be added and guide the delivery of exocytotic vesicles to the new branch. In addition, the activity of Sns might be regulated through phosphorylation of its intracellular tail or interaction with other adhesion molecules from the extracellular environment.

Accordingly, this idea would imply that the action of Sns promotes the formation of new branches on the dendritic arbour of md-da neurons. How does this fit to the phenotypes seen in the vpda and ddaE neurons? If Sns

promotes the branch formation in dendrites, the dendrites of md-da neurons in *sns* mutants should consequently create less branches. This is partially seen in ddaE neurons of mutant line *sns*^{S660}. In contrast, the vpda neuron produced a reliable overbranching phenotype in *sns* mutants, which means that Sns limits the formation of high order branches in this neuron. This could indicate that Sns is also involved in a different signal event that limits the activity of an independent cellular machinery that is responsible for the creation of high order branches.

5.16. Outlook

For several reasons, the nature of the Sns function in dendrite morphogenesis can not be yet conclusively described here. First, the individual dendritic phenotypes of each md-da neuron in *sns* mutants could not be demonstrated so far. Due to this limitation, the overbranching phenotype of the dorsal cluster neurons in the line *sns*⁹⁰⁴ can not be ultimately resolved. Furthermore, a cell-autonomous function of *sns* in dendrite differentiation of md-da neurons, as suggested by the cell-specific rescue, needs to be confirmed. Useful insights, to clarify these issues, could be provided by completed MARCM and the FLP-out labeling of md-da neurons. In the case that a cell-autonomous function of *sns* in md-da neurons is verified by MARCM, it would be necessary to explore the cellular function of Sns during the dendritic development of these neurons. Genetic analysis of putative intracellular interactors, known from the studies of myoblast fusion or Sns homologues in other model systems, could provide a starting point to understand how this molecule acts to control branch formation of md-da neurons. In addition to classical mutant analysis in the embryos, the usage of *UAS*-RNAi lines to knock down candidate genes specifically in md-da neuron could be an interesting tool to conduct such an analysis. Moreover, mutations of the putative phosphorylation sites in the intracellular tail of Sns, could reveal whether kinase activity is involved in the regulation of Sns. Possible extracellular ligands of Sns required for dendrite development are not known, but could be useful for the understanding of the

biological role of Sns. Likely candidates are Duf and especially Rst that are known interactors of Sns during myoblast fusion.

Finally, the analysis of Sns in other neuronal model systems of *Drosophila* could offer the chance to prove whether Sns is a more general regulator of dendrite development and allow studying its function from a different point of view.

6. Bibliography

Acebes, A. and Ferrus, A. (2000). Cellular and molecular features of axon collaterals and dendrites. *Trends Neurosci* **23**, 557-65.

Adams, C. M., Anderson, M. G., Motto, D. G., Price, M. P., Johnson, W. A. and Welsh, M. J. (1998). Ripped pocket and pickpocket, novel Drosophila DEG/ENaC subunits expressed in early development and in mechanosensory neurons. *J Cell Biol* **140**, 143-52.

Ainsley, J. A., Pettus, J. M., Bosenko, D., Gerstein, C. E., Zinkevich, N., Anderson, M. G., Adams, C. M., Welsh, M. J. and Johnson, W. A. (2003). Enhanced locomotion caused by loss of the Drosophila DEG/ENaC protein Pickpocket1. *Curr Biol* **13**, 1557-63.

Andersen, R., Li, Y., Resseguie, M. and Brenman, J. E. (2005). Calcium/calmodulin-dependent protein kinase II alters structural plasticity and cytoskeletal dynamics in Drosophila. *J Neurosci* **25**, 8878-88.

Artero, R. D., Castanon, I. and Baylies, M. K. (2001). The immunoglobulin-like protein Hibris functions as a dose-dependent regulator of myoblast fusion and is differentially controlled by Ras and Notch signaling. *Development* **128**, 4251-64.

Balagopalan, L., Chen, M. H., Geisbrecht, E. R. and Abmayr, S. M. (2006). The CDM superfamily protein MBC directs myoblast fusion through a mechanism that requires phosphatidylinositol 3,4,5-triphosphate binding but is independent of direct interaction with DCrk. *Mol Cell Biol* **26**, 9442-55.

Bate, M. (1990). The embryonic development of larval muscles in Drosophila. *Development* **110**, 791-804.

Bate, M. (1993). The mesoderm and its derivatives. In *The Development of Drosophila melanogaster*, vol. 2 (ed. M. Bate and A. M. Arias), pp. 1013-1090. Cold Spring Harbour: Cold Spring Harbour Laboratory Press.

Baylies, M. K., Bate, M. and Ruiz Gomez, M. (1998). Myogenesis: a view from Drosophila. *Cell* **93**, 921-7.

Bellen, H. J., Levis, R. W., Liao, G., He, Y., Carlson, J. W., Tsang, G., Evans-Holm, M., Hiesinger, P. R., Schulze, K. L., Rubin, G. M. et al. (2004). The BDGP gene disruption project: single transposon insertions associated with 40% of *Drosophila* genes. *Genetics* **167**, 761-81.

Berger, J., Suzuki, T., Senti, K. A., Stubbs, J., Schaffner, G. and Dickson, B. J. (2001). Genetic mapping with SNP markers in *Drosophila*. *Nat Genet* **29**, 475-81.

Bettencourt da Cruz, A., Schwarzel, M., Schulze, S., Niyati, M., Heisenberg, M. and Kretzschmar, D. (2005). Disruption of the MAP1B-related protein FUTSCH leads to changes in the neuronal cytoskeleton, axonal transport defects, and progressive neurodegeneration in *Drosophila*. *Mol Biol Cell* **16**, 2433-42.

Bodmer, R. and Jan, Y. N. (1987). Morphological differentiation of the embryonic peripheral neurons in *Drosophila*. *Roux's Arch Dev Biol* **196**, 67-77.

Bonhoeffer, T. and Yuste, R. (2002). Spine motility. Phenomenology, mechanisms, and function. *Neuron* **35**, 1019-27.

Borst, A. and Haag, J. (2002). Neural networks in the cockpit of the fly. *J Comp Physiol A Neuroethol Sens Neural Behav Physiol* **188**, 419-37.

Bour, B. A., Chakravarti, M., West, J. M. and Abmayr, S. M. (2000). *Drosophila* SNS, a member of the immunoglobulin superfamily that is essential for myoblast fusion. *Genes Dev* **14**, 1498-511.

Brand, A. H. and Perrimon, N. (1993). Targeted gene expression as a means of altering cell fates and generating dominant phenotypes. *Development* **118**, 401-15.

Brewster, R. and Bodmer, R. (1995). Origin and specification of type II sensory neurons in *Drosophila*. *Development* **121**, 2923-36.

Buday, L., Wunderlich, L. and Tamas, P. (2002). The Nck family of adapter proteins: regulators of actin cytoskeleton. *Cell Signal* **14**, 723-31.

Bustelo, X. R., Sauzeau, V. and Berenjano, I. M. (2007). GTP-binding proteins of the Rho/Rac family: regulation, effectors and functions in vivo. *Bioessays* **29**, 356-70.

Calabrese, B., Wilson, M. S. and Halpain, S. (2006). Development and regulation of dendritic spine synapses. *Physiology (Bethesda)* **21**, 38-47.

Carmena, A., Bate, M. and Jimenez, F. (1995). Lethal of scute, a proneural gene, participates in the specification of muscle progenitors during *Drosophila* embryogenesis. *Genes Dev* **9**, 2373-83.

Casso, D., Ramirez-Weber, F. and Kornberg, T. B. (2000). GFP-tagged balancer chromosomes for *Drosophila melanogaster*. *Mech Dev* **91**, 451-4.

Chen, B., Chu, T., Harms, E., Gergen, J. P. and Strickland, S. (1998). Mapping of *Drosophila* mutations using site-specific male recombination. *Genetics* **149**, 157-63.

Chen, B. E., Kondo, M., Garnier, A., Watson, F. L., Puettmann-Holgado, R., Lamar, D. R. and Schmucker, D. (2006). The molecular diversity of Dscam is functionally required for neuronal wiring specificity in *Drosophila*. *Cell* **125**, 607-20.

Chen, E. H. and Olson, E. N. (2001). Antisocial, an intracellular adaptor protein, is required for myoblast fusion in *Drosophila*. *Dev Cell* **1**, 705-15.

Chen, E. H., Pryce, B. A., Tzeng, J. A., Gonzalez, G. A. and Olson, E. N. (2003). Control of myoblast fusion by a guanine nucleotide exchange factor, loner, and its effector ARF6. *Cell* **114**, 751-62.

Cho, R. J., Mindrinos, M., Richards, D. R., Sapolsky, R. J., Anderson, M., Drenkard, E., Dewdney, J., Reuber, T. L., Stammers, M., Federspiel, N. et al. (1999). Genome-wide mapping with biallelic markers in *Arabidopsis thaliana*. *Nat Genet* **23**, 203-7.

Craig, A. M. and Banker, G. (1994). Neuronal polarity. *Annu Rev Neurosci* **17**, 267-310.

Dickson, B. J. (2002). Molecular mechanisms of axon guidance. *Science* **298**, 1959-64.

Dietzl, G., Chen, D., Schnorrer, F., Su, K. C., Barinova, Y., Fellner, M., Gasser, B., Kinsey, K., Oettel, S., Scheiblauer, S. et al. (2007). A genome-wide transgenic RNAi library for conditional gene inactivation in *Drosophila*. *Nature* **448**, 151-6.

Doberstein, S. K., Fetter, R. D., Mehta, A. Y. and Goodman, C. S. (1997). Genetic analysis of myoblast fusion: blown fuse is required for progression beyond the prefusion complex. *J Cell Biol* **136**, 1249-61.

Duan, H., Skeath, J. B. and Nguyen, H. T. (2001). Drosophila *Lame duck*, a novel member of the Gli superfamily, acts as a key regulator of myogenesis by controlling fusion-competent myoblast development. *Development* **128**, 4489-500.

Dworak, H. A., Charles, M. A., Pellerano, L. B. and Sink, H. (2001). Characterization of *Drosophila hibris*, a gene related to human nephrin. *Development* **128**, 4265-76.

Dworak, H. A. and Sink, H. (2002). Myoblast fusion in *Drosophila*. *Bioessays* **24**, 591-601.

Emoto, K., He, Y., Ye, B., Grueber, W. B., Adler, P. N., Jan, L. Y. and Jan, Y. N. (2004). Control of dendritic branching and tiling by the Tricornered-kinase/Furry signaling pathway in *Drosophila* sensory neurons. *Cell* **119**, 245-56.

Emoto, K., Parrish, J. Z., Jan, L. Y. and Jan, Y. N. (2006). The tumour suppressor Hippo acts with the NDR kinases in dendritic tiling and maintenance. *Nature* **443**, 210-3.

Erickson, M. R., Galletta, B. J. and Abmayr, S. M. (1997). *Drosophila* myoblast *city* encodes a conserved protein that is essential for myoblast fusion, dorsal closure, and cytoskeletal organization. *J Cell Biol* **138**, 589-603.

Faix, J. and Rottner, K. (2006). The making of filopodia. *Curr Opin Cell Biol* **18**, 18-25.

Furrer, M. P., Kim, S., Wolf, B. and Chiba, A. (2003). Robo and Frazzled/DCC mediate dendritic guidance at the CNS midline. *Nat Neurosci* **6**, 223-30.

Galletta, B. J., Chakravarti, M., Banerjee, R. and Abmayr, S. M. (2004). SNS: Adhesive properties, localization requirements and ectodomain dependence in S2 cells and embryonic myoblasts. *Mech Dev* **121**, 1455-68.

Galletta, B. J., Niu, X. P., Erickson, M. R. and Abmayr, S. M. (1999). Identification of a *Drosophila* homologue to vertebrate Crk by interaction with MBC. *Gene* **228**, 243-52.

Gao, F. B., Brenman, J. E., Jan, L. Y. and Jan, Y. N. (1999). Genes regulating dendritic outgrowth, branching, and routing in *Drosophila*. *Genes Dev* **13**, 2549-61.

Gao, F. B., Kohwi, M., Brenman, J. E., Jan, L. Y. and Jan, Y. N. (2000). Control of dendritic field formation in *Drosophila*: the roles of *flamingo* and competition between homologous neurons. *Neuron* **28**, 91-101.

Gerke, P., Benzing, T., Hohne, M., Kispert, A., Frotscher, M., Walz, G. and Kretz, O. (2006). Neuronal expression and interaction with the synaptic protein CASK suggest a role for Neph1 and Neph2 in synaptogenesis. *J Comp Neurol* **498**, 466-75.

Gerke, P., Huber, T. B., Sellin, L., Benzing, T. and Walz, G. (2003). Homodimerization and heterodimerization of the glomerular podocyte proteins nephrin and NEPH1. *J Am Soc Nephrol* **14**, 918-26.

Giot, L., Bader, J. S., Brouwer, C., Chaudhuri, A., Kuang, B., Li, Y., Hao, Y. L., Ooi, C. E., Godwin, B., Vitols, E. et al. (2003). A protein interaction map of *Drosophila melanogaster*. *Science* **302**, 1727-36.

Grueber, W. B., Jan, L. Y. and Jan, Y. N. (2002). Tiling of the *Drosophila* epidermis by multidendritic sensory neurons. *Development* **129**, 2867-78.

Grueber, W. B., Jan, L. Y. and Jan, Y. N. (2003a). Different levels of the homeodomain protein cut regulate distinct dendrite branching patterns of *Drosophila* multidendritic neurons. *Cell* **112**, 805-18.

Grueber, W. B., Ye, B., Moore, A. W., Jan, L. Y. and Jan, Y. N. (2003b). Dendrites of distinct classes of *Drosophila* sensory neurons show different capacities for homotypic repulsion. *Curr Biol* **13**, 618-26.

Grueber, W. B., Ye, B., Yang, C. H., Younger, S., Borden, K., Jan, L. Y. and Jan, Y. N. (2007). Projections of *Drosophila* multidendritic neurons in the central nervous system: links with peripheral dendrite morphology. *Development* **134**, 55-64.

Hakeda-Suzuki, S., Ng, J., Tzu, J., Dietzl, G., Sun, Y., Harms, M., Nardine, T., Luo, L. and Dickson, B. J. (2002). Rac function and regulation during *Drosophila* development. *Nature* **416**, 438-42.

Hand, R., Bortone, D., Mattar, P., Nguyen, L., Heng, J. I., Guerrier, S., Boutt, E., Peters, E., Barnes, A. P., Parras, C. et al. (2005). Phosphorylation of Neurogenin2 specifies the migration properties and the dendritic morphology of pyramidal neurons in the neocortex. *Neuron* **48**, 45-62.

Hanley, J. G., Koulen, P., Bedford, F., Gordon-Weeks, P. R. and Moss, S. J. (1999). The protein MAP-1B links GABA(C) receptors to the cytoskeleton at retinal synapses. *Nature* **397**, 66-9.

Hausser, M., Spruston, N. and Stuart, G. J. (2000). Diversity and dynamics of dendritic signaling. *Science* **290**, 739-44.

Horton, A. C. and Ehlers, M. D. (2004). Secretory trafficking in neuronal dendrites. *Nat Cell Biol* **6**, 585-91.

Hoskins, R. A., Phan, A. C., Naeemuddin, M., Mapa, F. A., Ruddy, D. A., Ryan, J. J., Young, L. M., Wells, T., Kopczynski, C. and Ellis, M. C. (2001). Single nucleotide polymorphism markers for genetic mapping in *Drosophila melanogaster*. *Genome Res* **11**, 1100-13.

Huang, E. J. and Reichardt, L. F. (2003). Trk receptors: roles in neuronal signal transduction. *Annu Rev Biochem* **72**, 609-42.

Huet, F., Lu, J. T., Myrick, K. V., Baugh, L. R., Crosby, M. A. and Gelbart, W. M. (2002). A deletion-generator compound element allows deletion saturation analysis for genomewide phenotypic annotation. *Proc Natl Acad Sci U S A* **99**, 9948-53.

Hughes, C. L. and Thomas, J. B. (2007). A sensory feedback circuit coordinates muscle activity in *Drosophila*. *Mol Cell Neurosci* **35**, 383-96.

Hughes, M. E., Bortnick, R., Tsubouchi, A., Baumer, P., Kondo, M., Uemura, T. and Schmucker, D. (2007). Homophilic Dscam interactions control complex dendrite morphogenesis. *Neuron* **54**, 417-27.

Hummel, T., Krukkert, K., Roos, J., Davis, G. and Klambt, C. (2000). *Drosophila* Futsch/22C10 is a MAP1B-like protein required for dendritic and axonal development. *Neuron* **26**, 357-70.

Hummel, T. and Zipursky, S. L. (2004). Afferent induction of olfactory glomeruli requires N-cadherin. *Neuron* **42**, 77-88.

Jan, Y. N. and Jan, L. Y. (1993). The Peripheral Nervous system. In *The Development of Drosophila melanogaster*, vol. 2 (ed. M. Bate and A. M. Arias), pp. 1207-1244. Cold Spring Harbour: Cold Spring Harbour Laboratory Press.

Jarman, A. P., Grau, Y., Jan, L. Y. and Jan, Y. N. (1993). *atonal* is a proneural gene that directs chordotonal organ formation in the *Drosophila* peripheral nervous system. *Cell* **73**, 1307-21.

Jefferis, G. S. and Hummel, T. (2006). Wiring specificity in the olfactory system. *Semin Cell Dev Biol* **17**, 50-65.

Johnson, O. L. and Ouimet, C. C. (2006). A regulatory role for actin in dendritic spine proliferation. *Brain Res* **1113**, 1-9.

Jones, N., Blasutig, I. M., Eremina, V., Ruston, J. M., Bladt, F., Li, H., Huang, H., Larose, L., Li, S. S., Takano, T. et al. (2006). Nck adaptor proteins link nephrin to the actin cytoskeleton of kidney podocytes. *Nature* **440**, 818-23.

Kaplan, D. R. and Miller, F. D. (2000). Neurotrophin signal transduction in the nervous system. *Curr Opin Neurobiol* **10**, 381-91.

Kaufmann, W. E. and Moser, H. W. (2000). Dendritic anomalies in disorders associated with mental retardation. *Cereb Cortex* **10**, 981-91.

Kesper, D. A., Stute, C., Buttgereit, D., Kreiskother, N., Vishnu, S., Fischbach, K. F. and Renkawitz-Pohl, R. (2007). Myoblast fusion in *Drosophila melanogaster* is mediated through a fusion-restricted myogenic-adhesive structure (FuRMAS). *Dev Dyn* **236**, 404-15.

Kim, M. D., Jan, L. Y. and Jan, Y. N. (2006). The bHLH-PAS protein Spineless is necessary for the diversification of dendrite morphology of *Drosophila* dendritic arborization neurons. *Genes Dev* **20**, 2806-19.

Kim, S., Shilagardi, K., Zhang, S., Hong, S. N., Sens, K. L., Bo, J., Gonzalez, G. A. and Chen, E. H. (2007). A critical function for the actin cytoskeleton in targeted exocytosis of prefusion vesicles during myoblast fusion. *Dev Cell* **12**, 571-86.

Koch, R., van Luenen, H. G., van der Horst, M., Thijssen, K. L. and Plasterk, R. H. (2000). Single nucleotide polymorphisms in wild isolates of *Caenorhabditis elegans*. *Genome Res* **10**, 1690-6.

Komiyama, T., Johnson, W. A., Luo, L. and Jefferis, G. S. (2003). From lineage to wiring specificity. POU domain transcription factors control precise connections of *Drosophila* olfactory projection neurons. *Cell* **112**, 157-67.

Komiyama, T., Sweeney, L. B., Schuldiner, O., Garcia, K. C. and Luo, L. (2007). Graded expression of semaphorin-1a cell-autonomously directs dendritic targeting of olfactory projection neurons. *Cell* **128**, 399-410.

Konur, S. and Ghosh, A. (2005). Calcium signaling and the control of dendritic development. *Neuron* **46**, 401-5.

Lee, A., Li, W., Xu, K., Bogert, B. A., Su, K. and Gao, F. B. (2003). Control of dendritic development by the *Drosophila* fragile X-related gene involves the small GTPase Rac1. *Development* **130**, 5543-52.

Lee, T. and Luo, L. (1999). Mosaic analysis with a repressible cell marker for studies of gene function in neuronal morphogenesis. *Neuron* **22**, 451-61.

Lee, Y., Lee, Y., Lee, J., Bang, S., Hyun, S., Kang, J., Hong, S. T., Bae, E., Kaang, B. K. and Kim, J. (2005). Pyrexia is a new thermal transient receptor potential channel endowing tolerance to high temperatures in *Drosophila melanogaster*. *Nat Genet* **37**, 305-10.

Li, H., Zhu, J., Aoudjit, L., Latreille, M., Kawachi, H., Larose, L. and Takano, T. (2006). Rat nephrin modulates cell morphology via the adaptor protein Nck. *Biochem Biophys Res Commun* **349**, 310-6.

Li, W., Li, Y. and Gao, F. B. (2005). Abelson, enabled, and p120 catenin exert distinct effects on dendritic morphogenesis in *Drosophila*. *Dev Dyn* **234**, 512-22.

Li, W., Wang, F., Menut, L. and Gao, F. B. (2004). BTB/POZ-zinc finger protein abruptly suppresses dendritic branching in a neuronal subtype-specific and dosage-dependent manner. *Neuron* **43**, 823-34.

Liao, G. C., Rehm, E. J. and Rubin, G. M. (2000). Insertion site preferences of the P transposable element in *Drosophila melanogaster*. *Proc Natl Acad Sci U S A* **97**, 3347-51.

Lin, H. H., Lai, J. S., Chin, A. L., Chen, Y. C. and Chiang, A. S. (2007). A map of olfactory representation in the *Drosophila* mushroom body. *Cell* **128**, 1205-17.

Liu, L., Yermolaieva, O., Johnson, W. A., Abboud, F. M. and Welsh, M. J. (2003). Identification and function of thermosensory neurons in *Drosophila* larvae. *Nat Neurosci* **6**, 267-73.

Lohmann, C., Myhr, K. L. and Wong, R. O. (2002). Transmitter-evoked local calcium release stabilizes developing dendrites. *Nature* **418**, 177-81.

- London, M. and Hausser, M.** (2005). Dendritic computation. *Annu Rev Neurosci* **28**, 503-32.
- Luo, L.** (2002). Actin cytoskeleton regulation in neuronal morphogenesis and structural plasticity. *Annu Rev Cell Dev Biol* **18**, 601-35.
- Luo, L., Liao, Y. J., Jan, L. Y. and Jan, Y. N.** (1994). Distinct morphogenetic functions of similar small GTPases: Drosophila Drac1 is involved in axonal outgrowth and myoblast fusion. *Genes Dev* **8**, 1787-802.
- Mack, T. G., Koester, M. P. and Pollerberg, G. E.** (2000). The microtubule-associated protein MAP1B is involved in local stabilization of turning growth cones. *Mol Cell Neurosci* **15**, 51-65.
- Martin, S. G., Dobi, K. C. and St Johnston, D.** (2001). A rapid method to map mutations in Drosophila. *Genome Biol* **2**, RESEARCH0036.
- Massarwa, R., Carmon, S., Shilo, B. Z. and Schejter, E. D.** (2007). WIP/WASp-based actin-polymerization machinery is essential for myoblast fusion in Drosophila. *Dev Cell* **12**, 557-69.
- Matthews, B. J., Kim, M. E., Flanagan, J. J., Hattori, D., Clemens, J. C., Zipursky, S. L. and Grueber, W. B.** (2007). Dendrite self-avoidance is controlled by Dscam. *Cell* **129**, 593-604.
- Matus, A.** (1994). Stiff microtubules and neuronal morphology. *Trends Neurosci* **17**, 19-22.
- Matus, A.** (2005). Growth of dendritic spines: a continuing story. *Curr Opin Neurobiol* **15**, 67-72.
- McAllister, A. K., Katz, L. C. and Lo, D. C.** (1996). Neurotrophin regulation of cortical dendritic growth requires activity. *Neuron* **17**, 1057-64.
- Menon, S. D. and Chia, W.** (2001). Drosophila rolling pebbles: a multidomain protein required for myoblast fusion that recruits D-Titin in response to the myoblast attractant Dumbfounded. *Dev Cell* **1**, 691-703.
- Meriane, M., Tcherkezian, J., Webber, C. A., Danek, E. I., Triki, I., McFarlane, S., Bloch-Gallego, E. and Lamarche-Vane, N.** (2004). Phosphorylation of DCC by Fyn mediates Netrin-1 signaling in growth cone guidance. *J Cell Biol* **167**, 687-98.

Meyer-Franke, A., Wilkinson, G. A., Kruttgen, A., Hu, M., Munro, E., Hanson, M. G., Jr., Reichardt, L. F. and Barres, B. A. (1998). Depolarization and cAMP elevation rapidly recruit TrkB to the plasma membrane of CNS neurons. *Neuron* **21**, 681-93.

Moore, A. W., Jan, L. Y. and Jan, Y. N. (2002). hamlet, a binary genetic switch between single- and multiple- dendrite neuron morphology. *Science* **297**, 1355-8.

Morita, A., Yamashita, N., Sasaki, Y., Uchida, Y., Nakajima, O., Nakamura, F., Yagi, T., Taniguchi, M., Usui, H., Katoh-Semba, R. et al. (2006). Regulation of dendritic branching and spine maturation by semaphorin3A-Fyn signaling. *J Neurosci* **26**, 2971-80.

Nairz, K., Stocker, H., Schindelholz, B. and Hafen, E. (2002). High-resolution SNP mapping by denaturing HPLC. *Proc Natl Acad Sci U S A* **99**, 10575-80.

Nolan, K. M., Barrett, K., Lu, Y., Hu, K. Q., Vincent, S. and Settleman, J. (1998). Myoblast city, the Drosophila homolog of DOCK180/CED-5, is required in a Rac signaling pathway utilized for multiple developmental processes. *Genes Dev* **12**, 3337-42.

Parks, A. L., Cook, K. R., Belvin, M., Dompe, N. A., Fawcett, R., Huppert, K., Tan, L. R., Winter, C. G., Bogart, K. P., Deal, J. E. et al. (2004). Systematic generation of high-resolution deletion coverage of the Drosophila melanogaster genome. *Nat Genet* **36**, 288-92.

Parrish, J. Z., Emoto, K., Jan, L. Y. and Jan, Y. N. (2007a). Polycomb genes interact with the tumor suppressor genes hippo and warts in the maintenance of Drosophila sensory neuron dendrites. *Genes Dev* **21**, 956-72.

Parrish, J. Z., Emoto, K., Kim, M. D. and Jan, Y. N. (2007b). Mechanisms that Regulate Establishment, Maintenance, and Remodeling of Dendritic Fields. *Annu Rev Neurosci* **30**, 399-423.

Parrish, J. Z., Kim, M. D., Jan, L. Y. and Jan, Y. N. (2006). Genome-wide analyses identify transcription factors required for proper morphogenesis of Drosophila sensory neuron dendrites. *Genes Dev* **20**, 820-35.

Patapoutian, A. and Reichardt, L. F. (2001). Trk receptors: mediators of neurotrophin action. *Curr Opin Neurobiol* **11**, 272-80.

Paululat, A., Holz, A. and Renkawitz-Pohl, R. (1999). Essential genes for myoblast fusion in Drosophila embryogenesis. *Mech Dev* **83**, 17-26.

Pedrotti, B., Colombo, R. and Islam, K. (1994). Microtubule associated protein MAP1A is an actin-binding and crosslinking protein. *Cell Motil Cytoskeleton* **29**, 110-6.

Polleux, F., Morrow, T. and Ghosh, A. (2000). Semaphorin 3A is a chemoattractant for cortical apical dendrites. *Nature* **404**, 567-73.

Putala, H., Soininen, R., Kilpelainen, P., Wartiovaara, J. and Tryggvason, K. (2001). The murine nephrin gene is specifically expressed in kidney, brain and pancreas: inactivation of the gene leads to massive proteinuria and neonatal death. *Hum Mol Genet* **10**, 1-8.

Ramos, R. G., Igloi, G. L., Lichte, B., Baumann, U., Maier, D., Schneider, T., Brandstatter, J. H., Frohlich, A. and Fischbach, K. F. (1993). The irregular chiasm C-roughest locus of Drosophila, which affects axonal projections and programmed cell death, encodes a novel immunoglobulin-like protein. *Genes Dev* **7**, 2533-47.

Rau, A., Buttgereit, D., Holz, A., Fetter, R., Doberstein, S. K., Paululat, A., Staudt, N., Skeath, J., Michelson, A. M. and Renkawitz-Pohl, R. (2001). rolling pebbles (rols) is required in Drosophila muscle precursors for recruitment of myoblasts for fusion. *Development* **128**, 5061-73.

Redmond, L., Kashani, A. H. and Ghosh, A. (2002). Calcium regulation of dendritic growth via CaM kinase IV and CREB-mediated transcription. *Neuron* **34**, 999-1010.

Reiter, C., Schimansky, T., Nie, Z. and Fischbach, K. F. (1996). Reorganization of membrane contacts prior to apoptosis in the Drosophila retina: the role of the IrreC-rst protein. *Development* **122**, 1931-40.

Ruiz-Gomez, M. (1998). Muscle patterning and specification in Drosophila. *Int J Dev Biol* **42**, 283-90.

Ruiz-Gomez, M., Coutts, N., Price, A., Taylor, M. V. and Bate, M. (2000). Drosophila dumbfounded: a myoblast attractant essential for fusion. *Cell* **102**, 189-98.

Ruiz-Gomez, M., Coutts, N., Suster, M. L., Landgraf, M. and Bate, M. (2002). myoblasts incompetent encodes a zinc finger transcription factor required to specify fusion-competent myoblasts in Drosophila. *Development* **129**, 133-41.

Ruiz Gomez, M. and Bate, M. (1997). Segregation of myogenic lineages in Drosophila requires numb. *Development* **124**, 4857-66.

Rushton, E., Drysdale, R., Abmayr, S. M., Michelson, A. M. and Bate, M. (1995). Mutations in a novel gene, myoblast city, provide evidence in support of the founder cell hypothesis for Drosophila muscle development. *Development* **121**, 1979-88.

Ryder, E., Blows, F., Ashburner, M., Bautista-Llacer, R., Coulson, D., Drummond, J., Webster, J., Gubb, D., Gunton, N., Johnson, G. et al. (2004). The DrosDel collection: a set of P-element insertions for generating custom chromosomal aberrations in Drosophila melanogaster. *Genetics* **167**, 797-813.

Schneider, T., Reiter, C., Eule, E., Bader, B., Lichte, B., Nie, Z., Schimansky, T., Ramos, R. G. and Fischbach, K. F. (1995). Restricted expression of the irreC-rst protein is required for normal axonal projections of columnar visual neurons. *Neuron* **15**, 259-71.

Schroter, R. H., Buttgereit, D., Beck, L., Holz, A. and Renkawitz-Pohl, R. (2006). Blown fuse regulates stretching and outgrowth but not myoblast fusion of the circular visceral muscles in Drosophila. *Differentiation* **74**, 608-21.

Schroter, R. H., Lier, S., Holz, A., Bogdan, S., Klambt, C., Beck, L. and Renkawitz-Pohl, R. (2004). kette and blown fuse interact genetically during the second fusion step of myogenesis in Drosophila. *Development* **131**, 4501-9.

Schubert, V. and Dotti, C. G. (2007). Transmitting on actin: synaptic control of dendritic architecture. *J Cell Sci* **120**, 205-12.

Sepp, K. J. and Auld, V. J. (2003). Reciprocal interactions between neurons and glia are required for Drosophila peripheral nervous system development. *J Neurosci* **23**, 8221-30.

Shen, K. and Bargmann, C. I. (2003). The immunoglobulin superfamily protein SYG-1 determines the location of specific synapses in *C. elegans*. *Cell* **112**, 619-30.

Sin, W. C., Haas, K., Ruthazer, E. S. and Cline, H. T. (2002). Dendrite growth increased by visual activity requires NMDA receptor and Rho GTPases. *Nature* **419**, 475-80.

Soba, P., Zhu, S., Emoto, K., Younger, S., Yang, S. J., Yu, H. H., Lee, T., Jan, L. Y. and Jan, Y. N. (2007). Drosophila sensory neurons require Dscam for dendritic self-avoidance and proper dendritic field organization. *Neuron* **54**, 403-16.

Song, W., Onishi, M., Jan, L. Y. and Jan, Y. N. (2007). Peripheral multidendritic sensory neurons are necessary for rhythmic locomotion behavior in *Drosophila* larvae. *Proc Natl Acad Sci U S A* **104**, 5199-204.

Spradling, A. C., Stern, D. M., Kiss, I., Roote, J., Laverly, T. and Rubin, G. M. (1995). Gene disruptions using P transposable elements: an integral component of the *Drosophila* genome project. *Proc Natl Acad Sci U S A* **92**, 10824-30.

Strunkelberg, M., Bonengel, B., Moda, L. M., Hertenstein, A., de Couet, H. G., Ramos, R. G. and Fischbach, K. F. (2001). *rst* and its paralogue *kirre* act redundantly during embryonic muscle development in *Drosophila*. *Development* **128**, 4229-39.

Sugimura, K., Satoh, D., Estes, P., Crews, S. and Uemura, T. (2004). Development of morphological diversity of dendrites in *Drosophila* by the BTB-zinc finger protein *abrupt*. *Neuron* **43**, 809-22.

Sugimura, K., Yamamoto, M., Niwa, R., Satoh, D., Goto, S., Taniguchi, M., Hayashi, S. and Uemura, T. (2003). Distinct developmental modes and lesion-induced reactions of dendrites of two classes of *Drosophila* sensory neurons. *J Neurosci* **23**, 3752-60.

Sweeney, N. T., Li, W. and Gao, F. B. (2002). Genetic manipulation of single neurons in vivo reveals specific roles of *flamingo* in neuronal morphogenesis. *Dev Biol* **247**, 76-88.

Szebenyi, G., Bollati, F., Bisbal, M., Sheridan, S., Faas, L., Wray, R., Haferkamp, S., Nguyen, S., Caceres, A. and Brady, S. T. (2005). Activity-driven dendritic remodeling requires microtubule-associated protein 1A. *Curr Biol* **15**, 1820-6.

Taylor, W. R. and Vaney, D. I. (2003). New directions in retinal research. *Trends Neurosci* **26**, 379-85.

Togel, M., Wiche, G. and Propst, F. (1998). Novel features of the light chain of microtubule-associated protein MAP1B: microtubule stabilization, self interaction, actin filament binding, and regulation by the heavy chain. *J Cell Biol* **143**, 695-707.

Tower, J., Karpen, G. H., Craig, N. and Spradling, A. C. (1993). Preferential transposition of *Drosophila* P elements to nearby chromosomal sites. *Genetics* **133**, 347-59.

Tracey, W. D., Jr., Wilson, R. I., Laurent, G. and Benzer, S. (2003). *painless*, a *Drosophila* gene essential for nociception. *Cell* **113**, 261-73.

Van Aelst, L. and Cline, H. T. (2004). Rho GTPases and activity-dependent dendrite development. *Curr Opin Neurobiol* **14**, 297-304.

Van Aelst, L. and D'Souza-Schorey, C. (1997). Rho GTPases and signaling networks. *Genes Dev* **11**, 2295-322.

Whitford, K. L., Marillat, V., Stein, E., Goodman, C. S., Tessier-Lavigne, M., Chedotal, A. and Ghosh, A. (2002). Regulation of cortical dendrite development by Slit-Robo interactions. *Neuron* **33**, 47-61.

Winzler, E. A., Richards, D. R., Conway, A. R., Goldstein, A. L., Kalman, S., McCullough, M. J., McCusker, J. H., Stevens, D. A., Wodicka, L., Lockhart, D. J. et al. (1998). Direct allelic variation scanning of the yeast genome. *Science* **281**, 1194-7.

Wong, R. O. and Ghosh, A. (2002). Activity-dependent regulation of dendritic growth and patterning. *Nat Rev Neurosci* **3**, 803-12.

Wu, G. Y. and Cline, H. T. (1998). Stabilization of dendritic arbor structure in vivo by CaMKII. *Science* **279**, 222-6.

Yamamoto, M., Ueda, R., Takahashi, K., Saigo, K. and Uemura, T. (2006). Control of axonal sprouting and dendrite branching by the Nrg-Ank complex at the neuron-glia interface. *Curr Biol* **16**, 1678-83.

Yamamoto, N., Tamada, A. and Murakami, F. (2002). Wiring of the brain by a range of guidance cues. *Prog Neurobiol* **68**, 393-407.

Ye, B., Petritsch, C., Clark, I. E., Gavis, E. R., Jan, L. Y. and Jan, Y. N. (2004). Nanos and Pumilio are essential for dendrite morphogenesis in Drosophila peripheral neurons. *Curr Biol* **14**, 314-21.

Yeh, E., Gustafson, K. and Boulianne, G. L. (1995). Green fluorescent protein as a vital marker and reporter of gene expression in Drosophila. *Proc Natl Acad Sci U S A* **92**, 7036-40.

Yu, X. and Malenka, R. C. (2003). Beta-catenin is critical for dendritic morphogenesis. *Nat Neurosci* **6**, 1169-77.

Zhai, R. G., Hiesinger, P. R., Koh, T. W., Verstreken, P., Schulze, K. L., Cao, Y., Jafar-Nejad, H., Norga, K. K., Pan, H., Bayat, V. et al. (2003). Mapping *Drosophila* mutations with molecularly defined P element insertions. *Proc Natl Acad Sci U S A* **100**, 10860-5.

Zhu, H., Hummel, T., Clemens, J. C., Berdnik, D., Zipursky, S. L. and Luo, L. (2006). Dendritic patterning by Dscam and synaptic partner matching in the *Drosophila* antennal lobe. *Nat Neurosci* **9**, 349-55.

Zhu, H. and Luo, L. (2004). Diverse functions of N-cadherin in dendritic and axonal terminal arborization of olfactory projection neurons. *Neuron* **42**, 63-75.

First of all, I have to thank my family for their help and support during the years of my study and PhD, despite the fact that I always failed to explain what I was actually doing and were all this will finally end. I thank Gaia Tavosanis for giving me the chance to perform my PhD in her lab and sharing all her practical experience with me. In addition, I am very grateful to Alexander Borst and Rüdiger Klein for their supervision of my PhD. The SNP-mapping would not have been possible without the instructions and incubators of Takashi Suzuki. I am thankful to Karl-Friedrich Fischbach, Susan Abmayr, Eric Olson and again Takashi Suzuki for the anti-sns antibody and/or fly stocks. Furthermore, I am also thankful for all the valuable advice and comments that I got from various members of the Tavosanis, Bradke, Suzuki and Klein labs in the numerous seminars that I had to give during the last four years. Most important, many thanks to Ewa for all her help, ideas, surprises, jokes, smiles, tears and the insights into the polish side of life that made everything so much easier and brighter for me.

Personal Data

Name	Andre Reissaus
Date of Birth	06.05.1978
Place of Birth	Leipzig
Nationality	German

Education

since 11/2003	Doctoral Thesis Laboratory of Dr. Gaia Tavosanis Max Planck Institut for Neurobiology
04/2002-02/2003	Diploma thesis Laboratory of Prof. Wolfhard Bandlow Ludwig-Maximilians-University, Munich
09/1997-02/2003	Diploma in Biology University of Leipzig

Publications

Rützler, M.; Reissaus, A.; Budzowska, M.; Bandlow W. (2004). SUT2 is a novel multi-copy-suppressor of low activity of the cAMP/PKA pathway in yeast. *Eur.J.Biochem.*;271;1284-1291.